

**STOKES POLARIMETRY
AND
THE MEASUREMENT OF
VECTOR MAGNETIC FIELDS
IN SOLAR ACTIVE REGIONS**

A Thesis

Submitted for the Degree of

Doctor of Philosophy

in the Faculty of Science

by

K. S. BALASUBRAMANIAM



INDIAN INSTITUTE OF SCIENCE
JOINT ASTRONOMY PROGRAM
DEPARTMENT OF PHYSICS
BANGALORE-560 012.

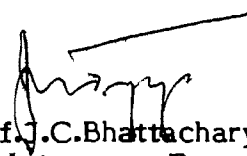
JULY 1988

To

MOM

CERTIFICATE

The thesis entitled '**Stokes Polarimetry and the Measurement of Vector Magnetic Fields in Solar Active Regions**' is a record of the work done by Shri.K.S.Balasubramaniam under my supervision. It has not formed the basis for the award to him of any Degree, Diploma, Associateship, Fellowship or other similar titles. This thesis represents independent work on the part of Shri.K.S.Balasubramaniam.



Prof. J.C. Bhattacharyya
Joint Astronomy Program
Indian Institute of Astrophysics
Bangalore 560034

July 1988
Bangalore

DECLARATION

I hereby declare that the work reported in this thesis is entirely original. This work was carried out by me at the Joint Astronomy Program, Department of Physics, Indian Institute of Science, Bangalore under the supervision of Prof.J.C.Bhattacharyya, Indian Institute of Astrophysics, Bangalore. The work reported here was executed by me at the Indian Institute of Astrophysics, Bangalore and its field stations at the Kodaikanal Observatory, Kodaikanal and the Vainu Bappu Observatory, Kavalur. I further declare that this work has not formed the basis for the award of any Degree, Diploma, Membership, Associateship or similar title of any University or Institution.

K. S. Balasubramaniam

K.S.Balasubramaniam
Joint Astronomy Program
Department of Physics
Indian Institute of Science
Bangalore 560012

and

Indian Institute of Astrophysics
Bangalore 560034

July 1988
Bangalore

ACKNOWLEDGEMENTS

It hardly took forty-five minutes for me to decide to work on measuring solar vector magnetic fields, after just one convincing meeting with Prof. J.C.Bhattacharyya, in July 1983. From then on there has been no looking back. His generous encouragement, help, suggestions and advice at every stage of this work, as my teacher, as my research supervisor and as the Director of the Indian Institute of Astrophysics has indeed gone a long way in the outcome of this work. My gratitude to him.

Dr.P.Venkatakrisnan, has been a continuous source of inspiration, encouragement and help through the course of this work. His experience and balancing influence has been of invaluable help in charting the course of this thesis over the last five years. My gratitude to him.

Dr. T.P.Prabhu has enormously helped me with the data reduction procedures. His ready answers to my ever nagging questions and his keen interest in every aspect of the data reduction has greatly helped me in this endeavour. My gratitude to him.

Another source of big help has been Ms. G.C.Anupama. Her constant and ever ready help during the phases of the reductions and, at all times has been of enormous use. Dr. T.P.Prabhu, Ms. G.C.Anupama and Dr.S.Giridhar have taken great pains to explain the workings of the spectroscopic reduction package RESPECT.

Mr. P.Devendran has extended his help, both during the course of observations as well as in the reductions at the PDS facility. He and Mr. Hariharan have spent long hours helping me at the observing floor. The Workshop staff at the Kodaikanal Observatory have helped me with all mechanical problems relating to the construction of the polarimeter and the ellipsometer and, the scientific staff

there have also been of help whenever required. My thanks to them.

I wish to thank Mr. Ashok Pati for all his encouragement and help. His presence, particularly at Kavalur during the computational stages had been very useful. Invaluable help came from Dr. K.K. Ghosh and his colleagues at the VAX 11/780 Installation of the Vainu Bappu Observatory, who have spent several months of their valuable time. Dr. Srinivasan, Mr K.Subramanian and their colleagues have taken pains to keep the vital power supply lines to the the computer system alive, inspite of unforeseen difficulties like breakdowns and lightning disruption of the electrical systems during a crucial stage of this work. Mr. V.Chandramouli, CMC, has helped me to trouble shoot several software problems and data handling difficulties. I thank them all for their wonderful help.

Drs. K.N.Nagendra, D.Mohan Rao, K.E.Rangarajan, and G.Som Sunder, and P.Joarder have all helped me at different phases of this work. The expertise of Dr. K.N.Nagendra in handling the polarised radiative problems has been extremely useful. The solar physics community at the Indian Institute of Astrophysics have always lent a helping hand during this work. Profs. K.R.Sivaraman and M.H.Gokhale have been very enthusiastic about this work. Dr. Jagdev Singh provided the much needed introduction to the art of observations. His tips to the observations have been useful. Frequent discussions with Dr. S.K.Jain has helped me to widen my understanding of several concepts in polarimetry. The library staff of IIA, particularly Ms. A.Vagiswari, Ms. Christina Louis and Mr. Manjunath have taken great pains to retrieve information whenever required. I thank them all for their gracious help.

Drs. A.D.Wittmann and E.Landi Degl'Innocenti sent me the computer codes for polarised radiative transfer and related material. I thank them and Drs. W.Livingston and

V.I.Makarov for showing keen interest in this work.

I wish to thank Dr. R.Rajamohan for his 'pep-talk' and advice during moments of depression. Dr. R.Rjamohan and Mr. V.Chinnappan have lightened the task of preparing this thesis by making available the personal computers, in its preparation.

Mr Arvind Paranjpye has been a great source of moral support throught the course of this work. His understanding of the word processing software has enormously reduced my troubles. This thesis would not have been completed in time but for the tremendous support of Dr.T.P.Prabhu, Ms.G.C.Anupama, Dr.P.Venkatakrishnan, Mr.Arvind Paranjpye Mr.Divakara Mayya and Mr M.Venkatesh. They have spent several sleepless nights and have taken the trouble to ensure the smooth completion of the thesis during its final stages. Mr.A.Elangovan and Mr.H.Inbaraj have helped in preparing some of the illustrations. Mr. and Mrs. Krishnamurthy and their colleagues at the binding section taken trouble to see the thesis in its final form.

I wish to thank all the staff members of the Indian Institute of Astrophysics for their timely help.

Finally I wish to thank the Chairman, and all the staff members of the Department of Physics, IISc for their timely help. Drs. B.Ramakrishnan and R.H.Premchandran have enthusiastically helped me whenever I needed their help.

PREFACE

The thesis titled 'Stokes Polarimetry and the Measurement of Vector Magnetic Fields in Solar Active Regions', describes an attempt to measure the Stokes polarisation profiles of Zeeman sensitive spectral lines to use these profiles to infer the vector magnetic field and other physical parameters in sunspots.

Chapter I spells out the need for the measurement of solar vector magnetic fields. Although techniques for the measurement of vector fields have evolved since 1913, no perfect method has emerged. It also gives a schematic preview of the later chapters and compares the present work with that done elsewhere.

Chapter II discusses the instrumentation used. The Solar Tower/Tunnel Telescope, spectrograph and the camera system is described first. For the sake of completeness, a brief introduction to Stokes parameters and Mueller Calculus has been included.

This is followed by detailed analysis of the instrumental polarisation produced by the coelostat system. The instrumental polarisation is next estimated for various hour angles and declinations. The implication of these estimates for the observation are pointed out. The positioning of the primary of the coelostat system is then compared with that predicted from the formulae developed for the analysis.

The spectroscopic principles underlying the observations are outlined, which is followed by some arguments that lead to the present choice of using Zeeman sensitive spectral lines for polarisation measurements, in the $\lambda 6300 \text{ \AA}$ region.

The construction of polarimeter used in these

measurements is described and errors in the measurement of the Stokes parameters due to this system are then evaluated.

The measured separation of the Stokes V components of the two Zeeman sensitive spectral lines Fe I $\lambda 6301.5$ and Fe I $\lambda 6302.5$ are shown to be consistent with their Lande g values thus confirming the reliability of the polarimeter. Attempts to improve the seeing conditions within the telescope as well as to remove suspended dust particles, (which introduces scattered light), are reported.

Chapter III outlines the procedures followed for the data analysis. A summary of the observations made are given. The first step in the data analysis is the conversion of photographic densities into a digital format. This is followed by a description of the stages involved in the reduction of the data which include the noise filtering, wavelength calibration, conversion from densities to intensities, deriving the the spectral line-to-continuum ratios, algebraic operation on the data to extract the Stokes profiles, and finally, the off-line correction for the instrumental polarisation.

Chapter IV describes the analytical formulation for the transfer of polarised radiation in a magnetic field. These analytical formulae are then used in the non-linear least squares fitting of the observed profiles.

The problem encountered in the conventional Marquardt scheme for the non-linear least squares fitting are enumerated. Modifications to these techniques are then attempted. Rigorous tests on the modified algorithms for both synthetic as well as real data proved to be successful. This modified scheme was applied to the Stokes profiles obtained from the unipolar sunspot KKL 18303 (NDAA 4810). A set of eight parameters namely, the strength, inclination, and azimuth of the magnetic field

vector, the line-centre wavelength, opacity ratio, Doppler widths, slope of the source function and damping constant are then retrieved from the observed Stokes Q, U, and V profiles, for one scan across the sunspot.

Chapter V summarises the previous chapters and highlights the strength and weakness of the observational scheme used here. Improvements to the data acquisition methods as well as the subsequent inversion of the Stokes profiles are suggested.

In the Appendix, the design and construction of an ellipsometer to measure the complex refractive indices of the coelostat mirror surfaces is described. This device is necessary to monitor the changes in the refractive index caused by the ageing of the aluminised mirror surfaces. The refractive indices determine the Mueller matrix of the coelostat system.

LIST OF SCIENTIFIC PAPERS

1. Journal : Measurement of vector magnetic fields
1. Theoretical approach to the instrumental polarisation of the Kodaikanal Solar Tower. Balasubramaniam, K.S., Venkatakrisnan, P. & Bhattacharyya, J.C., (1985) Solar Physics. 99, 333
2. Proceedings : Measurement of Solar Magnetic fields. Bhattacharyya, J.C., & Balasubramaniam, K.S. (1986) Proceedings of National Workshop on Solar Physics. Kodaikanal Observatory Bulletin (Special Issue) Vol. 6
3. Preprint : Design considerations for fabricating an ellipsometer to measure the complex refractive indices of aluminised mirrors. Balasubramaniam, K.S., (1986) IIA Preprint
4. Proceedings : "Asymmetry of Stokes profiles across a sunspot - Measurements". Contributed paper presented at the D - E - S Workshop on The Role of fine-scale magnetic fields of the structure of the solar atmosphere. Canary Islands October 1986. (in press) Balasubramaniam, K.S.
5. Conference : A proposal for the construction of a vector magnetograph at the Tower Telescope at Kodaikanal and a vector magnetograph for the proposed polarisation-free Vacuum Telescope. Bhattacharyya, J.C., & Balasubramaniam, K.S., National workshop on astronomical instrumentation Past, present and Future. August 1987 Kodaikanal, India

CONTENTS

	PAGE
PREFACE	i
CHAPTER I	INTRODUCTION
1	The need for Stokes polarimetry and the measurement of vector magnetic fields 1
2	Historical perspective 3
3	What does this thesis attempt to do 13
4	A comparision 16
CHAPTER II	INSTRUMENTATION
1	The tower/tunnel telescope 18
2	The spectrograph and camera system 19
3	Stokes parameters 20
4	Mueller calculus 22
5	The instrumental polarisation of the coelostat mirrors 23
5.1	The telescope geometry 23
5.2	Derivation of the Mueller matrices of the telescope 24
5.3	Determination of the angles of incidence 25
5.4	Determination of the angles of rotation 28
6	Estimation of instrumental polarization 29
7	Implication of the instrumental polari- sation for actual observations 31
8	Experimental verification of the accuracy of the positioning of the coelostat system and its comparison with formulae derived in section II-5.3 33
9	Spectroscopic principles 34
9.1	The Zeeman effect 34
9.2	Choice of the spectral lines 35
10	The polarimeter 37

CHAPTER II

11	Errors in the measurement of the Stokes parameters	40
12	Observational checks on the complex refractive indices of the coelostat mirrors	41

CHAPTER III DATA ANALYSIS

1	The observations	43
2	Conversion of photographic densities into digital densities	45
3	Reduction of the data using the VAX 11/780 computer facility and the RESPECT package	46
3.1	The calibration for converting the data from densities to intensities	46
3.2	Reduction of the observed spectrum	47
4	Correction for instrumental polarisation of the telescope	53

CHAPTER IV INVERSION OF STOKES PROFILES

1	The equations of radiative transfer	58
2	Analytical solutions of the polarised	
3	The inversion scheme	
3.1	Simultaneous fitting of the Stokes Q, U, and V profiles	62
3.2	Calculations of Stokes Q, U and V profiles and their derivatives	62
3.3	Test on the non-linear least square fitting algorithms	64
4	Test runs on real data	65
5	Results on non-linear least square fitting algorithm	65

CHAPTER V SUMMARY AND CONCLUSIONS

1	Overview	68
2	Future improvements	70

APPENDIX	72
REFERENCES	76

CHAPTER I
INTRODUCTION

1. THE NEED FOR STOKES POLARIMETRY AND THE MEASUREMENT OF VECTOR MAGNETIC FIELDS

Magnetic fields play an important role in the energy balance of the atmospheres of our Sun and the solar-type stars. They wield dominant influence on the formation of various observed structures and control the physical processes that take place on the Sun. The Sun is a giant laboratory providing us with examples of a wide variety of structures formed under the simultaneous influence of the thermodynamic, hydrodynamic and radiative processes. The observed features vary from scale sizes ranging from a few kilometres to several tens of thousands of kilometres. It is now well known that the interaction of magnetic fields, convection and radiation are responsible for the formation of active chromospheres and coronae of Sun and possibly the solar type stars. Our knowledge of the magnetic field strength present in the various structures on the Sun and, to a small extent, its direction, has aroused serious questions on its role, in the evolutionary course of these objects.

The three dimensional structure of the solar active regions is still an enigma; the need for an understanding of the three-dimensional magnetic field configuration here becomes immediately obvious. To understand the underlying physical and magnetohydrodynamic nature of these structures, a knowledge of the vector magnetic field will be very useful. We have to answer such questions as: What is the role of the magnetic field in the formation and evolution of sunspots? Do they influence the Evershed flow - the radial movement of material in sunspot penumbrae? How does the vector magnetic field influence the energy balance in sunspots? How does the vector magnetic field affect the formation of complex sunspots whose energetics and dynamics result in the occurrence of

solar flares - a consequence of the departures of these magnetic structures from force-free equilibrium? It is now well known that the large scale structures in the solar atmosphere are rooted in foot-points on the turbulent solar photosphere. What changes in the vector magnetic fields at these foot-points will produce those observable changes of these structures at the chromosphere and the corona?

The measurement of Stokes polarisation profiles arising from the Zeeman sensitive magnetic field regions, apart from yielding the direction and strength of the magnetic fields, have themselves been an important diagnostic tool for unraveling the underlying thermodynamical and physical properties of these structures (*Solanki 1986; Solanki and Stenflo 1984, 1985; Stenflo et.al. 1984*). Usage of the Stokes polarisation profiles of the Zeeman effected lines in such diagnostics, particularly the Q, U and V profiles vector magnetic field measurements will go a long way in understanding the temperature, pressure, density and the vector magnetic configuration of these structures. We are yet to understand the departures of the shapes of the Stokes profiles from their symmetrical or anti-symmetrical nature(e.g. *Illing et.al. 1974; Stenflo et.al. 1984; Landolfi et.al. 1984; Landi Degl'Innocenti, Landi Degl'Innocenti 1977; Balsubramanian 1986*), ascribed to gradients in either the vector magnetic field parameters (strength and directions) or the physical parameters (temperature, velocities, densities, pressure etc).

We are still unable to understand the effect of such complex situations on the transfer of polarised radiation. Several anomalies seem to exist in comparing observations of the Stokes profiles when they are compared with that of the theoretically generated polarised radiative transfer equations (*West and Hagyard 1983*). It is necessary to develop quicker ways of deriving the vector magnetic field

from the measurement of Stokes profiles across spectral lines.

2.HISTORICAL PERSPECTIVE

The first questions about the presence of the magnetic fields on the Sun were raised by *Schuster* (1892,1912). Beginning with the assumption that every rapidly rotating large body must produce a magnetic field, he calculated the Earth's magnetic field and even the Sun's magnetic field and said that it should be about 440 times greater than the Earth's field. Indirect evidences indicating the presence of magnetic fields on the Sun was noticed by several astronomers. *Bigelow* (1889) suggested that the Sun must be a magnet because coronal streamers near the poles of the Sun agree well in form with the lines of force of a bar magnet. *Strömer* (1892)calculated trajectories of electrical corpuscles moving out of the Sun under an assumed magnetic field and the resulting curves resembled the structure of the corona. *Deslandres* (1912) applied the same idea to the case of prominences and concluded from their forms and radial velocities that, the ions which compose them are moving under the influence of the magnetic field.

With the discovery of the splitting of the spectral lines, when a light source was placed under the influence of magnetic field, by *Pieter Zeeman* (1896), *Hale* (1913) used the Zeeman effect to measure the magnetic fields on the Sun . He used a Nicol prism and a quarter wave plate to measure the magnetic fields in sunspots in several spectral lines. From his observations Hale first arrived at the general magnetic field of the Sun to be about 50 Gauss. He also analysed the magnetic structure of sunspots and their bi-polar nature. His observations reaffirmed the earlier beliefs that the magnetism of the Sun is due to the axial rotation of a body as though it carried a

residual volume charge.

The observations of Hale was put on a sound theoretical basis by *Sears* (1913). In an attempt to understand the polarisation of the spectral lines caused by the solar magnetic field, he was the first person to emphasize the importance of the instrumental polarisation due to the telescope and the intervening optics. He derived the relative intensities of the σ and π components of the Zeeman splitting. They are

$$I_{\sigma^-} = 0.25 (1 \pm \cos \gamma)^2$$
$$I_{\pi} = 0.5 \sin^2 \gamma$$
$$I_{\sigma^+} = 0.25 (1 \mp \cos \gamma)^2,$$

where γ is the inclination of the magnetic field vector to the line-of-sight.

Hale and Nicholson (1938) devised a simple grid to measure the circular polarisation of the Zeeman broadened spectral lines. The grid simply divides the spectrograph slit into short segments and transmits right and left circularly polarised light in the alternate segments. The grid consists of strips of $\lambda/4$ plate, followed by a polaroid. The strips of the $\lambda/4$ plate are oriented so as to alternately suppress each sigma component. For measuring the transverse magnetic field, $\lambda/2$ plate-strips are used.

Babcock (1953) invented the solar longitudinal magnetograph to measure the weak longitudinal magnetic fields on the Sun. Using the Fe I $\lambda 5250.22 \text{ \AA}$ spectral line (Lande's g factor is 3), the circular polarisation from the wings on either side of the spectral line was isolated with a pair of exit slits. The polarisation of the beam was modulated at the entrance of the spectrograph with the help of an electro-optic modulator followed by a polariser, to alternately isolate the right and left circular polarisations from the spectral line-wings. Photomultipliers at the exit slits detected the circular

polarisation which was then fed to a differential amplifier, whose signal was proportional to the magnetic field. Babcock's magnetograph was able to measure fields between 1-20 Gauss. Using the magnetograph he produced maps of the general magnetic field of the Sun (magnetograms). He was able to show that there was a persistent magnetic field in the heliographic latitudes above $\pm 65^\circ$ and also confirmed the Sears displacement law.

In an attempt to explain the formation of the solar magnetic field and the various magnetic structures on the Sun, *Babcock* (1961) proposed the first solar dynamo model based on the his observations of the magnetograms. His dynamo theory was able to explain the formation of the bipolar magnetic regions, the Sporer's law as well as the butterfly diagram. He was also able to explain the magnetic polarities of sunspots as well as the reversal of the dipolar magnetic field on the Sun.

The first magnetograph to measure transverse magnetic fields was due to the pioneering work of Severny and his coworkers at the Crimean Astrophysical Observatory (*Stepanov and Severny* 1962; *Nikulín* 1964; *Severny* 1964, 1965). Their transverse magnetograph was a modification of an existing longitudinal magnetograph at the λ 5250.2 Å spectral line. A $\lambda/4$ plate was introduced, in addition to the existing $\pm \lambda/4$ ADP electro-optic modulator, to achieve a $\lambda/2$ modulation, to detect the transverse magnetic field. The signals from the photomultipliers located at the wing of the Zeeman broadened line was added, instead of subtracting them, as in the Babcock's scheme.

To measure the magnetic fields on the Sun in a 'one-stroke' recording, *Leighton* (1956) invented a technique to measure the longitudinal magnetic fields on the Sun. Two spectro-heliograms are separately, and simultaneously recorded at the exit of the spectrograph,

each on one wing of the Zeeman sensitive line to record the circularly polarised intensities. While one spectroheliogram is for the right circularly polarised intensities, the other is for the left circularly polarised intensities. In areas where there are magnetic fields, the relative displacements of the σ - components result in an increase in the intensity of one spectroheliogram and a decrease in the other. To take the algebraic differences in intensity of the spectroheliograms corresponding to the longitudinal magnetic fields, a positive transparency is made of one of the spectroheliograms, and is superposed on the other. A print through the two then constitutes a photograph of the magnetic field. One polarity of the magnetic field shows up as dark while the other shows up as bright. The results of the intimate relationship between the calcium plages and the coarse network with that of the magnetic fields has been established with this technique. The limitation of the technique is the inaccurate calibration of the magnetic field, whereas its advantage lies in the speed: the entire disc of the Sun could be measured in a few minutes.

It would be of interest to note here that the first measurements of the magnetic field at Kodaikanal was due to *Bhattacharyya* (1969), who built a longitudinal magnetograph to map the general magnetic field of the Sun. His technique was similar to that of Babcock's, in using an electro-optic modulator (an ADP crystal) to alternately chop the right and left circular polarised components of the Zeeman broadened lines. At the exit of the spectrograph the wings of the spectral line Fe I $\lambda 5250.22 \text{ \AA}$ as well as the line centre were isolated to simultaneously measure the magnetic and velocity fields.

Systematic measurements of the vector magnetic field of the Sun, particularly across sunspots was first taken up by *Treanor* (1960) and further improved by *Adams*

(1963). Their method of analysis consisted of using a Babinet compensator with a polaroid. They also made detailed analysis of the vector magnetic field, including the measurements of gradients in magnetic and velocity fields across a sunspot. The limitations included not considering the entire spectral line.

Unno (1956) first developed the theory of polarised radiative transfer and spectral line formation in a magnetic field. For an arbitrary inclination of the magnetic field, using all the four Stokes parameters he developed the solutions of these equations. His theory gave impetus to using the polarisation information along the entire spectral line and thus help in measuring other physical parameters apart from the purely vector magnetic field parameters. His theory was mainly based on pure absorption and a Milne-Eddington model atmosphere.

Stepanov in a series of papers published between 1958 and 1960, almost parallely improved the theory of polarised radiative transfer, computed the effective absorption coefficients as a function of the inclination of the magnetic field and included both scattering as well as true absorption and attempted at a more generalised formulations of these equations.

Since the measurement of the vector magnetic field cannot be isolated from the physical conditions in sunspots, *Rachkovsky* (1962) included the presence of magneto-optical effects. His contribution was a significant factor in understanding the effect of Faraday rotation of the linear polarisation and its influence on the results affecting the calculation of the transverse magnetic fields on the Sun.

Daily maps of the longitudinal magnetic field of the entire solar disc are now produced by the Kitt Peak National Observatory using their 512-channel magnetograph

(Livingston et.al 1976).The magnetograph uses the Fe I λ 5250.2 Å spectral line. The polarimetric optics essentially uses an electro-optic modulator to chop the right and left circular polarisation alternately.

Limitations of the measurement of both the transverse and the longitudinal field is mainly because of the following reasons: Magnetographs, both of the longitudinal as well as the transverse types, use only portions of the spectral line for measuring the magnetic fields. With narrow slits using only portions of the spectral line, the complete information is not fully extracted. Zeeman saturation occurs because of the non-linear behaviour of the line of sight component of the magnetic field. Physical parameters of the spectral line forming regions are also not completely extracted.

Improvements to the theory of spectral line formation was formulated by *Beckers* (1969), (including magneto-optical effects), by studying the Zeeman profiles of Fraunhofer lines in the presence of the magnetic field. Numerical studies in this direction have been made for both LTE as well as non-LTE conditions (*Rees* 1969; *Moe* 1968) by fixing the relevant model atmospheres.

Attempts to measure all the four Stokes profiles of a Zeeman broadened spectral line was systematically first done by *Wittmann* (1973) using a polarimeter arrangement. To help in the analysis of these Stokes profiles, *Wittmann* (1974, 1977) was the first to develop synthesis radiative transfer codes to generate the solar spectrum, using a detailed model atmosphere. He generated the Stokes profiles from the Unno-Beckers equations of polarised radiative transfer.

At about the same time, *Stenflo* (1973) invented the line-ratio technique. His idea was to verify the magnetic and physical properties derived from two spectral lines

formed under similar thermodynamic condition. Using the Stokes I and V profiles of the Fe I λ 5250.22 Å and Fe I λ 5247.06 Å spectral lines which differ mainly in the values of their Lande g-factors, he estimated that field strengths of the order of 2000 Gauss must be present in the photospheric network. He also calculated the extent to which the Fe I λ 5250.22 Å spectral line is weakened in the network structure and also calculated the downward velocities at the supergranular boundaries to be of the order of 0.5 Kms^{-1} . Such is the power of the line-ratio technique that, to the present day it has been able to obtain information on spatially unresolved flux tubes and the physical and thermodynamic properties of the medium, using the ratio's of the Stokes profiles.

A milestone in the theoretical formalism of the polarised radiative transfer equations was due to *Landi Degl' Innocenti and Landi Degl'Innocenti* (1972). Starting from the basic atomic physics and quantum mechanical formulations, they developed the equations of polarised radiative transfer in the most self consistent way, that included all possible physical processes. They have numerically computed the Stokes profiles derived from these equations for both LTE as well as NLTE. Analytical solutions of the Stokes profiles have also been developed for a restricted case of a homogenous atmosphere with the region of spectral line formation in the Milne-Eddington approximation (*Landolfi and Landi Degl' Innocenti*, 1978). All physical parameters within the depth of formation of the spectral line are assumed to be a constant.

Regular maps of the vector magnetic field in the form of transverse and longitudinal contour maps are produced from two places. The first one is from the NASA Marshall Space Flight Centre, Huntsville, Alabama. Using a telescope of 30cm aperture, and a polarimetric arrangement basically involving a KDP analyser followed by a

polarising optics, Stokes filtergrams are recorded. The filtergrams are recorded using a CCD device about the Fe I λ 5250.22 Å line. A birefringent tunable filter is used in conjunction with the polarisation optics to record the polarised filtergrams over a broad-band. The filtergrams cover either a 2x2 arcminute or a 5x5 arcminute field of view. The lower limits on the measurements is about 70 Gauss in the transverse field and about 4 Gauss in the longitudinal field. (*Hagyard et.al.* 1983; *Hagyard et.al.* 1982). The spectral resolution of the filtergrams is limited by the pass-band of the filter transmission profile which has a full-width-at-half-maximum (FWHM) of 0.125 Å.

The Tokyo Astronomical observatory also produces daily vector magnetograms (*Makita et.al.* 1985). Their method of detection uses four photomultipliers in the wings of the Fe I λ 5250.22 Å line to detect both the linear and circular polarisation. Their polarimetric arrangement consists of a rotating waveplate and a Wollaston prism. Although they use only a portion of the spectral line, their resolution corresponds to about 5 Gauss in the longitudinal direction and about 200G in the transverse direction.

One of the first attempts to produce complete vector magnetic field maps of sunspots using the entire Stokes line profile and integrating the observation with theory in terms of an inversion procedure was by *Kawakami* (1983). He developed a full line Stokes polarimeter using the Fe I λ 6301.5 Å ($g=1.667$) and Fe I λ 6302.5 Å ($g=2.5$) at the Tokyo Astronomical Observatory and used it to make maps of the vector magnetic field of unipolar sunspots. He, ofcourse, used the magneto-optical effects in a restricted sense. The magneto-optical effects were used to derive the azimuth of the magnetic field only, but were ignored while deriving the physical parameters like Doppler width, damping constant, velocities etc.

The Haleakala Stokes polarimeter uses a coronagraph to measure the Stokes profiles from solar active regions. (*Mickey* 1985). Very low scattered light levels and very high signal to noise have been the highlights of this instrument. The detection sensitivity involved is a few parts in 10^4 .

Noticeable in the literature, have been reports of measuring polarisation upto sensitivities of one part in ten million to one part in hundred million, (*Kemp et.al* 1987). Their instrument is essentially a polarimeter using photo-elastic modulators.

Stokes polarimetry with the Kitt Peak Fourier Transform Spectrometer at the Mc Math Telescope has yeilded valueable information on the nature of magnetic fields in solar active regions (*Harvey et.al* 1980; *Stenflo et.al* 1984)

One of the biggest stumbling blocks in Stokes polarimetry has been the extraction of the vector magnetic field and other physical parameters from the observations. Since the problem is an inverse one, of fitting the observed Stokes profiles with that of the theoretically generated ones, several attempts have been made to interpret the observations. Earliest of these have been to synthesize the Stokes profiles and then fit them to the observations (e.g., *Wittmann* 1976). Since synthesis itself is a laborious and time consuming task and, involves a large amount of computational work, it has so far not yet appealed as a quick and a relatively less model dependent method. Yet another method is the use of semi-emperical methods combined with the polarised radiative transfer equations (e.g. the work of Kawakami). In Kawakami's work, again the magneto-optical effects have been used in a restriced sense.

A more suitable method of comparing the observed Stokes profiles with the theoretically generated ones was first evolved by *Auer, Heasley and House* (1977), called the AHH routines. The method was a non-linear least square optimising technique using the Marquardt algorithm (in *Bevington* 1969). In the AHH routines, all the four Stokes profiles were attempted to be fitted with those of the profiles generated from the analytical solutions. The AHH method incorporated several simplifications to the line formation in magnetic field and had ignored the magneto-optical effects. They had effectively used a 4-parameter fit viz. the Doppler width, the ratio of the line centre-to continuum optical depth, the magnetic field strength and the inclination of the magnetic field strength to the line-of-sight.

Landi Degl'Innocenti, Landi Degl'Innocenti and Arena (1984), refined this technique of the non-linear least square technique using the Marquardt algorithm by including the magneto-optical effects. Inclusion of the magneto-optical effects as well as the damping parameter in their routine, called the ALL routine, which greatly helped in reproducing the theoretically generated profiles which they had used to test the routines. The ALL routines used a 6-parameter fit to their solution. apart from retaining those of the AHH.

In a recent development to this technique, *Skumanich and Lites* (1987), used only the Stokes Q, U and V profiles in their fit to compare the profiles. The reason for dropping the Stokes I profiles in their fit was that in any given observation, the I profiles is more likely to be contaminated by telescope parasitic light (the scattered light). Also since the I profile arises from both magnetic as well as non-magnetic elements, usage of the I profile would strongly influence the results in the non-linear least square fitting procedure. Since the Q, U and V polarisation profiles strictly arise from the

magnetic regions, these alone are considered. For the purpose of analysis one may treat both these effects -- the fraction of the I profile from non-magnetic regions as well as the fraction of I profile from parasitic light -- on the same footing, since they cannot be separated out. Skumanich and Lites made use of an 8-parameter fit to fit the observed profiles with that of the analytical solutions, namely, η_0 - the opacity ratio, $\Delta\lambda_D$ - Doppler width, H - Magnetic field strength, ψ - inclination of the magnetic vector, χ - azimuth of the magnetic field vector, α - damping constant, λ_0 - the line centre wavelength and μB_1 - the slope of the source function.

3. WHAT DOES THIS THESIS ATTEMPT TO DO ?

Since measurement of the Stokes polarisation profiles and the deduction of vector magnetic fields in solar active regions has been a primary goal in understanding the nature of the solar atmosphere, this thesis specifically attempts to devise a way to measure the Stokes profiles of Zeeman sensitive spectral lines. Using the Kodaikanal Solar Tower/Tunnel Telescope and Spectrograph, not originally meant for polarisation measurements, this detailed study is to exploit the feasibility of such telescopes to make the measurements, given its limitations. This study has evolved through several stages.

A detailed study of the instrumental polarisation of the Tower/Tunnel coelostat system and the limitations imposed by the instrumental polarisation, was made and a computer code for off-line corrections of the instrumental polarisation was first developed. This was followed by a choice of a reasonable Zeeman sensitive spectral lines that will be required to make the measurements. Next a polarimeter was designed and constructed to measure all four Stokes parameters based on the logistical and mechanical constraints imposed on the existing set-up.

Using the polarimeter in conjunction with the spectrograph, the Stokes spectra are recorded in form: I+Q, I-Q, I+V, I-V, I+U, I-U. The spectra are registered on a 35-mm spectroscopic emulsion, Kodak 103-aE, as density fluctuations, each frame covering a width of 50mm covering the spectral region between $\lambda\lambda$ 6299-6306 Å. An intervening lull in solar activity (an unusually long one too) because of the solar minimum (between the end of solar cycle no. 21 and the beginning of solar cycle no. 22), coupled with uncertain weather conditions at Kodaikanal, existed during the years 1983-1986. It was during this period that a prototype ellipsometer, was designed and developed, to measure the complex refractive indices of aluminised mirror surfaces - a vital ingredient in the knowledge of the instrumental polarisation due to the mirror reflections - as the reflectivity of the aluminised surfaces decreases with time. This aspect is mentioned in the appendix.

Observations and analysis of the measurement of the Stokes V profile asymmetries across a unipolar sunspot KKL No. 18213 was made on March 6, 1985 using the Fe I λ 6301.5 Å and Fe I λ 6302.5 Å spectral lines.

Daily observations of the Stokes profiles on three sunspots, KKL 18303 (NOAA 4810), KKL 18313 (NOAA 4811) and KKL 18315 (NOAA 4812) were made between the period of May 12-29, 1987. These photographic spectra have been converted to digital densities using a Photometric Data System Microdensitometer.

Using the spectroscopic reductions package RESPECT (*Prabhu, Anupama and Giridhar, 1987*) in conjunction with the VAX-11/780 Computer at the Vainu Bappu Observatory, IIA, Kavalur, a spectral reduction scheme was developed, to convert the digital densities of the spectrum to a useable form of intensities. The more agonising times have been due to the fixing of a proper continuum to the

spectrum. This was due to the presence of both parasitic light in the spectrum as well as the efficiency of the grating spectrograph for various relative orientations of the polaroid to the slit of the spectrograph.

The non-linear least square fitting technique using the Marquardt algorithm was first developed to compare the observed profiles with that of the Landolfi-Landi degl'Innocenti analytical solutions. The algorithms were based on the paper by Skumanich and Lites and have retained the eight parameters mentioned earlier. Several tests on this algorithm were made to check its efficiency on test fits, during which it was found that certain modifications of the algorithm as suggested by Fletcher (1971) were required. Use of Fletcher's algorithm to simultaneously fit the Stokes Q, U and V profiles certainly helped in a faster rate of convergence towards the solutions, but convergence rate decreased near the solutions. Thus only some of the modifications of the suggestion made by Fletcher were incorporated into the original algorithm. This proved to be of better use in reproducing the results. Repeated tests of the algorithm have been made on synthetic Stokes Q, U and V profiles, for various values of the B parameters before applying them to the actual measurements. In all these tests the synthetic profiles were perfectly reproduced and all the eight parameters perfectly retrieved.

Sunspots were chosen due to several reasons. They are strong magnetic field regions and hence a stable testing ground for the measurement of vector magnetic field. It was much easier to record Stokes profiles across sunspots than any other active region as the measurements were made during a minimum of the solar cycle and also sunspots were a good testing ground for the method. Observing time with favourable observing conditions like good seeing was restricted to a short period, not exceeding two hours on any day of observation. The photographic detection

technique was also a limitation on the sensitivity of detection. No on-line corrections for the instrumental polarisation was made.

The data was digitised using the PDS 1010M Microdensitomer, at IIA, Bangalore, and the spectral reductions were performed using the RESPECT package. Once the spectra were reduced, they were then added or subtracted to obtain the Stokes I, Q, U and V spectra. They were then corrected for the instrumental polarisation (which depended on the geometry of the telescope as well as on the coordinates from the Sun) based on the scheme mentioned earlier. The non-linear least square optimising technique was then used to fit the observed Stokes profiles with the profiles generated from the analytical solutions to derive vector magnetic and other physical parameters of the spectral line forming region.

4. A COMPARISON.

Where does this thesis stand compared to earlier attempts to make maps of the vector magnetic field? . As mentioned earlier, maps of the vector magnetic field are regularly being produced by only two observatories. The NASA MSFC and the Tokyo Astronomical Observatory. The present spectroscopic observations are of a better resolution than both of them, as it uses the entire spectral line profile in deriving the vector magnetic field. Hence the calibration of the magnetic field is better here. In terms of detection sensitivities, these observations are rather poor as instrumental polarisation is compensated off-line. Furthermore, photographic detection is an added disadvantage. However, in the methods of analysis, there lies an added advantage of using the non-linear least square fitting technique. Neither Kawakami (*ref. cit.*) nor the two vector magnetographs mentioned use this method and particularly

some of them ignore the magneto-optical effects. Again here, the vector magnetic field parameters as well as the physical parameters are determined simultaneously using the non-linear fitting technique in a 'single-shot'.

The MSFC magnetograph uses a KDP crystal in their polarimeter to chop the polarised signals. This introduces a large amount of cross-talk between the Stokes Q, U and V parameters. As a result, their method will be more suitable for measuring photospheric fields as well as sunspot penumbral field, but may not be very reliable for observing strong-field regions like sunspot umbrae as the cross-talk into the Q signal would proportionally increase with an increase in the V polarisation signal. The work mentioned in this thesis complements the MSFC system. As there is no KDP involved here, no cross-talk is introduced, hence strong fields can be safely measured. However, since signal-to-noise is poor because of no modulation, weak fields are not reliable here. It should also be noted that since the MSFC Magnetograph records the polarised filtergrams, a quick two dimensional vector magnetogram is produced, that makes morphological studies easily possible, whereas, since no 2-D imaging is used, discrete positions of the slit about various positions of the sunspot is necessary to get a two-dimensional picture of the vector magnetic field with our set up.

The experience gained out of these measurements will help in designing better vector magnetographs, including on-line corrections for the instrumental polarisation than the current off-line techniques, having solid state panoramic detectors for data acquisition, improved ways of handling the data and improving the reduction techniques and search for more efficient non-linear least square fitting techniques or optimisation techniques which can perform preferably better than the Marquardt algorithm.

CHAPTER II

INSTRUMENTATION

1. THE TOWER/TUNNEL TELESCOPE

The Kodaikanal Tower/Tunnel Telescope (*Bappu* 1967) is located at latitude $10^{\circ}14$ North and longitude $77^{\circ}5$ East. The three-mirror coelostat telescope system was manufactured by Grubb Parsons of U.K. and installed in 1959. The telescope essentially consists of a two-mirror, fused quartz 61cm diameter coelostat mounted on a 11-m tower, that vertically reflects down the light onto a third mirror, also made of fused quartz, which in turn reflects the beam horizontally onto a 60-m long underground tunnel. The parallel beam of light falls on to a 38-cm two-element achromatic objective of 36m focal length. This yields a 34-cm solar image that has a scale size of 5.5 seconds of arc per mm. The ray diagram showing the optical path is depicted in *Figure* II-1.1.

The primary coelostat, of equatorial mount tracks the Sun constantly in hour angle to feed the beam onto the secondary coelostat. This is achieved by a synchronous motor that is run by a crystal controlled frequency stabilised oscillator. The frequency of the oscillator can be tuned to vary the tracking rate (a function of the declination) during the course of the year. Apart from this, the primary coelostat moves on a North-South rail thereby enabling the light beam to completely fill the secondary coelostat. For every observational session, the primary coelostat is manually adjusted on these rails. Hence, the primary coelostat is made to execute a to-and-fro motion along these rails during the course of the year. A scale attached to the rails can read-off the position of the primary coelostat for each day of observation. The scale is accurate upto half a millimeter. During certain seasons of the year, when the elevation of

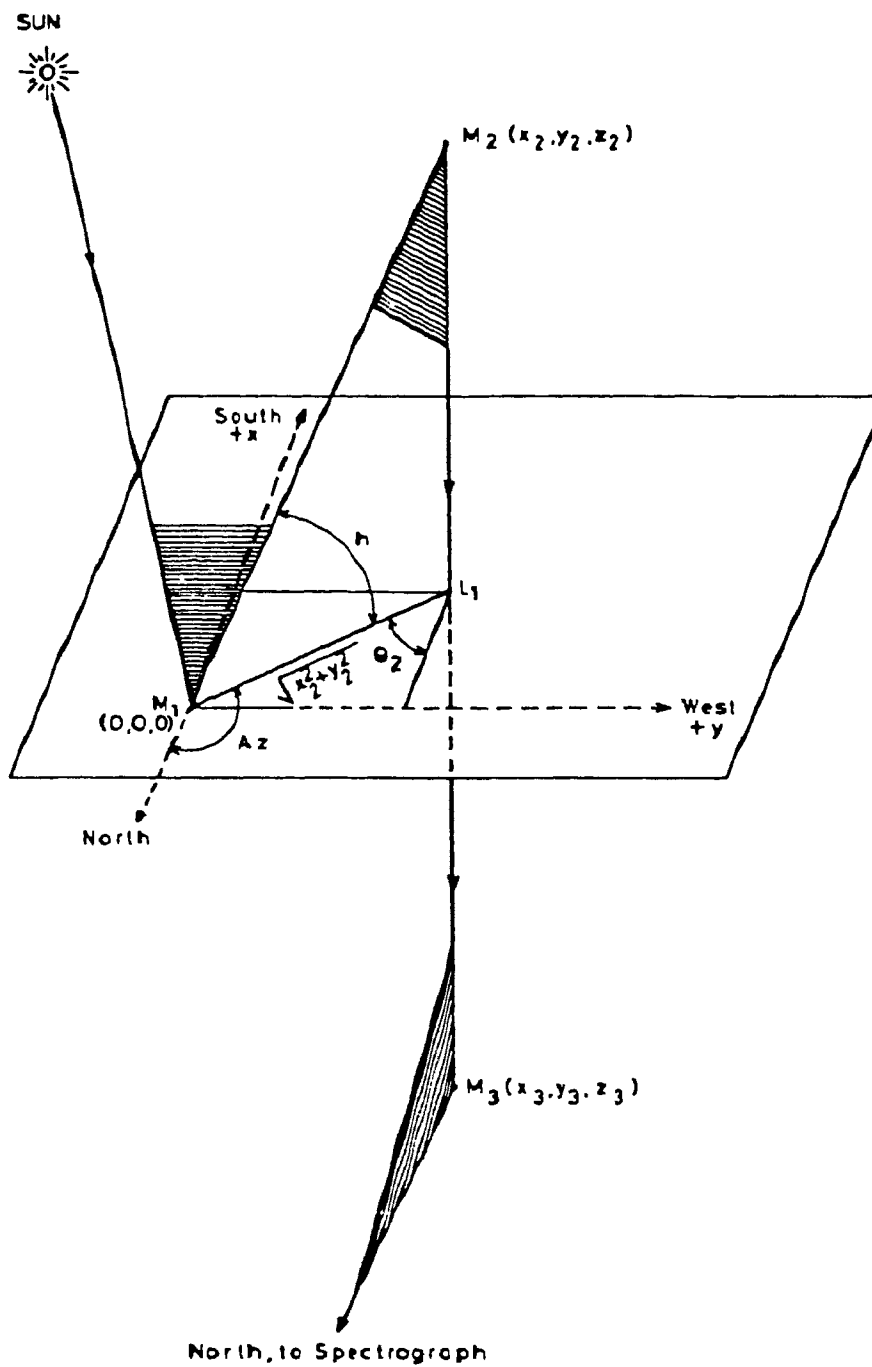


Fig.II-1.1 : Schematic representation of the 3-mirror system at Kodaikanal. M_1 , M_2 , and M_3 are the primary, secondary, and tertiary mirrors respectively. In practice y_2 and z_2 have fixed values of 83 cm and 74 cm respectively and x_2 changes with declination.

the Sun equals that of the secondary coelostat (as seen from the centre of the primary coelostat), a shadow of the secondary coelostat falls on the primary blocking its view of the Sun. To avoid this, the North-South rails on which the primary coelostat rests is in turn movable on an East-West rail system, to secure it in a symmetrically opposite position, East or West of the secondary coelostat.

2. THE SPECTROGRAPH AND CAMERA SYSTEM.

The spectrograph is a Littrow type spectrograph whose entrance slit is located at the image plane of the solar disc. The spectrograph is housed in a long cylindrical tube running along the length of the tunnel.

The light from the slit of the spectrograph falls on a 18.3-m focal length, two-element Hilger achromat, in conjunction with a 600 lines/mm Babcock grating, ruled over an area of 200 x 135 mm and blazed in the fifth order at $\lambda 5000 \text{ \AA}$. The theoretical resolving power of the spectrograph is 600,000. Tests by *Nirupama* (1965) using an iodine absorption source have shown that this theoretical resolving power is achieved in the observed spectrum.

Since this is a Littrow type spectrograph, the Hilger achromat itself acts as a camera lens to image the spectrum onto a plate holder or a film-transport system. A one-to-one correspondence exists between every point along the length of the slit and the length of the spectrum (in a direction perpendicular to the dispersion direction). A cross-wire, 200 microns thick, serves as a reference for identifying any point along the slit serving as fiducial mark. This fiducial mark along the dispersion direction also serves as an indicator of the exact dispersion direction. For the spectra reported in this thesis, the observations have been carried out in the $\lambda 6300 \text{ \AA}$ region, using the fourth order spectrum, which corresponds to a

resolution of 480,000 and a dispersion of 0.15 \AA mm^{-1} .

3. STOKES PARAMETERS

Consider an electromagnetic beam of wavelength λ propagating along the positive Z-direction. Its electrical variations along two orthogonal directions are given by (e.g. see Clarke and Grainger 1971).

$$\left. \begin{aligned} E_x &= E_{x0} \cos(\omega t - (2\pi z/\lambda) + \delta_x) \\ E_y &= E_{y0} \cos(\omega t - (2\pi z/\lambda) + \delta_y) \end{aligned} \right\} \quad \text{-- (II-3.1)}$$

From equation (II-3.1) E_x and E_y may be related to each other in the form

$$\frac{E_x^2}{E_{x0}^2} + \frac{E_y^2}{E_{y0}^2} - \frac{2 E_x E_y \cos(\delta_y - \delta_x)}{E_{x0} E_{y0}} = \sin^2(\delta_y - \delta_x) \quad \text{-- (II-3.2)}$$

which represents the equation of a polarisation ellipse (see *Figure* II-3.1). The four quantities E_{x0} , E_{y0} , δ_x and δ_y describe the polarisation ellipse. We require two more quantities, ζ - the orientation of the semi-major axis of the ellipse with respect to the x-axis (or the azimuth of the ellipse) and its helicity (or the handedness).

Since a lot of confusion has existed in the literature on the measurement of polarisation of Zeeman-broadened line profiles, the following sign convention is adopted. The helicity is right handed when the E-vector rotates clockwise as viewed from the positive z-direction, $\Pi > (\delta_y - \delta_x) > 0$, and the helicity is left-handed when the E-vector rotates in an anticlockwise sense, $0 > (\delta_y - \delta_x) > -\Pi$. Define η as the ratio of the semi-minor axis to the semi-major axis of the ellipse. We may then further define the azimuth of the ellipse as (see *Figure* II-3.1)

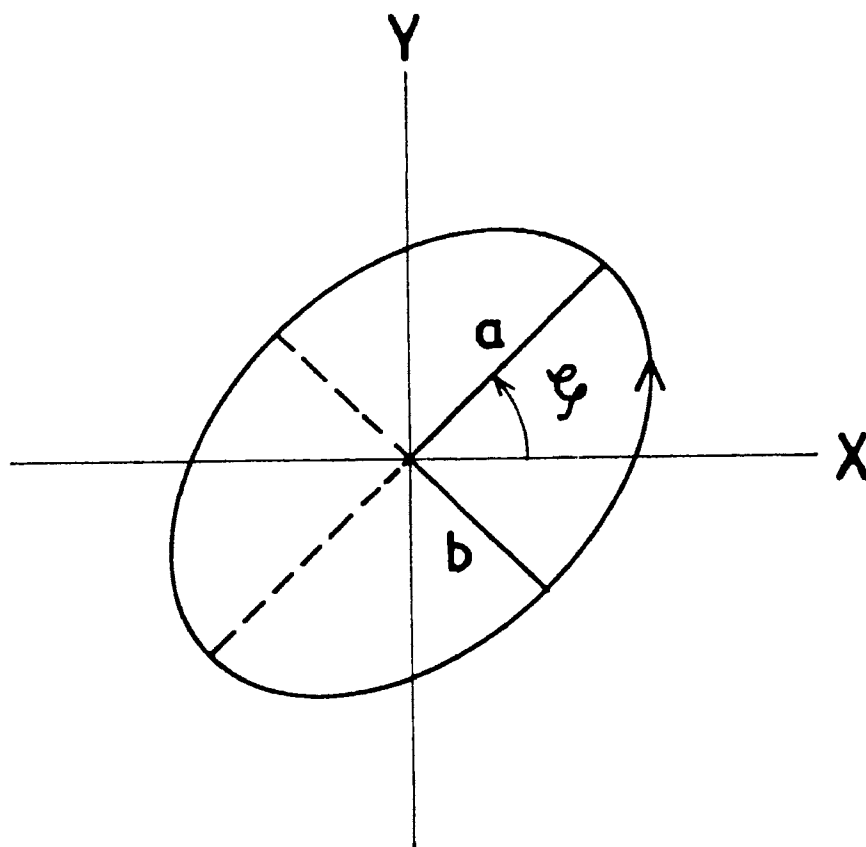


Fig.II-3.1 : The relation between the orthogonal electric vectors is represented in the form of an ellipse. The size of the ellipse is given by the semi-major axes 'a' and semi-minor axis 'b', while ξ represents the azimuth or orientation of the ellipse.

$$\tan(2\zeta) = \frac{2 E_x E_y \cos(\delta_y - \delta_x)}{E_{x0}^2 - E_{y0}^2} \quad \text{----(II-3.3)}$$

and the ellipticity as

$$\frac{2\eta}{1+\eta^2} = \frac{2 E_x E_y \cos(\delta_y - \delta_x)}{E_{x0}^2 + E_{y0}^2} \quad \text{----(II-3.4)}$$

We cannot directly observe the amplitudes and the phases of the E-vector. When light passes through appropriate optical devices, we can then measure the transmitted intensities.

The Stokes parameters evolve as a consequence of the relation between the observed polarised intensities of a beam of light and the polarisation ellipse. For a detailed description see *Clarke and Grainger* (1971) or *Rees* (1987). The Stokes parameters are defined as

$$\left. \begin{aligned} I &= \langle E_{x0}^2 \rangle + \langle E_{y0}^2 \rangle \\ Q &= \langle E_{x0}^2 \rangle - \langle E_{y0}^2 \rangle \\ U &= \langle 2 E_{x0} E_{y0} \cos(\delta_y - \delta_x) \rangle \\ V &= \langle 2 E_{x0} E_{y0} \sin(\delta_y - \delta_x) \rangle \end{aligned} \right\} \quad \text{----(II-3.5)}$$

where $\langle \rangle$ denotes the time average over the observation time interval which is $\gg \nu^{-1}$, the natural period of the wave. I represents the total intensity of the beam of light. Q represents the intensity difference measured along two orthogonal directions. The ratio U/Q would then determine the azimuth of ellipse and the sign of V would then determine the ^{helicity} ellipticity. If $(\delta_y - \delta_x) = \pi/2$ then V would be a perfect circular polarisation component. Hence the polarisation ellipse would be completely determined. One ambiguity, of course, remains: the orientation of the azimuth (the semimajor/semiminor axis) is ambiguous by

180° (see *Figure* II-3.1). We may now represent the intensity I of any beam of light as a sum of two components, of which one is the polarised part I_p and the other the unpolarised part I_u

$$I = I_p + I_u$$

$$I_p^2 = (Q^2 + U^2 + V^2)$$

4. MUELLER CALCULUS

Any optical component in the path of a light beam can be described by a 4X4 matrix, the Mueller matrix, which takes into account all forms of polarisation, retardation and extinction introduced by it.

If

$$[I] = (I, Q, U, V)^T$$

is the Stokes parameter of an incoming beam of light, then on passing through an optical component it transforms into the Stokes parameter

$$[I'] = (I', Q', U', V')^T$$

as

$$\begin{bmatrix} I' \\ Q' \\ U' \\ V' \end{bmatrix} = \begin{bmatrix} m_{11} & m_{12} & m_{13} & m_{14} \\ m_{21} & m_{22} & m_{23} & m_{24} \\ m_{31} & m_{32} & m_{33} & m_{34} \\ m_{41} & m_{42} & m_{43} & m_{44} \end{bmatrix} \begin{bmatrix} I \\ Q \\ U \\ V \end{bmatrix}$$

where m_{ij} represents the element of a Mueller matrix. This is the basic principle for the interaction of the polarised light with any optical medium.

5. THE INSTRUMENTAL POLARISATION OF THE COELOSTAT MIRRORS

Stokes profiles of Zeeman sensitive spectral lines are significantly distorted by reflecting mirrors. Physically this distortion can be understood in terms of the differential response of the electric vectors in and orthogonal to the plane of incidence respectively. Ideally, one must avoid several oblique reflections while measuring the polarisation of light. However, one cannot prevent this in existing installations not originally meant for polarisation measurements. For this reason, it is essential that the instrumental polarisation be determined precisely for all possible orientations of the telescope. This has been done by several groups (*Moe*, 1968; *Makita and Nishi*, 1970; *Livingston and Harvey*, 1971; *Bachman and Pflug*, 1983, *Bumba*, 1962) for their respective installations. A detailed description of the theoretical approach for estimating the instrumental response of the Kodaikanal Solar Tower to arbitrarily polarised light is presented here. The telescope reflection optics has been described in Section 1 of this chapter.

5.1 THE TELESCOPE GEOMETRY

Let us now consider a Cartesian coordinate system whose origin is the centre of the primary mirror (*Figure II-1.1*) i.e., $(0,0,0)$. The secondary mirror has the coordinates (X_2, Y_2, Z_2) and the tertiary mirror (X_3, Y_3, Z_3) . The coordinates are such that a positive Y -direction is towards the west, and a positive Z -direction is towards the zenith, all distances being reckoned from the centre of the primary mirror. As the primary mirror can be moved in the North-South direction in order to direct the sunlight on to the secondary for different declinations of the Sun, X_2 will change with a change in declination. When the primary mirror is secured to the West of the secondary, Y_2 becomes $-Y_2$. Thus Y_2 and Z_2 are fixed

quantities. The centre of the secondary mirror is fixed, but the mirror itself can be rotated about two axes to facilitate the diversion of the light beam vertically down to the tertiary mirror.

5.2 DERIVATION OF THE MUELLER MATRICES OF THE TELESCOPE

An incident Stokes vector $[I] = (I, Q, U, V)^T$ referred to coordinate system defined by the electric vector in and orthogonal to the plane of incidence on the primary mirror transforms to the observed Stokes vector

$$[I'] = (I', Q', U', V')^T$$

as

$$[I'] = [M_3] [R_2] [M_2] [R_1] [M_1] [I]$$

where $[M_1]$, $[M_2]$ and $[M_3]$ are the Mueller matrices of the primary, secondary and tertiary mirrors, $[R_1]$ and $[R_2]$ are the matrices describing the rotation of the planes of incidence between successive reflections. The output Stokes vector $[I']$ is analysed in a coordinate system where the plane of incidence of the third mirror coincides with the slit direction of the spectrograph. The Mueller matrix on reflection from a metallic surface is described by the Fresnel's equations (Kawakami, 1983)

$$[M] = 0.5 \begin{pmatrix} 1+X^2 & 1-X^2 & 0 & 0 \\ 1-X^2 & 1+X^2 & 0 & 0 \\ 0 & 0 & 2X \cos \tau & 2X \sin \tau \\ 0 & 0 & -2X \sin \tau & 2X \cos \tau \end{pmatrix} \quad \text{---(II-5.2.1)}$$

where X is ratio of the reflection coefficients of linearly polarised light perpendicular and parallel to the plane of incidence, and τ is the phase difference between reflected light polarised perpendicular and parallel to the plane of incidence (Makita and Nishi, 1970).

Here,

$$X^2 = \frac{a^2 + b^2 - 2a \sin i \tan i + \sin^2 i \tan^2 i}{a^2 + b^2 + 2a \sin i \tan i + \sin^2 i \tan^2 i} \quad \text{---(II-5.2.2)}$$

and

$$\tan \tau = \frac{2b \sin i \tan i}{\sin^2 i - (a^2 + b^2)} \quad \text{---(II-5.2.3)}$$

where

$$a^2 = 0.5 (n^2 - k^2 - \sin^2 i + \sqrt{(n^2 - k^2 - \sin^2 i)^2 + 4n^2 k^2}) \quad \text{---(II-5.2.4)}$$

and

$$b^2 = 0.5 (-n^2 + k^2 + \sin^2 i + \sqrt{(n^2 - k^2 - \sin^2 i)^2 + 4n^2 k^2}) \quad \text{---(II-5.2.5)}$$

i being the angle of incidence; n and k are the real and imaginary parts of the complex refractive index, respectively. The rotation matrix is given by

$$[R(\theta)] = \begin{bmatrix} 1 & 0 & 0 & 0 \\ 0 & \cos 2\theta & \sin 2\theta & 0 \\ 0 & \sin 2\theta & \cos 2\theta & 0 \\ 0 & 0 & 0 & 1 \end{bmatrix} \quad \text{---(II-5.2.6)}$$

where θ is the angle of rotation of the planes of incidence.

5.3 DETERMINATION OF THE ANGLES OF INCIDENCE.

The first step in determining the Mueller matrix of each reflection is to determine the angles of incidence. This is done in the following way: In spherical coordinates, let the origin be the centre of the primary mirror. The secondary mirror will then have coordinates,

$$\left. \begin{aligned} X_2 &= -d_1 \cosh \cos A_z \\ Y_2 &= d_1 \cosh \sin A_z \\ Z_2 &= d_1 \sin A_z \end{aligned} \right\} \quad \text{---(II-5.3.1)}$$

where h is the altitude, A_z is the azimuth of the secondary mirror as viewed from the origin and

$$d_1 = \sqrt{(x_2^2 + y_2^2 + z_2^2)}$$

is the distance from the centre of the primary to the secondary. The azimuth is positive when recorded from North to West.

Consider now the celestial sphere with origin at the centre of the primary mirror. Let the Sun have coordinates h_o and A_{zo} as its altitude and azimuth, respectively. Let t and δ be the hour angle of the Sun. The primary mirror is mounted equatorially and the normal to the primary mirror always points at the equator. Let the hour angle of the normal to the primary mirror be T . If ϕ is the latitude of the place, then from the spherical triangle PZM_2 (Figure II-5.3.1) we can write

$$\sin \delta = \sin \phi \sin h + \cos \phi \cos h \cos A_{zo} \quad \text{---(II-5.3.2)}$$

Substituting equation (II-5.3.2) in equation (II-5.3.1), we get

$$\sin \delta = \frac{x_2}{d_1} \cos \phi - \frac{z_2}{d_1} \sin \phi \quad \text{----(II-5.3.3)}$$

For a given declination of the Sun, the value of x_2 is unique so that the light from the primary is always reflected on to the secondary. One can solve for x_2 from equation (II-5.3.3) as

$$x_2 = R_2 \tan \beta \quad \text{----(II-5.3.4)}$$

where

$$\beta = A + \sin^{-1} ((\sin \delta) / B)$$

$$A = \tan^{-1} ((z_2 / R_2) \tan \phi)$$

$$B = (\cos^2 \phi + (z_2 / R_2)^2 \sin^2 \phi)$$

$$R_2 = \sqrt{(y_2^2 + z_2^2)}$$

Hence knowing the value of δ for the Sun at any given moment, we can adjust the position of the primary mirror. The maximum rate of change of declination is 24 arc-second day⁻¹ at $\delta = 0$ and the minimum rate of change of declination is zero at $\delta = \pm 23.5^\circ$. As a result the maximal positional error of X_2 in terms of declination, if the mirror is adjusted every one hour of observation, will be approximately one arc-second.

To determine the angles of incidence of the first mirror, consider the spherical triangle PZM_2 (Figure II-5.3.1). Knowing that

$$\begin{aligned} PZM_2 &= A_2 \\ PM_2 &= PG + GM_2 = 90 + \delta, \\ ZPM_2 &= (2T - t), \\ ZM_2 &= (90 - \lambda) \end{aligned}$$

we can apply the sine formula to obtain

$$\frac{\sin PZM_2}{\sin PM_2} = \frac{\sin ZPM_2}{\sin ZM_2},$$

or

$$\cos \lambda \sin A_2 = \cos \delta \sin(2T - t) \quad \text{----(II-5.3.5)}$$

Now consider the spherical triangle PSN. Here $PN = 90^\circ$, hence from the cosine formula (Smart, 1979)

$$\cos i_1 = \cos \delta \cos(T - t) \quad \text{----(II-5.3.6)}$$

Equations (II-5.3.5) and (II-5.3.6) can be used to determine i_1 (the angle of incidence of the light beam w.r.t the primary mirror) using the known values of λ and A_2 . To determine the angle of incidence of the secondary mirror (Figure II-1.1), consider the triangle defined by the centre of the primary mirror (M_1), the centre of the secondary mirror (M_2) and the point of intersection of the (X_2, Y_2) plane and the line joining the secondary and the tertiary mirrors, i.e., L_1 . The required angle of incidence

i_2 is half the angle $M_1M_2L_1$. Thus,

$$i_2 = 0.5 \tan^{-1} \left[\frac{M_1L_1}{M_2L_1} \right]$$

$$i_2 = 0.5 \tan^{-1} \left[\frac{\sqrt{x_2^2 + y_2^2}}{z_2} \right]$$

Since the third mirror merely reflects the beam from the secondary mirror into the horizontal direction towards its north (defined by the line joining the centre of the tertiary mirror and the centre of the slit of the spectograph), the angle of incidence i_3 is always 45° .

5.4 DETERMINATION OF THE ANGLES OF ROTATION

Since the rotation matrix $R(\theta)$ involves the terms $\cos 2\theta$ and $\sin 2\theta$ it is sufficient to determine the acute angles between the planes of incidence. However, the sense of rotation, namely, clockwise or anticlockwise, must be determined in each case with the convention that an anticlockwise rotation is positive when the light beam common to the planes of incidence is towards the observer. We will now proceed to determine the magnitudes and sign of the angles θ_1 and θ_2 .

a) The magnitude of θ_1

The magnitude of the angle θ_1 is the angle made by the plane containing the Sun (S), the primary mirror (M_1), the secondary mirror (M_2) with the plane containing the primary mirror (M_1), the secondary mirror (M_2) and the zenith (Z) (also refer *Figure II-5.3.1*). We are interested in the angle ZM_2S .

Here

$$ZM_2 = (90-h), \quad SM_2 = 2 i_1 \text{ and } ZS = (90-h_0).$$

Thus from the cosine formula we have

$$\cos(90-\lambda_0) = \cos(2i_1) \cos(90-\lambda) + \sin(2i_1) \sin(90-\lambda) \cos\theta_1$$

and hence

$$\cos(\theta_1) = \frac{\sin\lambda_0 - \cos(2i_1)\sin\lambda}{\sin(2i_1) \cos\lambda}$$

where the altitude of the Sun is given by (Smart, 1979)

$$\sin\lambda_0 = \sin\phi \sin\delta + \cos\phi \cos\delta \cos t$$

Table II-1 shows the sign of θ_1 obtained from geometrical considerations (Figure II-1.1).

b) The magnitude of θ_2

To determine the magnitude of θ_2 consider Figure II-1.1. It is immediately seen that $\tan\theta_2 = (|y_2|)/(|x_2|)$. The sign of θ_2 can be seen in Table II-2. The angle θ_1 varies on a shorter time-scale which is the function of the hour angle of the Sun whereas θ_2 varies on a longer time-scale which is a function of the declination.

6. ESTIMATION OF INSTRUMENTAL POLARISATION

In order to estimate the total effects of instrumental polarisation of the coelostat mirrors, we simulated the actual conditions for five declinations -23° , -13° , -3° , $+7^\circ$, and $+17^\circ$; for each fixed declination, running the hour angles from -90° to $+90^\circ$. The Mueller matrices due to each reflection was calculated assuming $n = 1.13$ and $k = 6.39$ valid at $\lambda 6300 \text{ \AA}$. This is

Table II-1
Sign convention for angle θ_1

	- x_2	+ x_2
- y_2	anticlock wise (+)	clock wise (-)
+ y_2	anticlock wise (-)	clock wise (+)

Table II-2
Sign convention for angle θ_2

	- x_2	+ x_2
- y_2	clock wise (+)	anticlock wise (-)
+ y_2	clock wise (-)	anticlock wise (+)

a good approximation according to *Makita and Nishi* (1970). We however plan to experimentally check the validity of this approximation. The Mueller matrices and the rotation matrices were combined to form a single Mueller matrix.

The Mueller matrix elements a_{ij} are shown as a function of hour angle and declination for various declinations (*Figures II-6.1a to II-6.1h*). The data for the Stokes parameters representing the following five forms was the input in our calculations: (a) unpolarised, (b) linearly polarised along the plane of incidence at the first mirror, (c) linearly polarised orthogonal to the plane of incidence at the first mirror, (d) right circularly polarised, and (e) left circularly polarised.

The output Stokes parameters was determined again as a function of hour angle for each of the five declinations. The following quantities were determined in each case from the output Stokes parameters (*Clarke and Grainger, 1971*):

(i) percentage polarisation

$$p = \frac{\sqrt{(Q'^2 + U' + V')}}{I'}$$

(ii) azimuth of the polarisation ellipse

$$\zeta = 0.5 \tan^{-1} (U'/Q')$$

(iii) ratio of the semi-major axis to the semi-minor axis of the polarisation ellipse, $b/a = \eta$, where

$$\frac{2\eta}{1+\eta} = \frac{|V'|}{I'}$$

The percentage of polarisation and η produced from unpolarised light is shown in *Figure II-6.2a*, while *Figure II-6.2b* shows η corresponding to the four polarised forms of

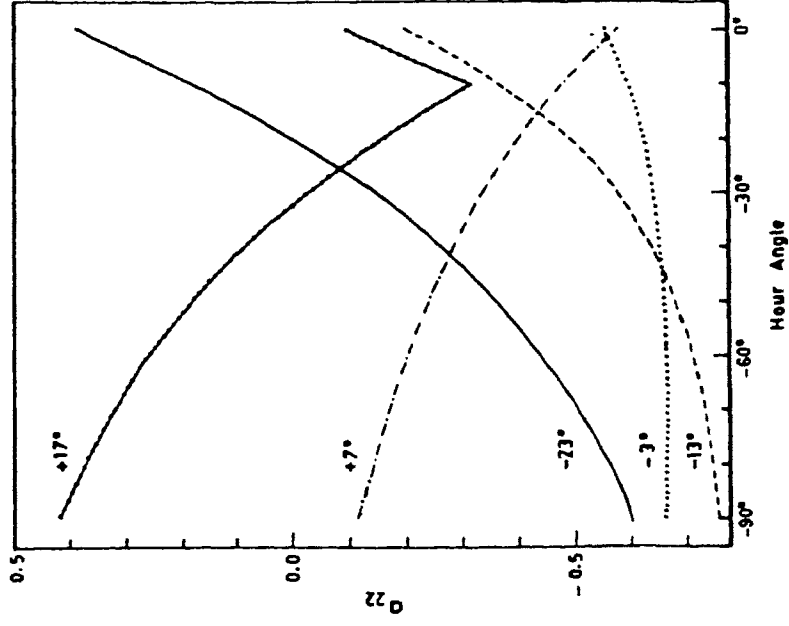


Fig. II-6.1b: Shows a_{22} as a function of hour angle. These curves are also symmetrical about 0° .

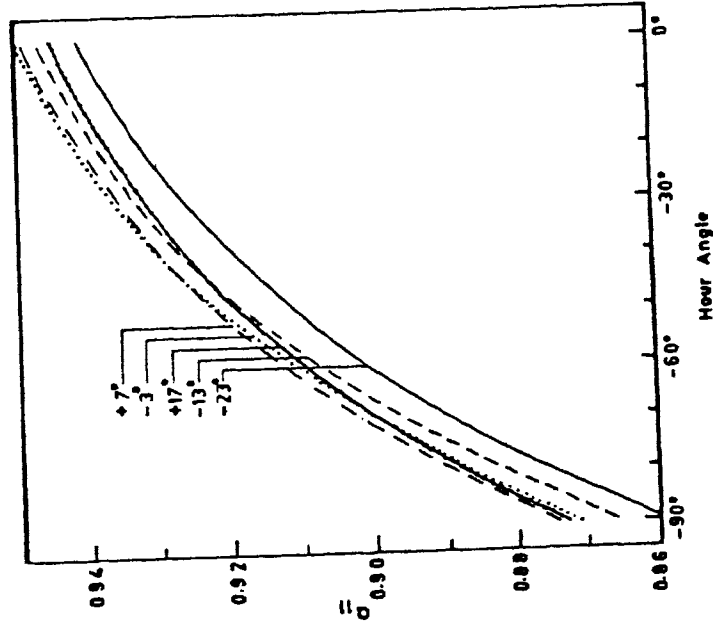


Fig. II-6.1a: Depicts a_{11} as a function of hour angle for various values of the declination (marked in the figure). Only one half of the day is shown since the curves are symmetrical about 0° .

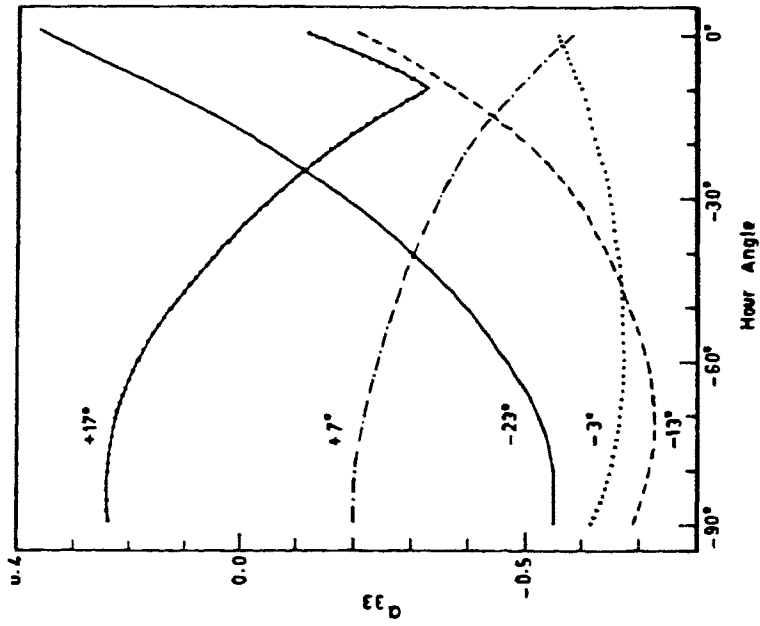


Fig.II-6.1c: Shows a_{33} as a function of hour angle. These curves are also symmetrical about 0° .

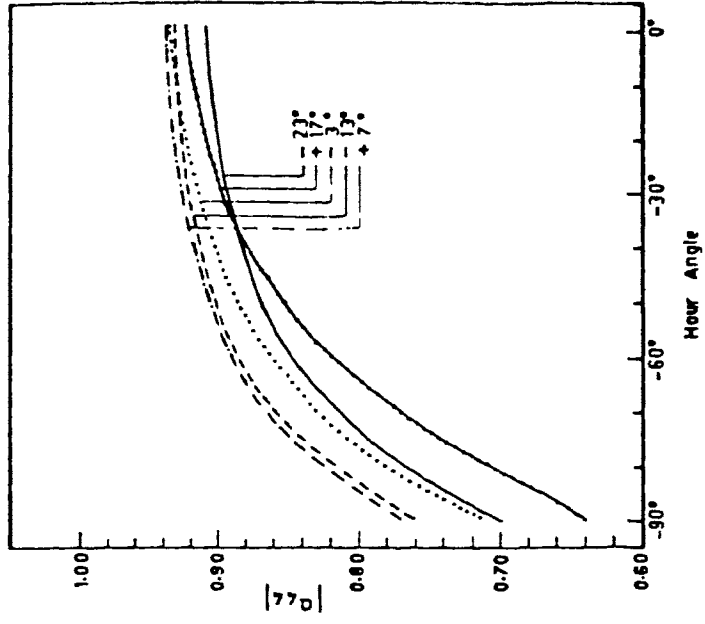


Fig.II-6.1d: Diagonal elements of the composite Mueller matrix.

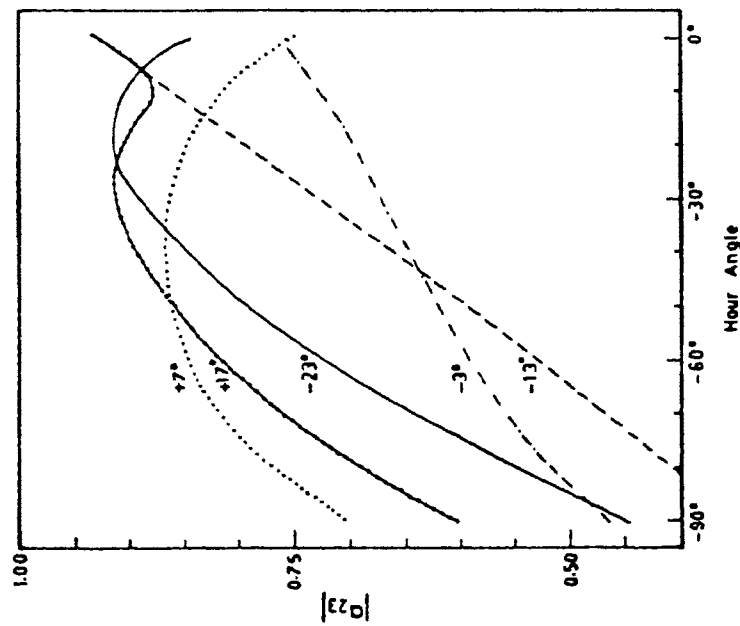


Fig. II-6.1e: a_{23} is antisymmetric about 0° and is positive for negative hour angles for declinations of -23° and -13° . It assumes opposite sign for declinations of -3° , $+7^\circ$, and $+17^\circ$.

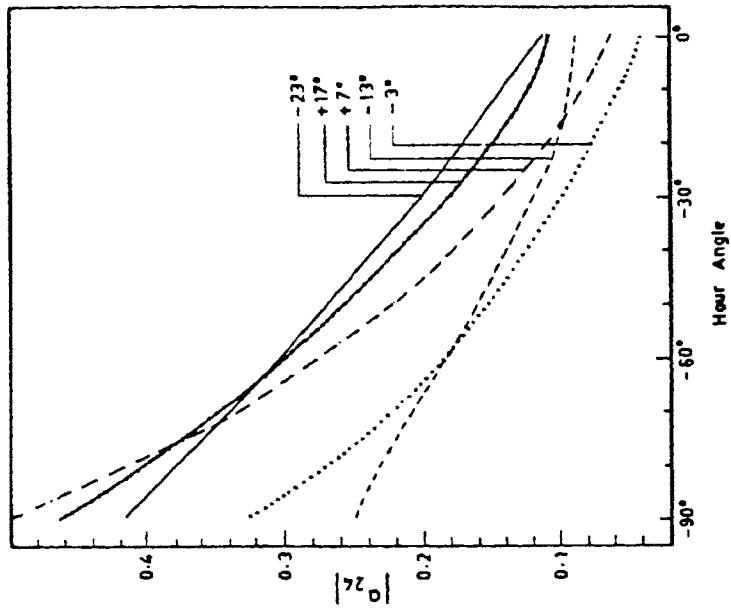


Fig. II-6.1f: a_{24} is also antisymmetric about 0° hour angle and takes on negative values for declinations of -23° and -13° . It assumes positive values for all other cases.

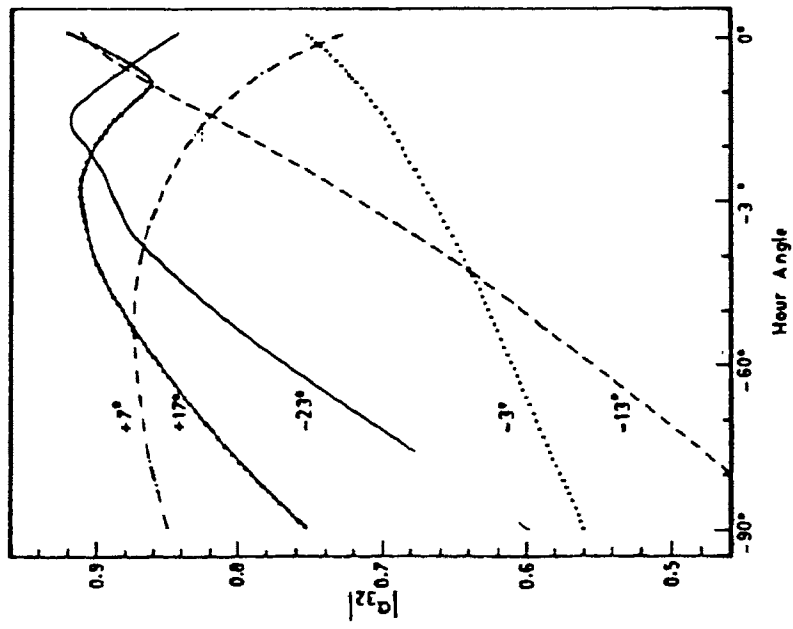


Fig. II-6.16: a_{32} has the same symmetry properties as a_{24} .

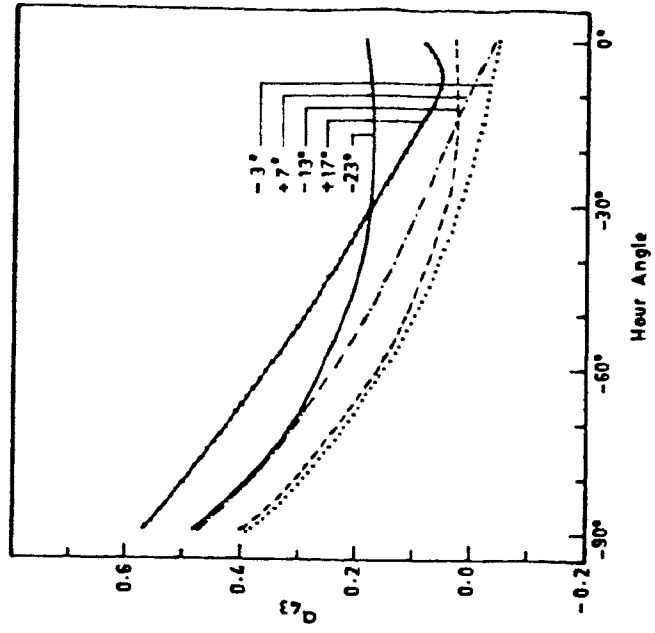


Fig. II-6.1h: a_{43} is symmetric about 0° hour angle.

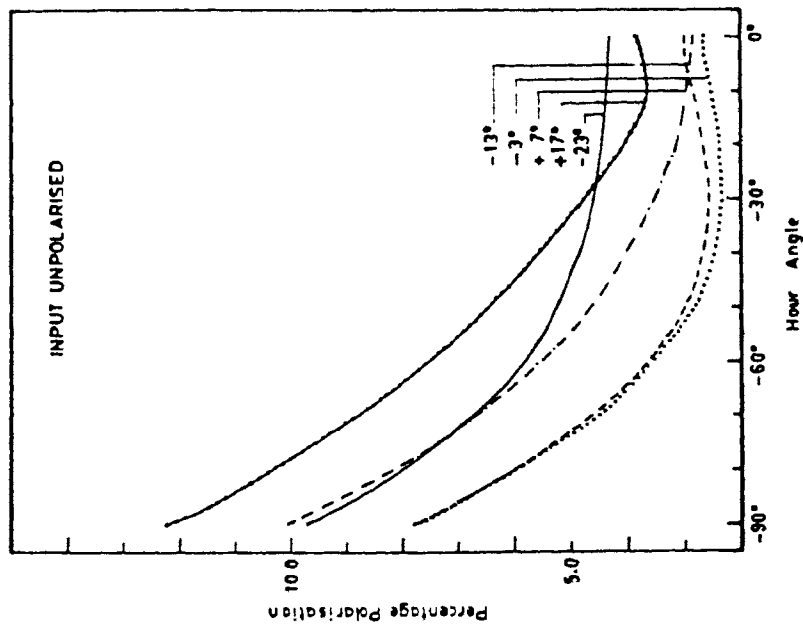


Fig. II-6.2a: Percentage of total polarisation produced by the mirrors as a function of hour angle for various declinations of the sun. The input beam is unpolarised.

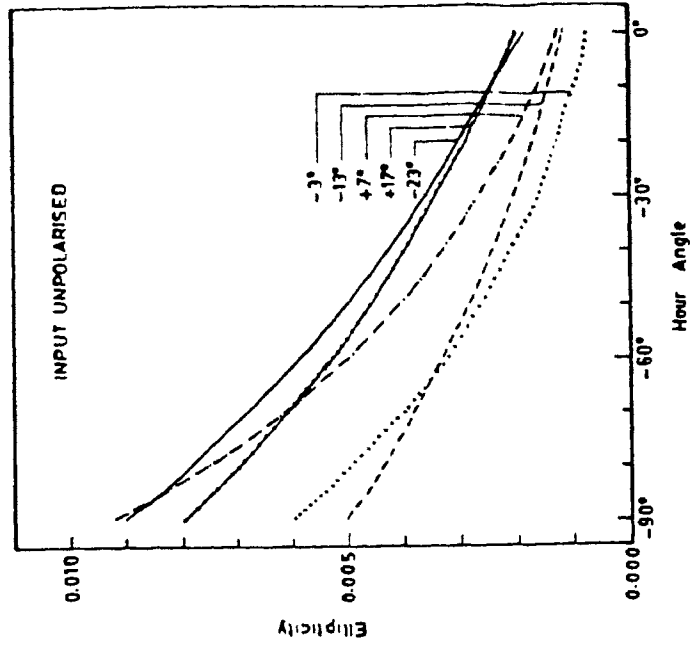


Fig. II-6.2b: The ellipticity of the polarised component of light produced by reflection of unpolarised light in the three-mirror system.

the input Stokes vectors.

7. IMPLICATION OF THE INSTRUMENTAL POLARISATION FOR ACTUAL OBSERVATIONS

Let us first look at the results for the variation of the elements of the composite Mueller matrix. The element a_{11} represents the scattering of I into I and thus is a measure of the partially polarising property of the system. It is seen that for all declinations, a_{11} is nearly unity thereby showing that not much partial polarisation is produced. The elements a_{12} , a_{13} and a_{14} represent the scattering of Q, U and V into I and are thus a measure of the depolarisation produced. These elements have a very small magnitude ($\approx 1\%$). Moreover in the measurement of the Stokes profiles of Zeeman sensitive lines, the Q, U and V would in general be very small thus reducing the contamination of I still further. The only context where these might assume some importance is the bisectors of the Zeeman sensitive line profiles.

The elements a_{21} , a_{31} and a_{41} are more serious as they represent the contamination of Q, U and V signals respectively, from the I profile. However, these elements also remain very small ($\approx 1\%$) and will pose no numerical problem while inverting the composite Mueller matrix for off-line compensation.

The diagonal elements a_{22} , a_{33} and a_{44} represent the sensitivity of the system to pick up the Q, U and V signals. Unfortunately, a_{22} and a_{33} are not very large and consequently require some care during the matrix inversion for off-line compensation. The element a_{44} is $\geq 80\%$ and thus the V measurements will be less prone to error.

The element a_{24} is particularly important for the measurement of the transverse component of the magnetic

fields which is inclined to a small angle to the line of sight. In this case V would be very much larger than Q and a_{24} would further contaminate the Q signal. Other off-diagonal elements that are significantly larger than zero are a_{23} , a_{32} and a_{43} . All the coefficients describing the cross talk are very serious and have to be carefully considered for a successful compensation.

Next let us consider the results of the percentage polarisation produced from natural light (randomly polarised). This is large ($\approx 12\%$) when the Sun is just rising but quickly drops to about 2% at hour angles of approximately -30° in spring and autumn. This value of about 2% is not a great impediment for the measurement of moderate field strengths. For weaker fields it would be necessary to introduce some on-line compensation. For purely polarised light it was seen that the percentage polarisation remained at 100% thereby indicating that no depolarisation was produced in the system.

However, linearly polarised light is converted to slightly elliptically polarised light as seen from the value of η plotted in *Figure* II-7.1 (≤ 0.1). Circularly polarised light is affected the same way whether it is right circular or left circular polarised (*Figure* II-7.2) and thus shows that no compensation is necessary if the system is used to feed a longitudinal magnetograph.

It is seen that the most favourable conditions for the measurement of polarisation of sunlight using the Kodaikanal Solar Tower Telescope are available between hour angles of -60° to $+60^\circ$ and during the seasons of small declinations. However, for any observing period, the off-line compensation requires careful consideration of the possible errors, in particular for the determination of the Stokes Q and U parameters.

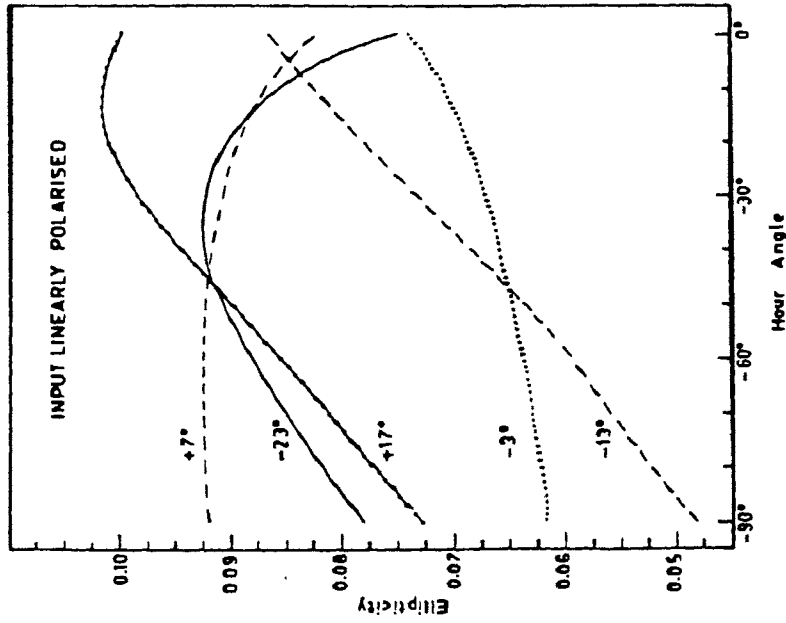


Fig. II-7.1: Ellipticity of the polarised light produced by reflection of linearly polarised light. The results for its orthogonally polarised component are very nearly the same and are not shown separately.

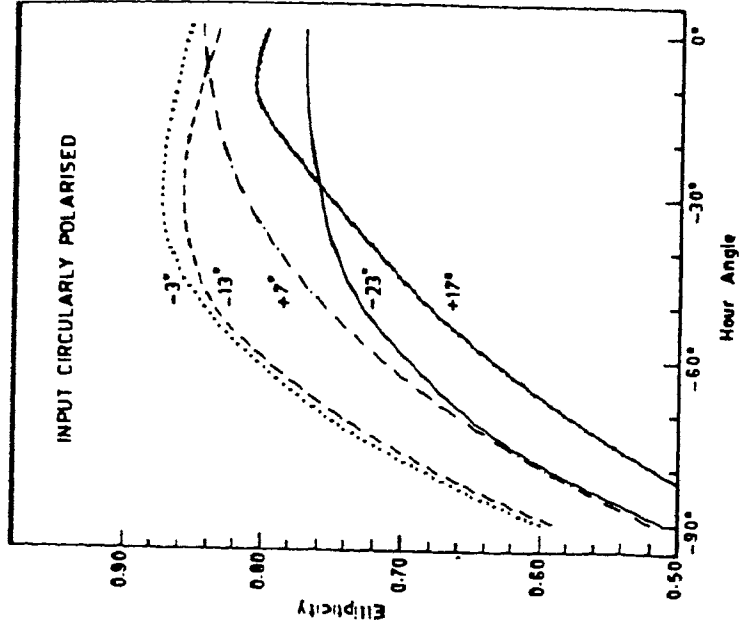


Fig. II-7.2: Ellipticity produced by reflection of circularly polarised light. The two orthogonal components show similar behaviour and, therefore, are not shown separately.

8. EXPERIMENTAL VERIFICATION OF THE ACCURACY OF THE POSITIONING OF THE COELOSTAT SYSTEM AND ITS COMPARISON WITH THE FORMUALE DERIVED IN SECTION II-5.3

To experimentally check our basic assumptions on the theoretical deductions of the telescope geometry and the existing pointing of the telescope, we made regular measurements of the positioning of the primary coelostat mirror throughout the year 1985. The measurements were based on the existing scale on the North-South guide rail that is used to position the primary mirror as the Sun moves in declination. The positioning in hour angle is achieved by rotating the primary coelostat about its axis, parallel to the Earth's equator. Positioning the primary coelostat (whose centre is the origin of the moving coordinates), changes the relative coordinates of the secondary, X_2 , (a function of hour angle and declination), while Y_2 and Z_2 are always kept fixed. Physically it is the primary coelostat that is made to move as a function of X_2 . The existing scale to read off X_2 is accurate within 0.5 mm. As the positioning of the primary coelostat was the main task, it did not matter whether the seeing conditions were good or not, as long as a discernable image of the Sun was placed at the image plane, with the centre of the image positioned at the centre of the slit. These measurements of the primary coelostat during a particular day and fraction thereof are plotted in *Figure II-8.1* with the points marked by a '+' sign. The declinations for each point in the figure for the moment of observation were calculated using a Chebychev polynomial expansion, whose coefficients are given in the *Almanac for Computers*, 1985. The relative position of the primary coelostat, X_2 was then reworked out using these declinations fitted into equation II-5.3.4. The points so derived are plotted in the same figure marked by the '*' sign. Notice that the measured and the calculated curves are anti-symmetric with each other. To match the two curves and bring them to the calculated scale (theory), it was necessary to invert the postional information in the

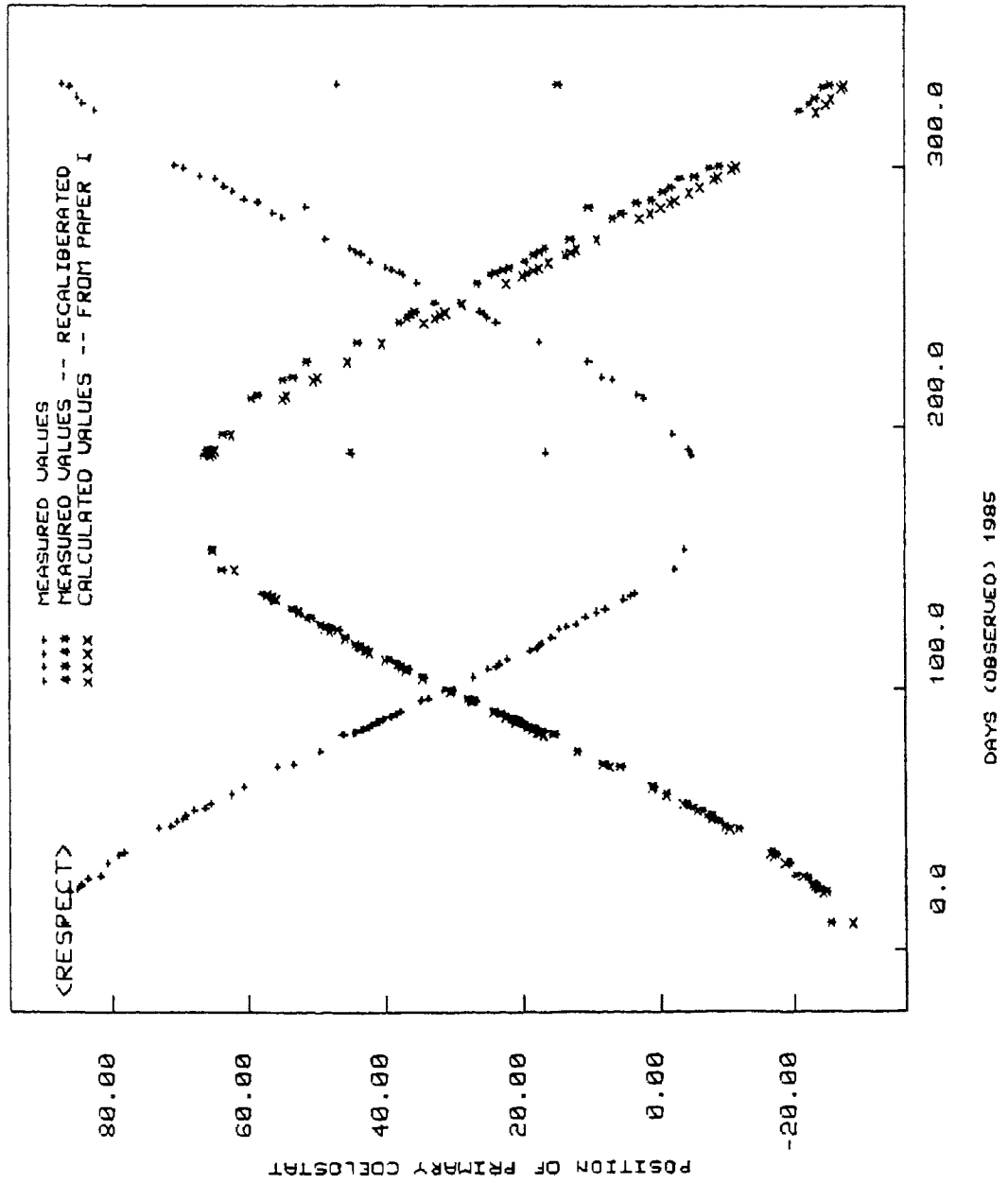


Fig.II-8.1 : Comparison of measured values of the position of the primary coelostat with those calculated from the formula II-5.3.1. The '+' represent measured values while 'x' represent the calculated values. The '*' represent recalibrated values after subtracting the '+' values from 60.

data by multiplying it by a factor of -1 and then adding to it a constant ($= 60$). The matched curves are also shown in the same figure marked by an 'x' sign. Notice that the curves do not match very accurately, on either side of the maximum. To ascertain the cause of these differences, we analytically calculated the gradient of X_2 with respect to each of Y_2 and Z_2 defined by equation II-5.3.4 and compared them with the differences (not shown here). This pointed out the possibility that the plane defined by the rails on which the primary coelostat rests, (the plane defined by the normal to the zenith) may possibly be slightly tilted and hence the measured values of Z_2 and Y_2 may be slightly off from true value. The values of X_2 themselves cannot lead to this discrepancy as we have noticed that even slight departures of the positioning of the primary coelostat on the north-south rail will show up as significant departures and that the light beam will not symmetrically fill the secondary mirror (stray points in the *Figure II-8.1*)

9. SPECTROSCOPIC PRINCIPLES

9.1 THE ZEEMAN EFFECT

Consider an atom radiating in a uniform magnetic field of strength H Gauss. The spectral line under the influence of the magnetic field is split into several components. Using the simplest pattern of a normal triplet, derived from the spectral line of a singlet series, and viewing along the direction of the magnetic field, we see two circularly polarised σ - components symmetrically placed at a wavelength separation of $\Delta\lambda_{\sigma}$ about the missing spectral line centre, λ_0 . The $-\Delta\lambda_{\sigma}$ component is right circularly polarised and the $+\Delta\lambda_{\sigma}$ component is left circularly polarised. Viewing about a direction perpendicular to the magnetic field, we see three linearly polarised components - one about the position of the undisturbed spectral line centre

(Π -component) whose polarisation sense is along the direction of the magnetic field and two symmetrically placed σ - components separated by $\Delta\lambda_{\text{H}}$ from the spectral line centre, whose polarisation sense is perpendicular to the magnetic field. The Zeeman splitting, in Angstroms is given by

$$\Delta\lambda_{\text{H}} = (e/4\pi m_e c^2) \lambda_0 g H = 4.67 \times 10^{-13} \lambda_0 g H \quad \text{--II-9.1.1}$$

where e is the electronic charge in e.s.u., m_e is the mass of the electron and c is the velocity of light. The Zeeman splitting is determined by the Lande' g factor. Under the assumptions of Russel-Saunders coupling (*Condon and Shortley 1935*),

$$g = 1 + [J(J+1) - L(L+1) + S(S+1)] / [2J(J+1)]$$

where L, S and J are the quantum numbers of the atomic states involved in the transition.

Fraunhofer lines are formed in the solar atmosphere under absorption, resulting in the inverse Zeeman effect, where the polarisation sense is reversed. This implies that the azimuth, of the observed polarisation in the spectral line wing is the same as that of the magnetic field.

The Zeeman components are not fully split but merely broaden the spectral line because the spectral lines are considerably broadened due to thermal motions. However, a wavelength dependent polarisation is present along the line profile. It is this wavelength dependent polarisation that is exploited in the measurements of the Stokes polarisation profiles to derive various properties of the magnetised medium in the solar atmosphere.

9.2 CHOICE OF THE SPECTRAL LINES

The choice of the Zeeman sensitive spectral lines for the measurement of the vector magnetic field, depends on several factors. A search in the solar spectrum was made,

to identify spectral lines that have the following criteria:

(i) spectral lines that can be located at longer wavelengths, since the Zeeman broadening is proportional to the square of the wavelength.

(ii) spectral lines that are not very far separated in wavelength, so that they can be observed simultaneously, given the limitations of the camera setting of the spectrograph.

(iii) spectral lines that have a sufficiently large value of the Lande' g factor so that the Zeeman splitting can be perceptibly measured.

(iv) spectral lines that are photospheric in origin - where the magnetic fields are very strong.

(v) spectral lines being preferably uncontaminated by blends, either of solar or terrestrial origin.

(vi) spectral lines that are not sensitive to changes in the temperature as one moves from the photosphere to the penumbra of a sunspot or to the umbra of a sunspot. Although the λ 5250 Å spectral line is widely used in magnetograph observations (due to its large value of the Lande' g factor), it is rather temperature sensitive (Stenflo 1971).

(vii) spectral lines that are well flanked by telluric spectral lines which are wavelength stable, thus affording a proper wavelength calibration.

(viii) spectral lines that are largely formed under pure absorption, where the scattering process in the spectral line formation does not become important. (see discussion by Stenflo 1971)

This search resulted in choice of the spectral region between $\lambda\lambda$ 6299-6306 Å which includes the spectral line pair Fe I λ 6301.5 Å ($g = 1.5$) and Fe I λ 6302.5 Å ($g = 2.5$). Both these spectral lines arise from the same multiplet, i.e., from the same physical conditions of the solar atmosphere but differing only in their values of the Lande' g factor. It may be noted that the FeI 6302.5

spectral line gives a normal Zeeman effect pattern giving rise to three components, whereas the FeI 6301.5 line behaves in the anomalous way. The telluric lines flanking these spectral lines have been well calibrated for their wavelengths using a Fabry-Perot spectrometer (Caccin *et al.* 1985) and have been found to be wavelength stable to an accuracy of 5 ms^{-1} . The spectral lines used in the wavelength calibration are $\lambda\lambda$ 6299.228, 6302.000, 6302.762 and 6305.810 Å) Table-III-2 of Chapter III gives the details of the spectral region that is observed.

10 THE POLARIMETER

Ideally the polarimeter used to measure polarisation content should be located just before the detector, assuming that the signal is not distorted by the instrumental polarisation generated by either the telescope optics or by the grating spectrograph. Unfortunately both of them do introduce a considerable amount of instrumental polarisation. One cannot avoid the coelostat system polarisation, here, by placing the polarisation-analysers at the entrance to the primary coelostat as the size of the optical components involved in the construction of the polarimeter would be too large. The grating spectrograph also introduces a considerable amount of instrumental polarisation (see e.g. Breckinridge, 1970, 1972; Hutley, 1982). We only know the response and sensitivity of grating spectrographs to linearly polarised light, as experimentally determined. The theory of grating and grating spectrographs are only in a scalar form and no vector electromagnetic theory is so far available to understand their behaviour. Hence efforts to understand the Mueller matrix of a grating spectrograph will prove to be difficult. These considerations have gone into locating the polarimeter just ahead of the slit of the spectrograph, before the light enters into it. The polarimeter housing is about 15cms ahead of the image-plane, the image plane coinciding

with the spectrograph slit. Since the focal ratio of the objective is F/96, (38-cm objective) it has a very large depth-of-focus. Hence any minor defocussing due to the polarimetric optics can be readjusted by repositioning the imaging objective. With such a large focal-ratio we are well within the acceptance angle constraints posed by polarisers as well as quater-wave plates.

A polarimeter has been designed and constructed for use at the existing spectrograph. Equal absorption through various components of the polarimeter (*J. H. Stone, 1963*), in recording all the polarisation profiles, has been a major consideration in the design. The polarisation analyser consists of a quartz quarter-wave plate (at λ 6302 Å) followed by a polaroid. The entire system is mounted atop a 1/2-cm thick brass plate. The quarter-wave plate and the polaroid can be independently turned by a mechanical wheel arrangement about an axis perpendicular to the direction of the incoming beam. The system is hooked on to the slit assembly during the polarimetric observations. A Hilger DG-1 filter isolates the red portion of the sunlight entering the slit. This is also located ahead of the quater-wave plate, within the polarimetric assembly. Attempts at using a narrow-band birefringent filter, centered at λ 6302 Å with a band-pass of 10 Å at FWHM, specially ordered for this purpose, failed as the filter itself developed non-uniformities when exposed to the light beam.

It may be worthwhile mentioning that an experimental arrangement was configured in the laboratory to measure the actual phase-difference introduced by the λ 6302 Å quarter-wave plate. A GDM 1000 double-pass monochromator, served as the reference source at the test wavelength - λ 6302 Å. The standard procedure of using a Babinet compensator in conjunction with two polaroids was employed to measure the phase difference introduced by the said phase plate and was found be $\pi/2$ within the accuracy of

the measurement itself.

The composite Mueller matrix of the polarimeter can be written as :

$$[M] = [P] [\alpha_2] [R_r] [\alpha_1]$$

where

$$[P] = \begin{pmatrix} 1 & 1 & 0 & 0 \\ 1 & 1 & 0 & 0 \\ 0 & 0 & 0 & 0 \\ 0 & 0 & 0 & 0 \end{pmatrix}$$

is the matrix due to the polaroid
and

$$[R_r] = \begin{pmatrix} 1 & 0 & 0 & 0 \\ 0 & 1 & 0 & 0 \\ 0 & 0 & \cos\delta_r & \sin\delta_r \\ 0 & 0 & -\sin\delta_r & \cos\delta_r \end{pmatrix}$$

is the matrix due to the retarder. Here δ_r is the retardance: for a quarter-wave plate $\delta_r = 90^\circ$. $[\alpha_1]$ and $[\alpha_2]$ are the rotation matrices required to transform from the reference frame denoted by XOY (Figure II-10.1) to the retarder frame (denoted by F and S), and from the retarder frame to the polaroid frame (denoted by transmission direction T), respectively.

The Stokes profiles are recorded in six successive combinations I+Q, I-Q, I+V, I-V, I-U and I+U (see Figure II-10.2) with a 35-mm camera at the exit of the spectrograph. The emulsion used for the entire observations was the Kodak 103-aE spectroscopic emulsion, having an rms grain-size of 20 microns and treated for low-intensity reciprocity failure. Unfortunately much finer grain-size emulsions, sensitive in the red region, were not used as they consume a longer time to reach the optimal density level above the background fog. Even with

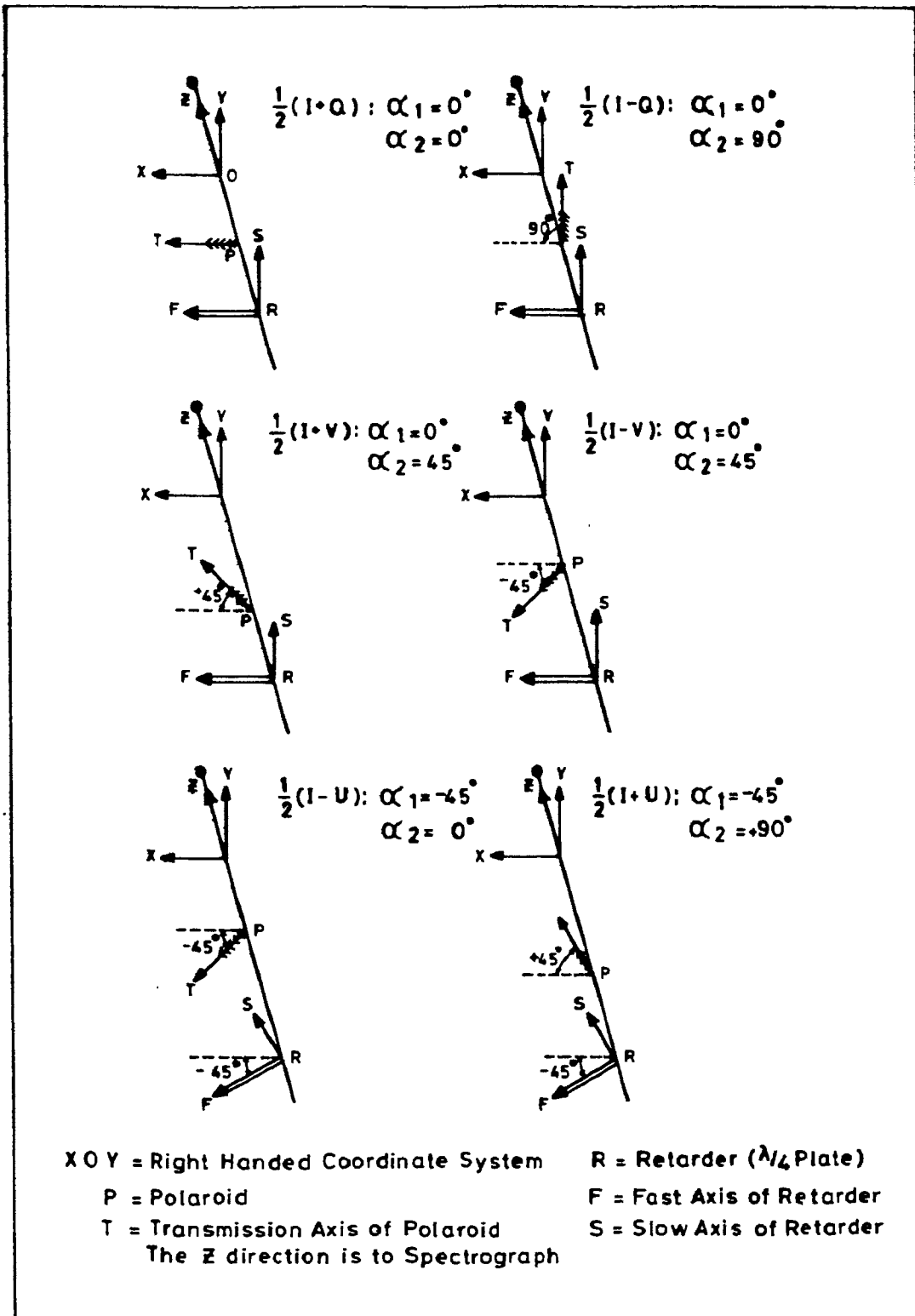


Fig.II-10.1: Schematic of the analysis procedure. The train consists of a quarter wave plate whose fast and slow axes are represented by F and S and a polaroid whose transmission direction is denoted by T. The different relative orientations of F(or S) with T transmit different combinations of the stokes parameters as depicted in the figure.

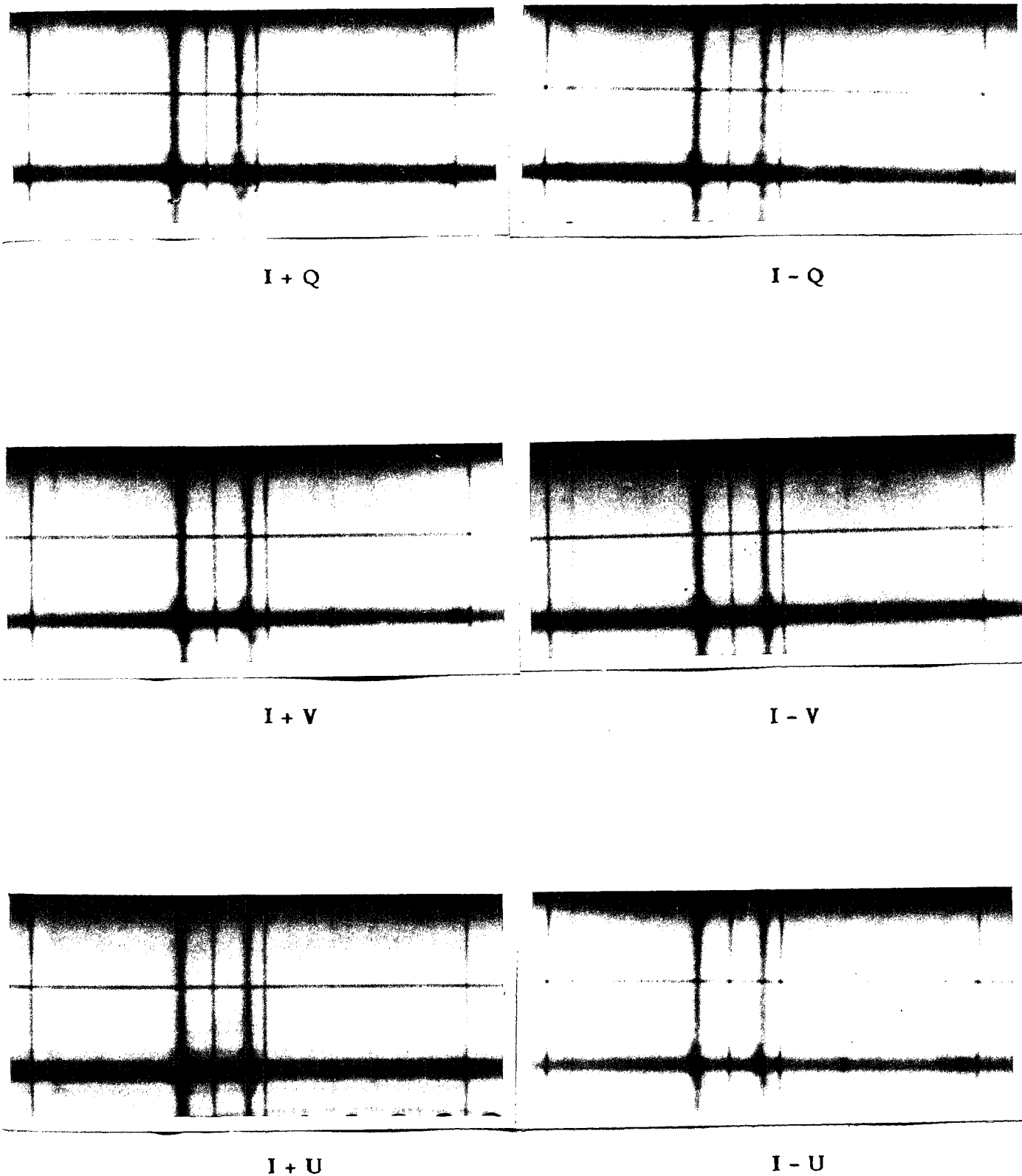


Figure II-10.1

Spectra of Stokes profiles recorded across sunspot KKL 18303 on May 12, 1987 at position 5. The fiducial cross wire is also seen dispersed along with the spectrum.

the 103-aE emulsion, it takes about 3-minutes to get a complete exposure set, covering one set of spectra for just one slit position and the entire useable observing time with good seeing does not last more than two hours a day, on the average.

11. ERRORS IN THE MEASUREMENT OF THE STOKES PARAMETERS

The errors in the measurement of the Stokes parameters come from the error in the positioning of the transmission axis of the polaroid and, the slow or fast axis of the quarter-wave plate. Since instrumental polarisation is also introduced in the polarimetric set-up, the uncertainty in the measured values need to be estimated. The errors in the measurement of Stokes parameters is given by the Mueller error matrix

$$\delta[M] = [P] \frac{\delta[\alpha_2]}{\delta\alpha_2} \delta\alpha_2 [R] [\alpha_1] + [P] [\alpha_2] [R] \frac{\delta[\alpha_1]}{\delta\alpha_1} \delta\alpha_1$$

We have evaluated these errors various input Stokes vectors and find that, for a positioning error of $\pm 0.5^\circ$, (the accuracy with which each of the polaroid and the quarter wave plate can be rotated about their centre of axis in the polarimetric system), the maximum errors ΔQ , ΔU and ΔV for the different orientations of the polaroid and quarter-wave plate do not exceed 2% of the Q, U and V signals.

12. OBSERVATIONAL CHECKS ON THE POLARIMETRIC SYSTEM

In order to observationally verify that the measurements of the magnetic field strength as derived from the Stokes V profiles were in tune with the theoretical Zeeman splitting, a comparison was made of the Zeeman displacement measured with the two FeI lines $\lambda\lambda$ 6301.5 Å (using $g = 1.5$) and 6302.5 Å (using $g = 2.5$). Assuming that the spectral lines form from approximately

the same level in the solar atmosphere where the magnetic field does not vary, the ratio of their Zeeman splitting (from equation II-9.1.1) their Zeeman splitting is given by

$$\frac{\Delta\lambda_{H_{6302.5}}}{\Delta\lambda_{H_{6301.5}}} = \frac{4.6375 \times 10^{-5} \text{ H}}{2.782 \times 10^{-5} \text{ H}} = 1.5097 \text{ (theoretical)}$$

Using observations of the Stokes V profiles from an umbral region, the splitting from the above formulae gave a magnetic field ratio of 1.513 which is very close to the expected value.

13. AN ELLIPSOMETER TO MEASURE THE COMPLEX REFRACTIVE INDICES OF THE COELOSTAT MIRRORS.

An ellipsometer was designed and constructed to measure the complex refractive indices of aluminised mirror surfaces . The complex refractive indices enter the Mueller matrices and hence any changes in them (due to the ageing of aluminium), will in turn change the quality as well as the quantity of instrumental polarisation (see Appendix-1)

14 IMPROVEMENTS TO THE SEEING CONDITIONS WITHIN THE TELESCOPE

The Tower/Tunnel telescope has an extremely long column of optical path, from the dome to the rear of the spectrograph. It was felt that the thermal gradients along the optical path would tend to degrade the image quality. Moreover, suspended dust particles in the optical path of the beam also tend to contribute to the scattered light. A smooth laminar flow of air along the length of the optical path of the light beam improves the internal seeing. (*Bray and Loughhead 1964*). In order to improve the seeing as well as to remove the suspended dust particles

within the Tower/Tunnel column, a powerful exhaust fan located at the exit door of the ante-room behind the grating spectrograph enclosure. Since the spectrograph itself is shielded by a cylindrical steel wall, it did not affect the conditions within the spectrograph. The ante-room itself was a bonus advantage as it buffered the powerful suction of air within it, resulting in a smooth laminar flow along the length of the optical path. Visual inspection of the image did show a marginal improvement in the image quality as seen from the solar granulation cells on the surface of the solar disc. Within about half-an-hour of the stabilisation of the laminar flow the suspended dust particles were drastically reduced. This has now been made a regular feature during the course of observations.

CHAPTER III DATA ANALYSIS

1. THE OBSERVATIONS

Using the polarimetric set up explained in Chapter II the observations were carried out on sunspots KKL 18303 (NOAA 4806), KKL 18312 (NOAA 4810), KKL 18313 (NOAA 4811) and KKL 18315 (NOAA 4812), where the numbers after the letters KKL correspond to the sunspot numbers designated at Kodaikanal, where everyday white-light pictures of the Sun are recorded using the 6-inch photoheliograph (*Bappu*, 1967) and the numbers mentioned in brackets correspond to the same sunspots designated at the National Oceanographic and Atmospheric Administration, Boulder, Colorado, U.S.A (*Solar Geophysical Data -Prompt Report No.515, Part I, July 1987*). The observations were carried out between May 12-30, 1987 on all the three sunspot groups. The details of the observations are mentioned in *Table III-1*. The list of spectral lines recorded in the spectrum are shown in *Table III-2* (*Moore et.al. 1966; Beckers, 1960; Pierce and Breckinridge 1974; Beckers et.al., 1976*).

The scheme of observations is shown in *Figure II-10.1* of Chapter II. For each sunspot the observations were carried out in the following fashion. Beginning with one edge of the sunspot, the image was placed on the slit of the spectrograph, corresponding to 25mm (138 arc-seconds) along the length of the slit. The width of the slit during the entire course of observations was kept at 100 microns (0.55 arc-seconds). *Figure III-1.1* shows a sketch of the position of the slit relative to the sunspot. The crosswire serves as a fiducial mark to read the location of the spectra along the slit. Subsequently, with the polarimeter in position, the Stokes spectra were recorded as six successive frames on Kodak 103-aE emulsion. This

TABLE III-1

Date of Observat.	Sunspot No.		B	L	No. of slit positions
	KKL	NOAA			
12/05/87	18303	4806	6°W	25°S	five
14/05/87	18303	4806	29°W	26°S	five
15/05/87	18303	4806	43°W	27°S	five
15/05/87	18312	4810	83°E	25°N	--
15/05/87	18313	4811	85°E	28°S	--
16/05/87	18303	4806	55°W	24°S	five
16/05/87	18312	4810	63°E	27°S	--
16/05/87	18313	4811	72°E	25°N	five
17/05/87	18303	4806	67°W	28°S	three
17/05/87	18312	4810	53°E	22°S	three
17/05/87	18313	4811	63°E	31°N	seven
18/05/87	18303	4806	At limb	At limb	--
18/05/87	18312	4810	38°E	22°S	--
18/05/87	18313	4811	45°E	31°N	--
19/05/87	18312	4810	--	--	--
19/05/87	18313	4811	--	--	--
20/05/87	18312	4810	--	--	nine
20/05/87	18313	4811	18°E	32°N	six
22/05/87	18313	4811	7°W	32°N	--
23/05/87	18313	4811	21°W	32°N	twelve

Table III-1 continued...

24/05/87	18313	4811	30°W	32°N	--
25/05/87	18313	4811	49°W	32°N	ten
26/05/87	18313	4811	58°W	32°N	eight
27/05/87	18313	4811	70°W	32°N	five
27/05/87	18315	4812	18°E	24°N	three
28/05/87	18315	4812	10°E	22°N	four
29/05/87	18315	4812	5°W	25°N	six
30/05/87	18315	4812	18°W	25°N	three

TABLE III-2

Sl. No.	Wavelength in Å	Atom/ Mol.	Ori [*]	Mult No.	E.P. (e.V.)		Transition
					low	high	
1	6299.2296	Atm. O ₂	T	--	--	--	---
2	6299.5957	Unidentified	S	--	--	--	---
3	6300.3178	O C I J	S	1F	0.0	1.96	2p ⁴ 3p-2p ⁴ 1D
4	6300.6843	Sc II	S	28	1.5	3.46	3p-z 3D ⁰
5	6301.5091	Fe I	S	816	3.64	5.60	z 5p-e 5D ⁰
6	6301.8450	Fe Ip	S	863	3.62	5.58	b 3D-x 3D ⁰
7	6302.0005	Atm. O ₂	T	--	--	--	---
8	6302.5017	Fe I	S	816	3.67	5.63	z 5p-e 5D
9	6302.7629	Atm. O ₂	T	--	--	--	---
10	6303.4671	Fe I	S	1140	4.30	6.26	z 5G-e 5G
11	6303.7619	Ti I	S	104	1.44	3.39	b 3F-y 3G ⁰
12	6304.3334	Zr I	S	24	0.54	2.50	a 3p-z 3P ⁰
13	6305.2538	Unidentified	S	--	--	--	---
14	6305.8101	Atm. O ₂	T	--	--	--	---

Note: * S and T stand for SOLAR and TELLURIC respectively.

was repeated for various such positions of the sunspot across the slit. *Figure III-1.1* shows the sketch of the Sunspot KKL 18303 on May 12, 1987 for various positions of the slit. A set of sample spectra corresponding to position 5 of this *Figure* is depicted in *Figure II-10.2*.

Experiments by *Breckinridge* (1970, 1972) on polarisation introduced by spectrograph slits have shown that the optimal sizes of the slits, for polarimetry, must necessarily be greater than about 100 times the wavelength, in order to avoid any additional polarisation introduced by the slit.

The emulsion records the spectrum as fluctuations in density. Use of the photographic characteristic curve must be made to convert these density fluctuations into intensity fluctuations. For every set of observations of a sunspot group, the calibration spectrum was recorded before and after the observations of that sunspot group on the same emulsion. This was done by using a standard Hilger density step-wedge that has six steps, of known percentage transmissions of light through each step (*Table III-3*). Each step delineates about 1.3mm along the length of the slit. The centre of the solar disc, slightly defocussed and activity free, served as the calibration light source. Since only six steps are available, we can effectively increase the number of steps, and hence the known transmittivities through these steps, by using various exposure times. Using a confusion free continuum in the λ 6300 Å region, the transmitted intensities across the density steps were recorded for various known time intervals corresponding to known exposures;

Exposure = Intensity x time,

intensity of the source being constant. The emulsions were developed in the standard Kodak D-19 developer for 4 minutes at 20° Celsius and fixed in the standard Kodak photographic fixer.

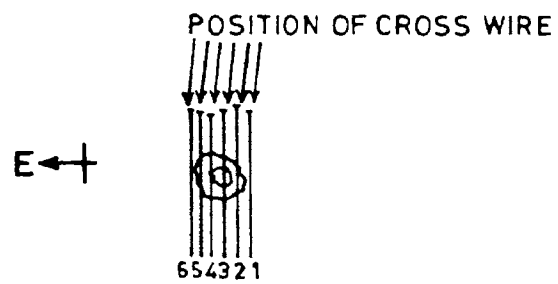


Fig.III-1.1 Sketch of the sunspot KKL 18303 with the positions of the slits (1-6) marked. Short bars at the top indicate the positions of the crosswire. North is top and east is to the left. Scale: 5.5 arcsec/mm.

TABLE III-3

Step No.	% of transmission
1	63.24
2	40.93
3	26.00
4	16.41
5	10.21
6	6.397

2 CONVERSION OF PHOTOGRAPHIC DENSITIES INTO DIGITAL DENSITIES

The density variations across the photographic spectra were digitised using the Photometric Data System 1010M Microdensitometer. Before digitising, the background fog-density was set to zero. The fiducial mark (cross wire) along the dispersion direction was then used to align the spectra. The spectra were digitised with a sampling resolution of 10 microns in the spectral direction, corresponding to a spectral resolution of 0.15 \AA mm^{-1} and 200 microns in the spatial direction (along the length of the slit), corresponding to an angular size of 1.1 arc-second on the Sun. Each of the six frames of the Stokes spectra for any single position of the slit are thus digitised in two dimensions, using the raster scanning. The spectral direction covers the wavelength range from 6299 \AA to 6306 \AA having 4800 points. The spatial direction covers between 50 - 110 points, depending on the spatial extent of the particular sunspot observed on a particular day. For the observations mentioned in *Table III-1*, there were a total of 700 frames, including the observations of the sunspot-free regions located at the solar disc centre and the calibrations of the density steps corresponding to known transmission functions for each density step. The time consumed for the entire conversion of the photographic densities to the digital form was three complete months and the data exists on 18 magnetic tapes (1600 BPI, 2400 feet).

The spectra have been digitised, in the dispersion direction at 10-micron intervals, finer than the photographic r.m.s grain size (20 microns) to include the grain noise of the emulsion. The grain noise can then be Fourier filtered by chopping all high frequency noise above the grain noise to improve the signal-to noise of the spectrum. By this way the problem of limitation of the grain-noise of the emulsion can be overcome. This is

because, if one were to have a larger pixel size for the digitisation then the grain noise would of course be averaged, but there is a loss in spectral resolution. In the spatial direction, the limitation of 1.1 arc-second is imposed by the seeing (atmospheric turbulence and scintillation) conditions. On no day, during the course of observations was the seeing less than 1 arc-second as determined by a visual inspection of the solar granulation pattern about the disc of the Sun. The granulation have sizes ranging from 0.5 to 2 arc-seconds.

3 REDUCTION OF THE DATA USING THE VAX 11/780 COMPUTER FACILITY AND THE RESPECT PACKAGE

The next phase of reductions involves the use of the VAX 11/780 computer at the Vainu Bappu Observatory, Kavalur. The VAX 11/780 computer in conjunction with the Tektronix 4115B work station and its color copier were very helpful in the reductions. For reduction of the spectra through various stages, the spectroscopic reduction package RESPECT (*Prabhu, Anupama and Giridhar 1987*) was used. The spectral reductions involve the following stages. (All commands mentioned in capital letters refer to the commands of the RESPECT package.)

3.1 THE CALIBRATION FOR CONVERTING THE DATA FROM DENSITIES TO INTENSITIES

The spectra need to be converted from the digital densities to digital intensities. In order to do so we need the photographic characteristic curve (see Section III-1). The density recording of the calibration step wedge, for each day of observation was used for this purpose (see *Table III-3*) This is represented in *Figure III-3.1.1*. Using the RESPECT package programs, the calibration steps shown in *Figure III-3.1.1* are interactively identified on the Tektronix monitor and are all scaled to actual exposure times of the spectral

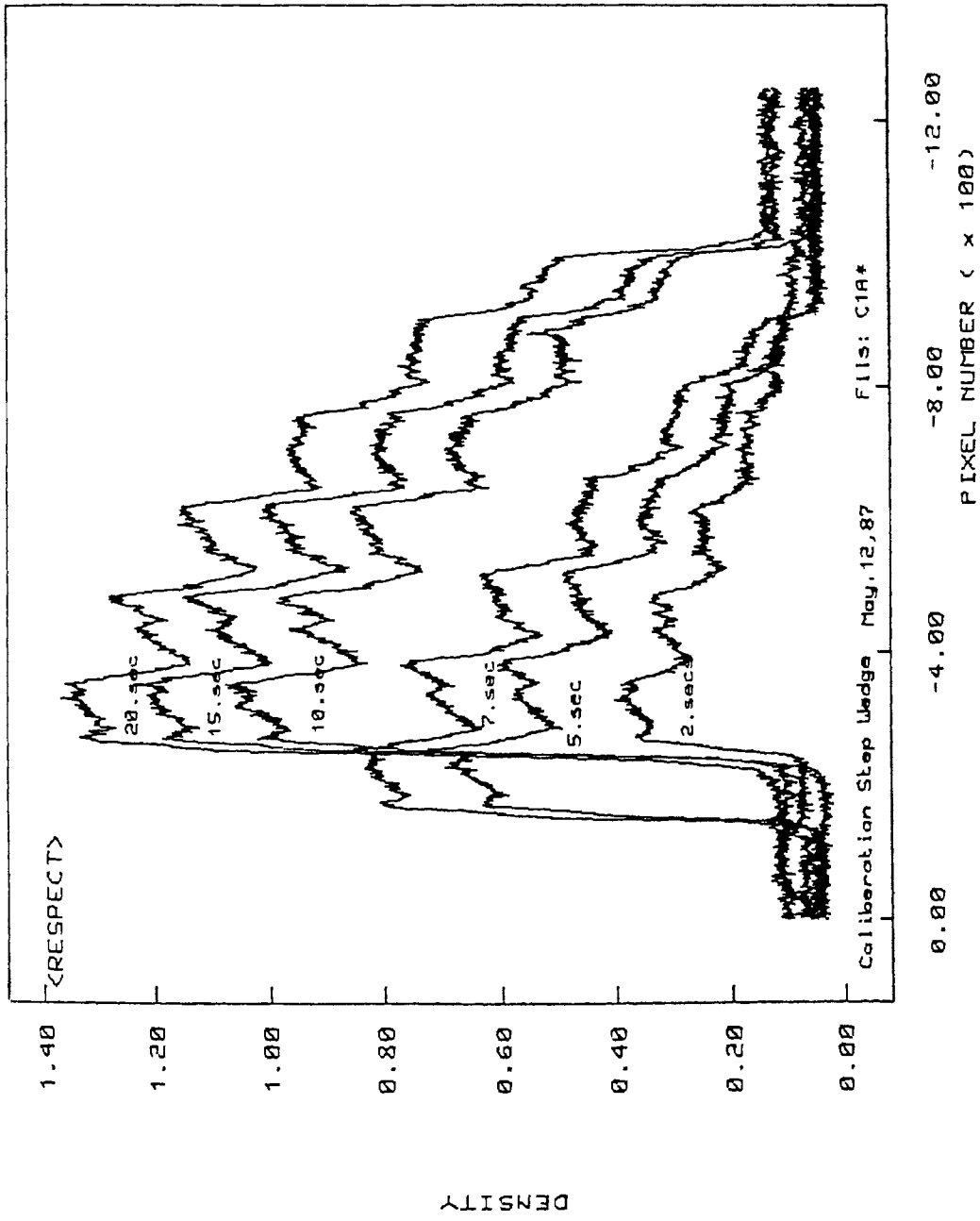


Fig. III-3.1.1 Response of the film as a function of wavelength to various levels of intensities transmitted through a step-wedge. The relative intensities are proportional to the exposure times marked against each curve.

observations. Using their known relative intensities corresponding to the measured densities, the characteristic curve of logarithmic intensity versus the Baker densities (*de Vaucouleurs, 1968*) is constructed. Such a curve for a particular days observation is shown in *Figure III-3.1.2.*, a third order polynomial fit the density steps, whose coefficients are used to convert the observed densities of the spectrum to the intensities.

The standard deviation of each of the observed density steps is then used to construct the signal-to-noise curves of the observed intensities using the characteristic curve and one such curve is depicted in *Figure III-3.1.3.* The signal-to-noise of the emulsion is maximum at a log intensity values of about 1.5 corresponding to densities around 0.5 above the background fog, which is typical of the emulsion used.

3.2 REDUCTION OF THE OBSERVED SPECTRUM

3.2.1 : Each spectrum containing 4800 pixels is first converted to a VAX compatible format by use of a command REFORM. A sample raw spectrum is shown in *Figure III-3.2.1.*

III-3.2.2: Next the data is smoothed with the help of the following operations.

a) Conversion to modified densities.

Since the photographic grain noise increases linearly with density, it is wise to bring the grain noise to a constant level at all densities as this will help in a more accurate removal of the grain noise. Such a transformation, for converting the densities to a state where the noise is constant, labelled as modified densities (*Anupama, 1987 ; Lindgren, 1975*) is given by

$$D_1 = A \ln (a + b D) + B$$

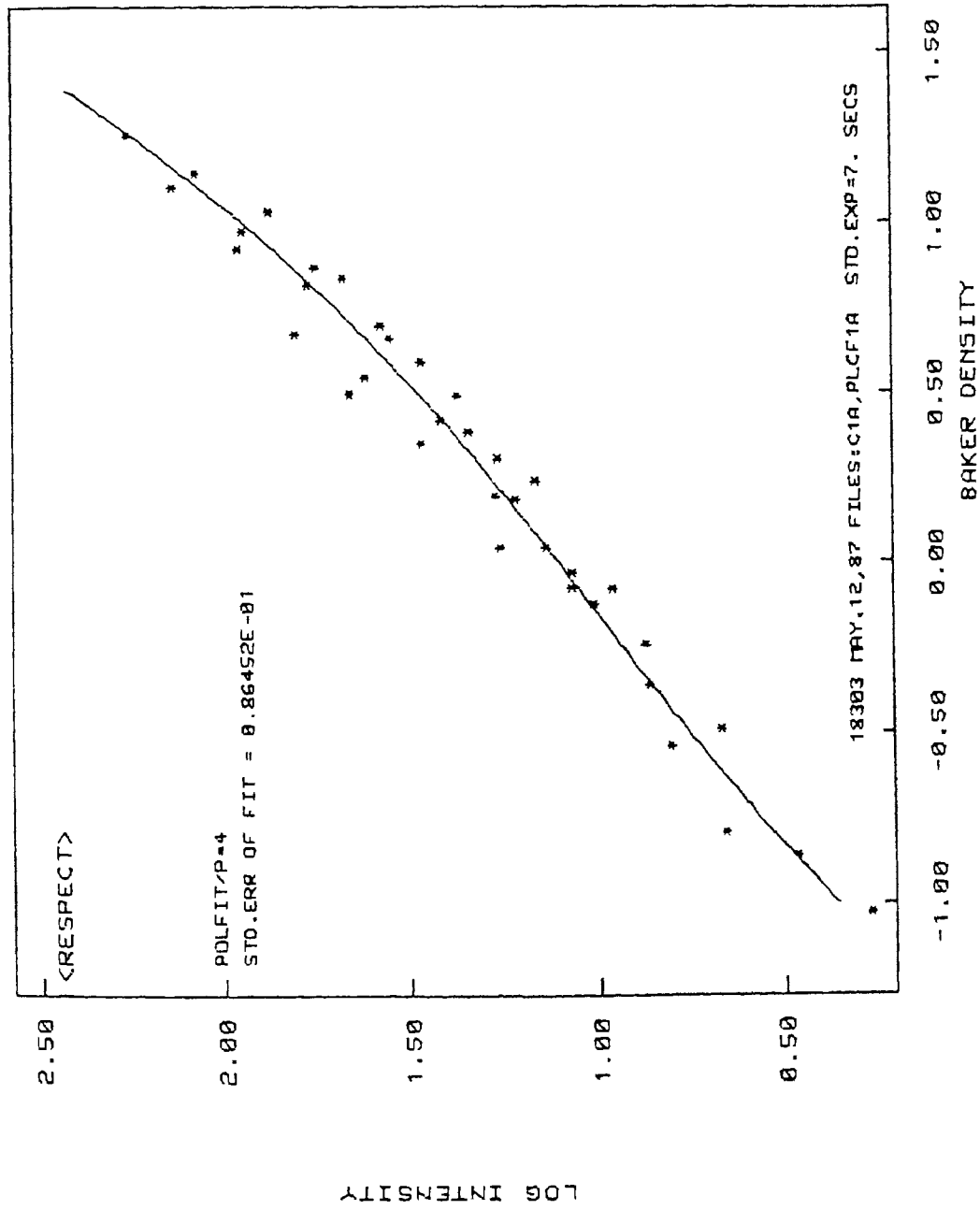


Fig. III-3.1.2 Characteristic curve of the emulsion used. Here log (intensity) is plotted as a function of Baker density. The solid curve is a polynomial fit of third order.

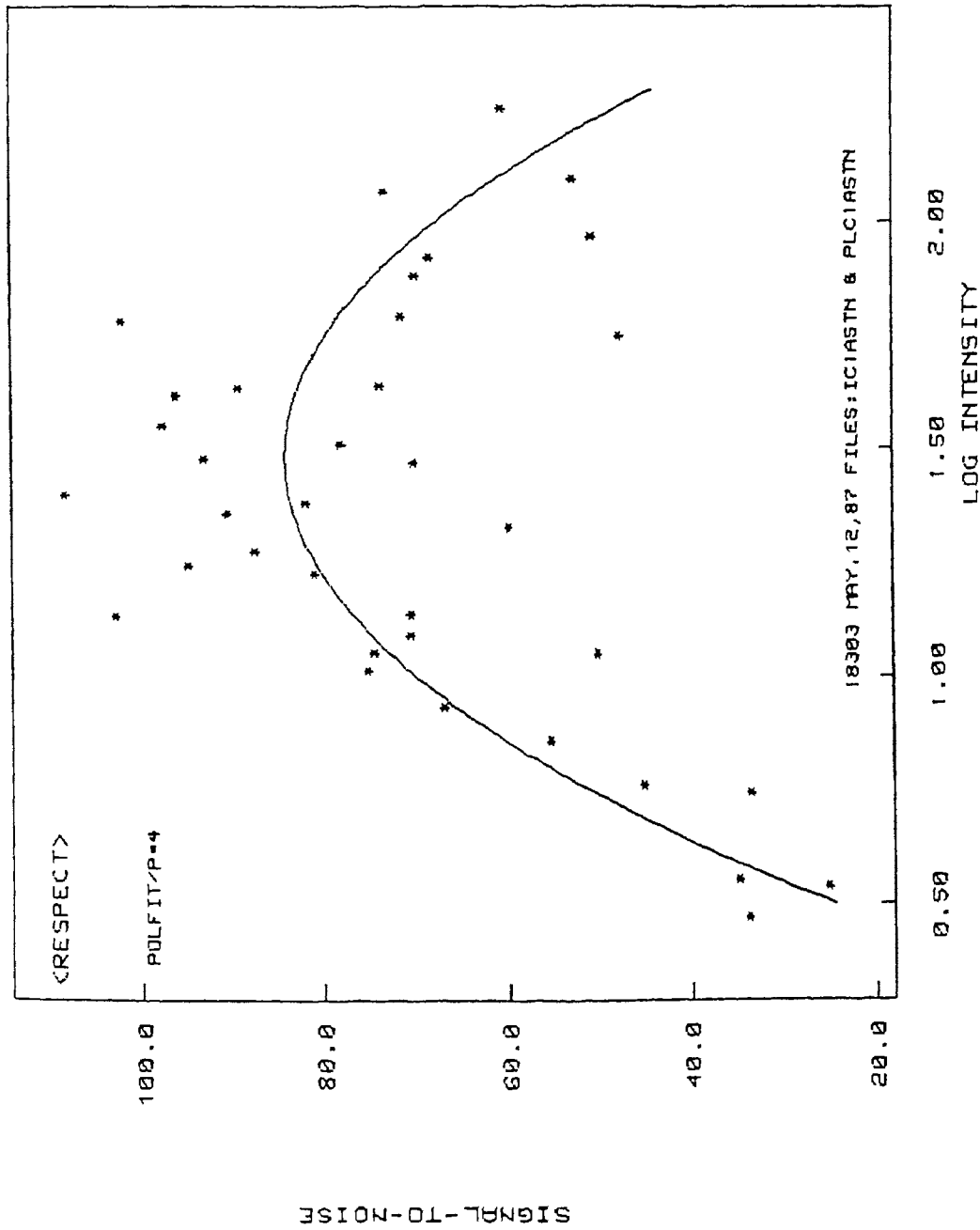


Fig. III-3.1.3 Signal-to-noise ratio of the spectra at various relative intensities, calculated from the standard deviation of the intensity fluctuations derived from the density fluctuations on the film. The solid curve is a polynomial fit of third order.

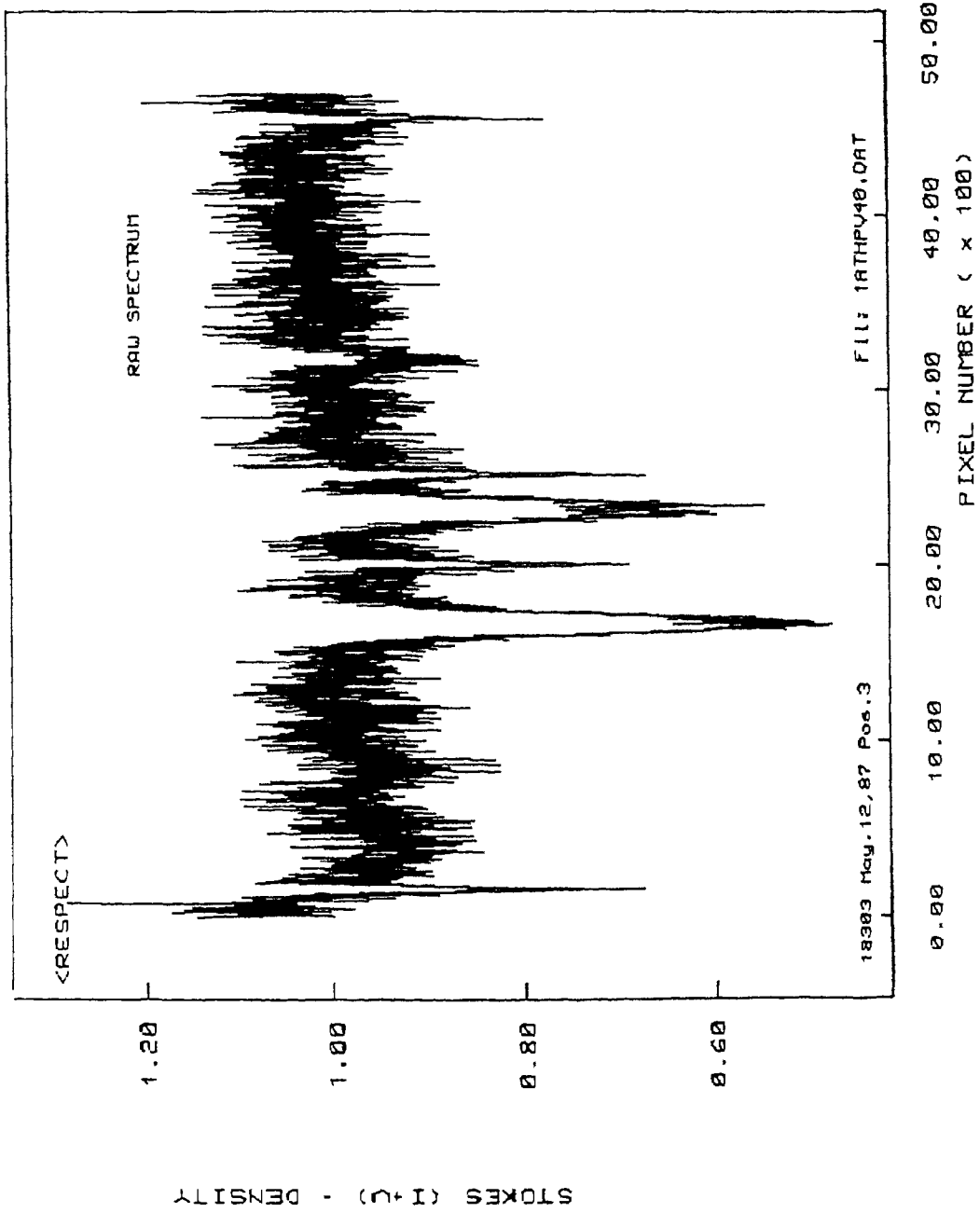


Fig.III-3.2.1 A sample raw spectrum of I + V .

where D is the density, A and B are arbitrary constants that are used to bring the magnitude of D_1 same as that of D . Here, the noise on the density domain is

$$\sigma_D = a + b D$$

and is actually the standard deviation in density. σ_D is derived from the calibration step-wedge densities, and has been explained before. The RESPECT command MDENS converts the data from ordinary densities to modified densities, given the coefficients of the linear fit between density and its standard deviation, obtained from the calibration curves.

b) Fourier smoothing of the data

Consider the density spectrum $D(x)$, where x is the pixel position of the recorded spectrum. Its Fourier transform is given by

$$D(\nu) = \int_{-\infty}^{+\infty} D(x) e^{i2\pi x\nu} dx$$

Then the power spectrum given by

$$P(\nu) = D(\nu) D(\nu)^*$$

gives the information on the power present in various frequencies.

A sample power spectrum of the data shown in *Figure III-3.2.1* is shown in *Figure III-3.2.2*. With the kind of spectrum recorded here, the signal is concentrated at the low frequencies. Since no information can be present at resolutions finer than the grain-size, only noise power dominates at high frequencies. Hence a low-pass filter was used to remove the noise at higher frequencies. The cut-off frequency is also marked in *Figure III-3.2.2*. After much experimentation, it was decided to use a cut-off frequency of $10 \text{ cycles mm}^{-1}$, corresponding to

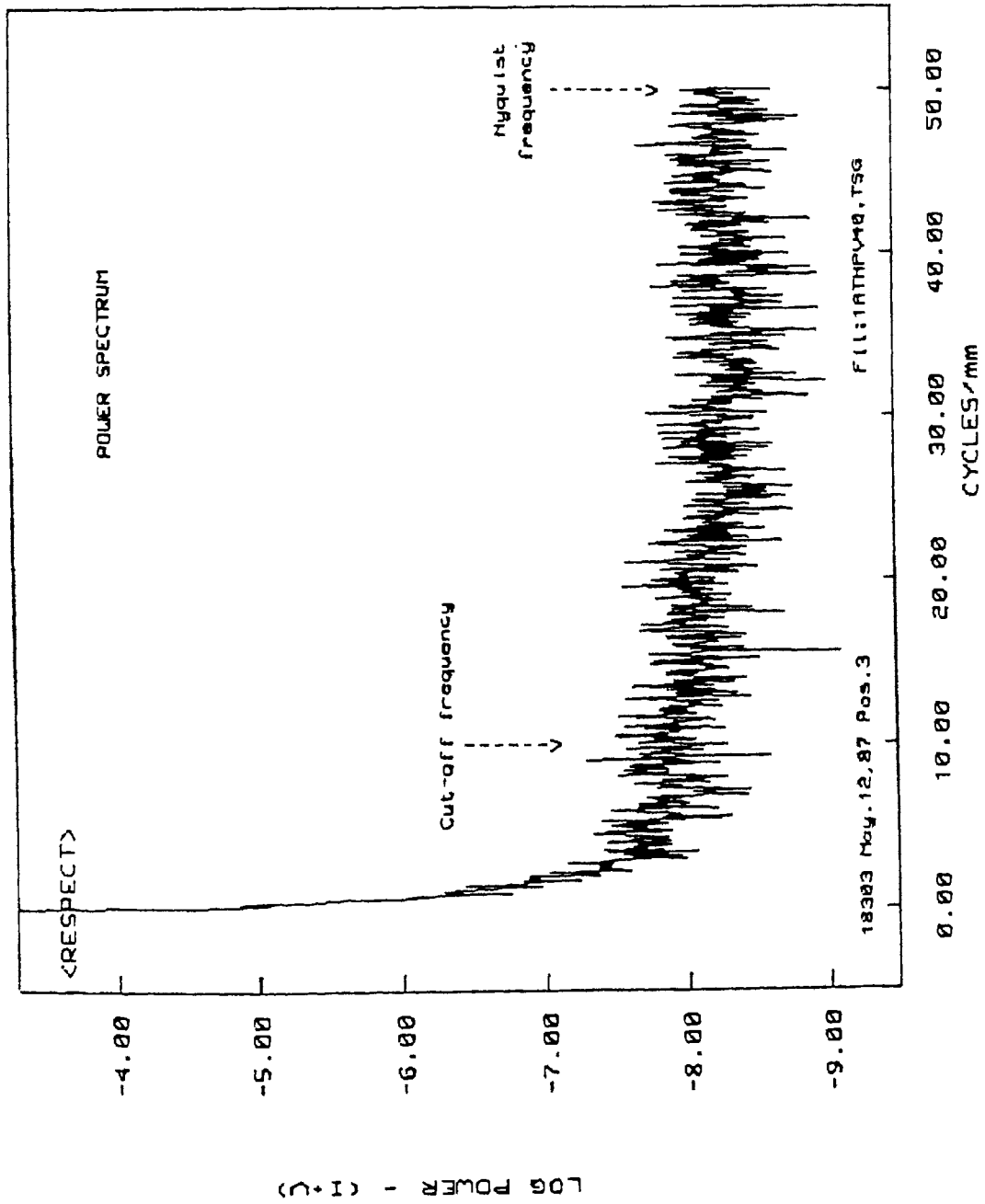


Fig. III-3.2.2 Power spectrum of an I + V profile. The data was oversampled to determine the noise in the emulsion. The cut-off frequency used in low-pass filtering for noise reduction is marked.

15 m Å . The low-pass filter has a strength of 1.0 upto the cut-off frequency and 0.0 at all higher frequencies. BSMOOTH converts the data to the Fourier domain, filters the data using the given cut-off frequency, and converts the data back to the modified densities.

c) A command MDENS/INV converts the data back to ordinary densities from modified densities. The data after smoothing is represented in *Figure III-3.2.3*

The response of the grating spectrograph to input linearly polarised light, perpendicular to the slit (I+Q) and along the length of the slit (I-Q) is shown in *Figure III-3.2.4*. Notice that the spectrograph is more efficient to linearly polarised light along the slit rather than orthogonal to it, in confirmity with the results of *Breckinridge (1972)*.

3.2.3 Automatic identification of the telluric lines in the spectrum for wavelenght calibration.

The DIPS routine identifies all the absorption lines within the spectrum against their pixel numbers. The identification is done after fitting a Gaussian profile through each one of them and noting their centroid pixel numbers. From an input line list containing the four telluric oxygen spectral line wavelenghts $\lambda 6299.228 \text{ \AA}$, $\lambda 6302.000 \text{ \AA}$, $\lambda 6302.764 \text{ \AA}$ and $\lambda 6305.810 \text{ \AA}$ the routine automatically identifies the centroid pixel numbers of corresponding telluric lines in the spectrum of interest. This is done based on the following input information: a) window-width within which the search should be done (corresponding to 2mm in the given spectrum), b) the approximate wavelenght of the first pixel of the spectrum (6299 Å), c) the approximate dispersion of the spectrum (0.15 \AA mm^{-1}), d) the criterion to identify only the true telluric spectral lines and reject sharp discontinuities (due to either scratches or dust on the emulsion). For

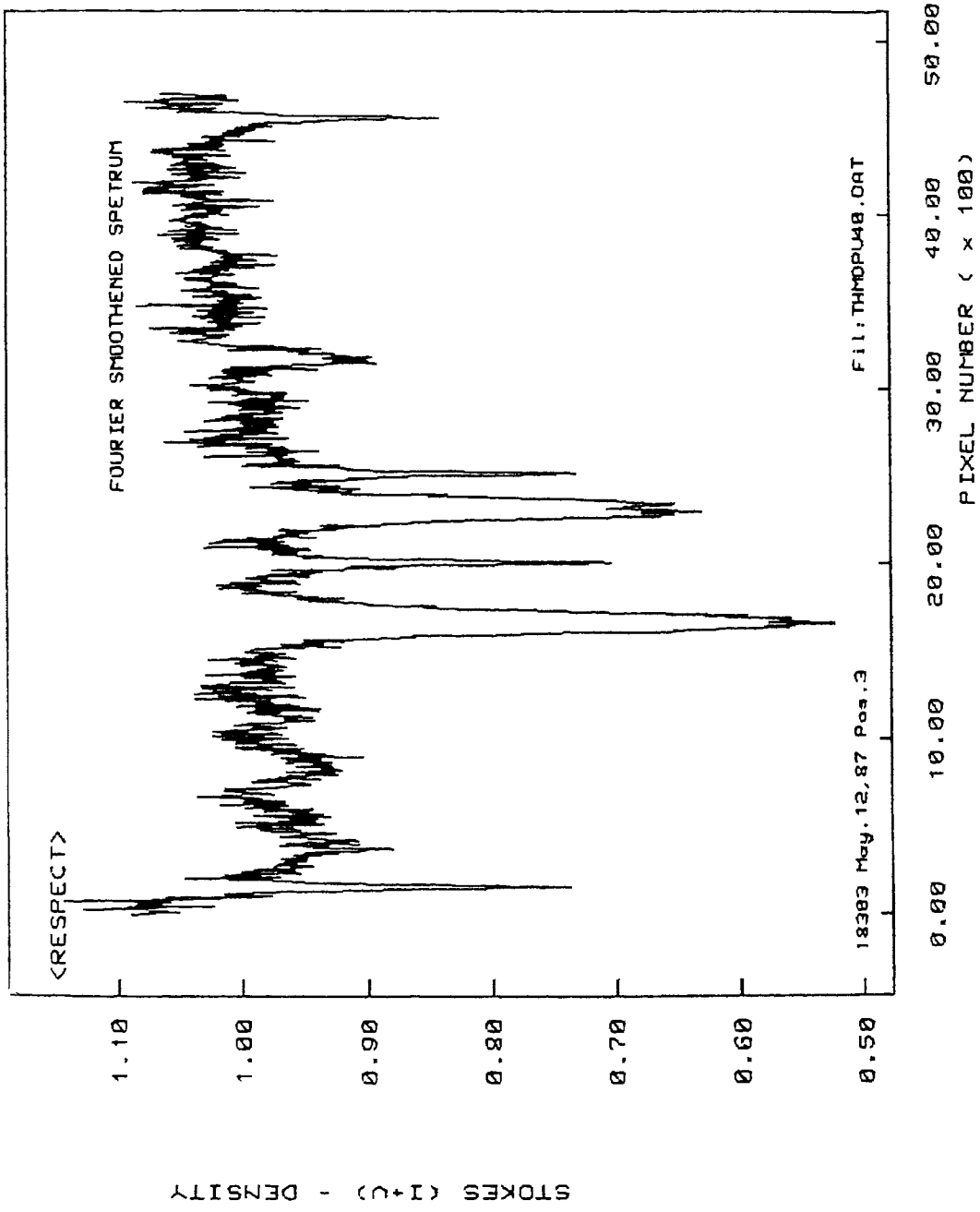


Fig. III-3.2.3 Typical I + V profile in the 6302 Å region after smoothing the raw spectrum.

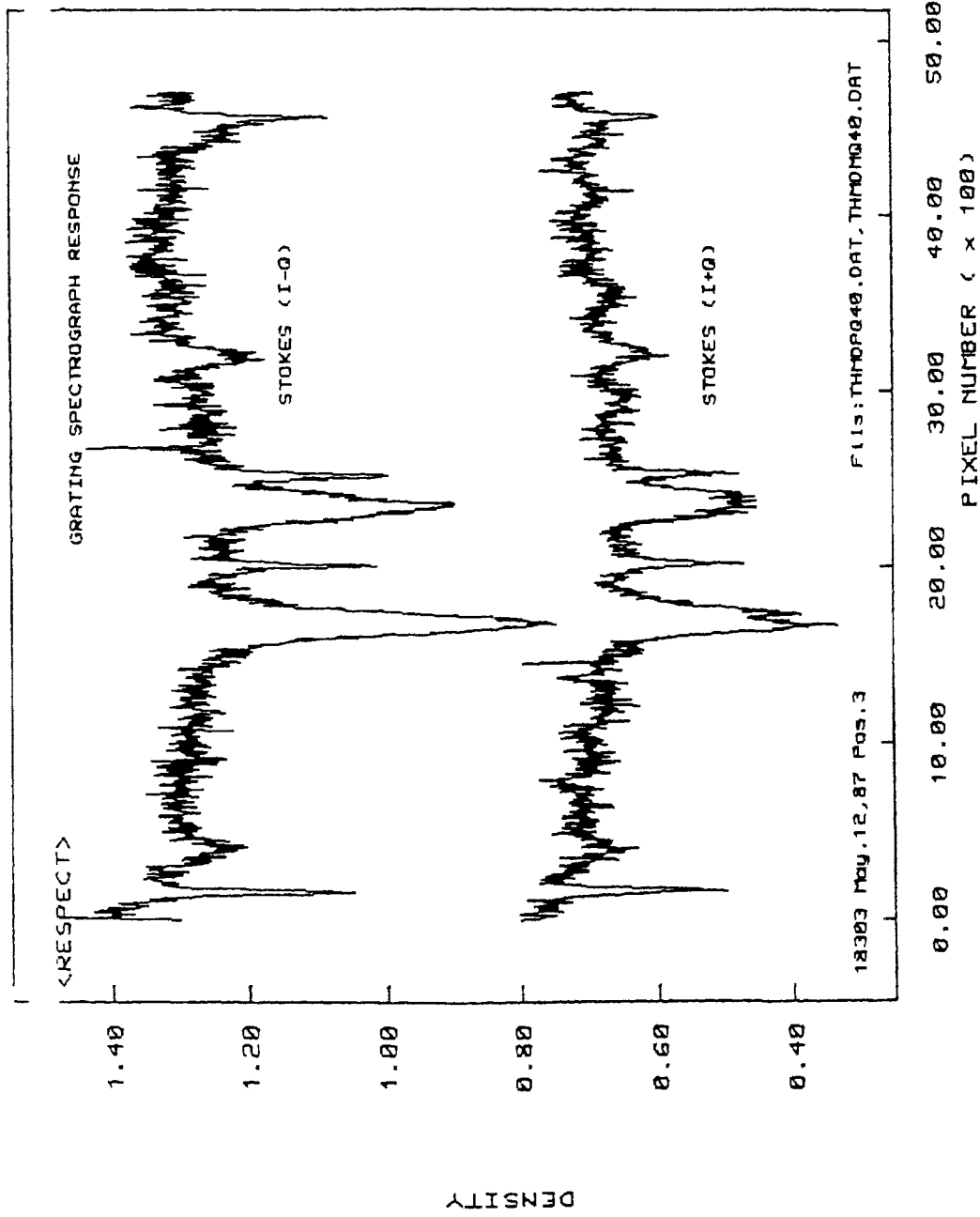


Fig. III-3.2.4 Raw spectra in Stokes I - Q (perpendicular to the slit) and I + Q (parallel to the slit), showing that the grating spectrograph is more efficient parallel to the slit.

the spectra under consideration, the criterion value was always less than 1.6mm corresponding to the largest width of the spectral line as recorded on the emulsion. e) the criterion to retain all coincidence pixels corresponding to the four telluric lines and weed out the rest.

All input information except (e) were manually determined by examining the spectrum, on the Tektronix Graphics Monitor, by trial and error, in several situations of both magnetically sensitive and insensitive regions, as the last two telluric spectral lines ($\lambda 6302.764 \text{ \AA}$ and $\lambda 6305.810 \text{ \AA}$) are each partially blended by their respective neighbouring spectral lines originating from the solar atmosphere. The blending increases in the presence of very strong magnetic fields. The four telluric lines were chosen as wavelength calibrators because of their high-stability in velocity not exceeding 5 m s^{-1} (Caccin *et al.*, 1978). DIPS measures the actual dispersion against the centroid pixel numbers of the four telluric lines with an accuracy of 0.002 \AA .

Since the spectrum will be curved along the length of the slit, in spite of the advantage of a large focal length of the Littrow spectrograph and since some turbulence effects within the spectrograph can also possibly change the dispersion, each individual spectrum corresponding to a physical point on the solar atmosphere (1.1 arc-second) was processed separately using all these programs, to measure their dispersions accurately.

3.2.4 The measured centroid pixels corresponding to the four oxygen lines are then subjected to a polynomial fitting of order two. The straight line fit is rather adequate.

3.2.5: Using these polynomial coefficients and the smoothed spectrum resulting from section III-2.3.3., the wavelengths against each pixel of the spectrum is

identified by WSCALE to bring the spectrum to the proper wavelength scale. The spectrum is interpolated to every mÅ by a cubic-spline interpolation. As the wavelength of the telluric oxygen lines are accurate upto 1 mÅ, and each pixel corresponds to 1.5 mÅ, the interpolation is carried out with the next smallest integer mÅ.

3.2.6: Since WSCALE generates a large amount of data points, which are essentially oversampled as far as the limitations of the spectrograph is concerned, the data is brought back to the original resolution of 15 mÅ per pixel by a running average about every 10 pixels.

3.2.7: Conversion of densities into intensities.

Using the polynomial coefficients of the calibration curve representing Baker-transformed density versus the logarithmic intensities for each sunspot group, the wavelength calibrated spectrum of Baker densities is converted to logarithmic intensities.

Sample representation of the spectra (I+Q), (I-Q), (I+V), (I-V), (I+U) and (I-U) are shown in *Figures III-3.2.7a to III-3.2.7f*. Each of these spectra have been measured across the sunspot KKL 18303 on May 12, 1987. The numbers indicated in the right hand side of the figures represent the pixel numbers measured from the fiducial mark on the spectrum, where each pixel is 200 microns (≈ 1.1 arcseconds). This gives the spatial information of the Stokes profiles as one moves from the penumbra of the sunspot towards the umbra. Notice the increase in the depth of the Ti I spectral line $\lambda 6303.76 \text{ \AA}$, as one moves from the penumbra towards the umbra, indicating stronger magnetic fields. Also, the spectral line of interest, the FeI $\lambda 6302.5 \text{ \AA}$ line, broadens due to an increase in the magnetic field strength, and hence the blending of it, with the terrestrial O₂ spectral line $\lambda 6302.76 \text{ \AA}$, increases.

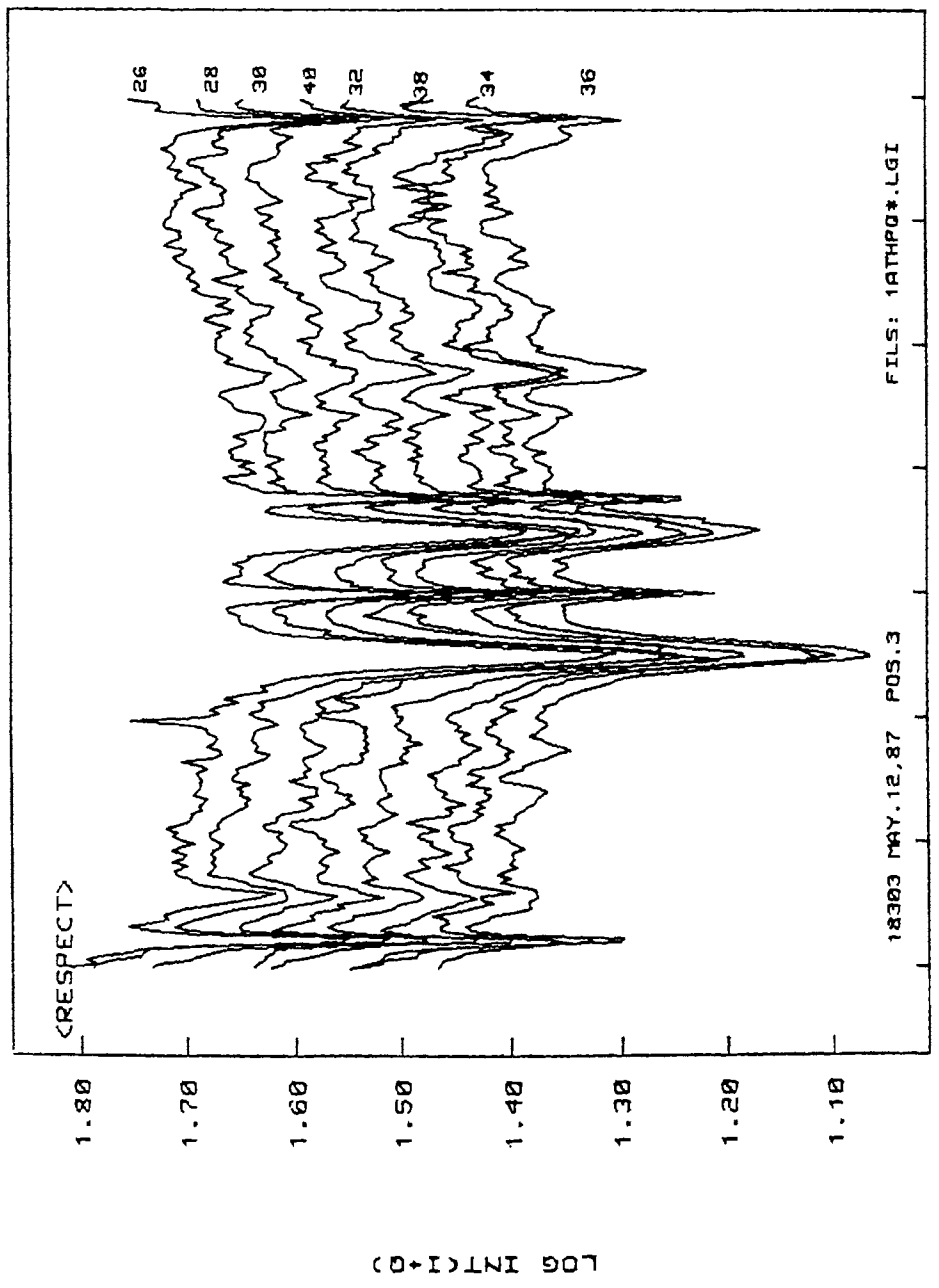


Fig. III-3.2.7a I + Q profiles in log(intensity) for eight positions along the slit.

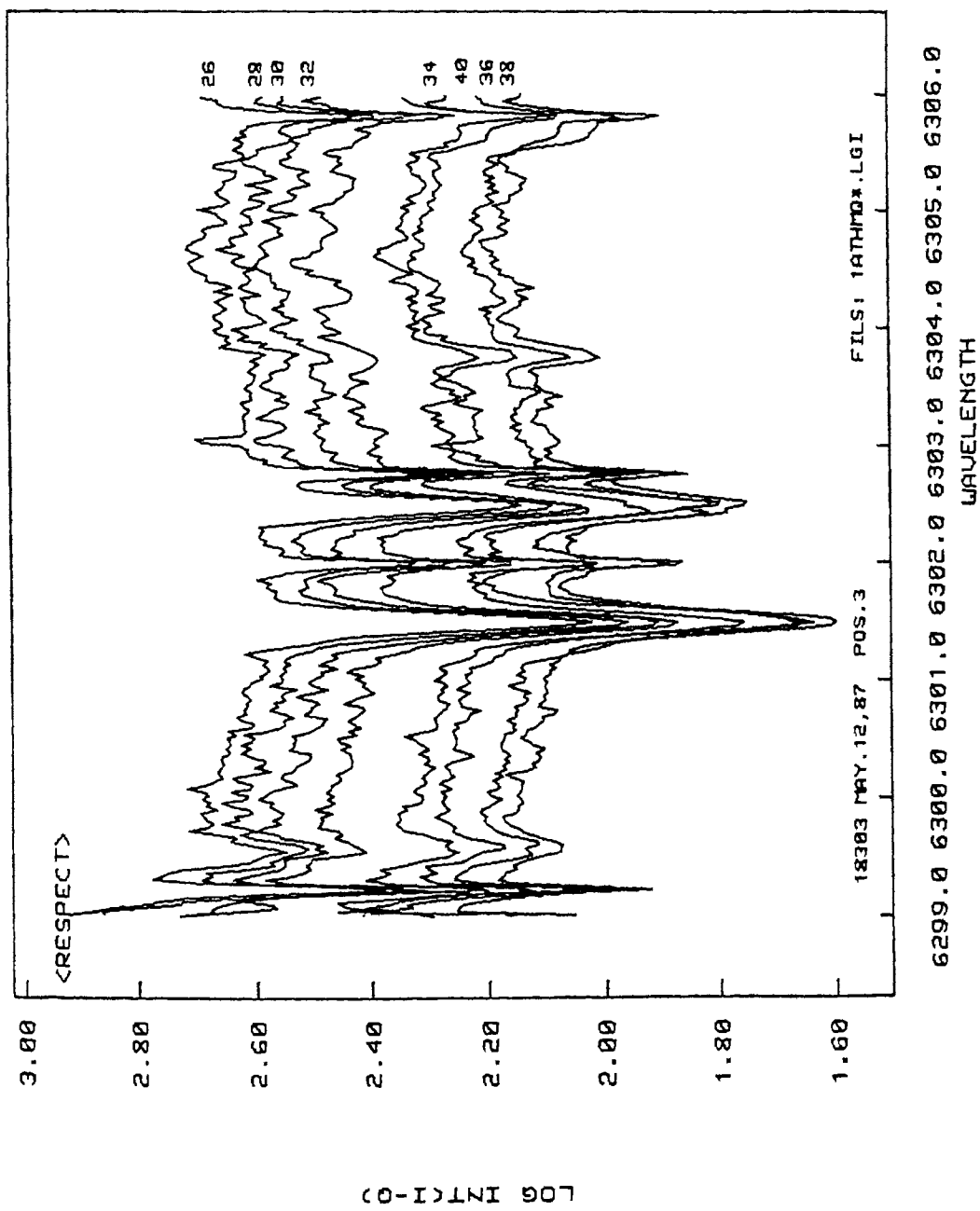


Fig.III-3.2.7b I - Q profiles for the same positions as in Fig.III-3.2.7a.

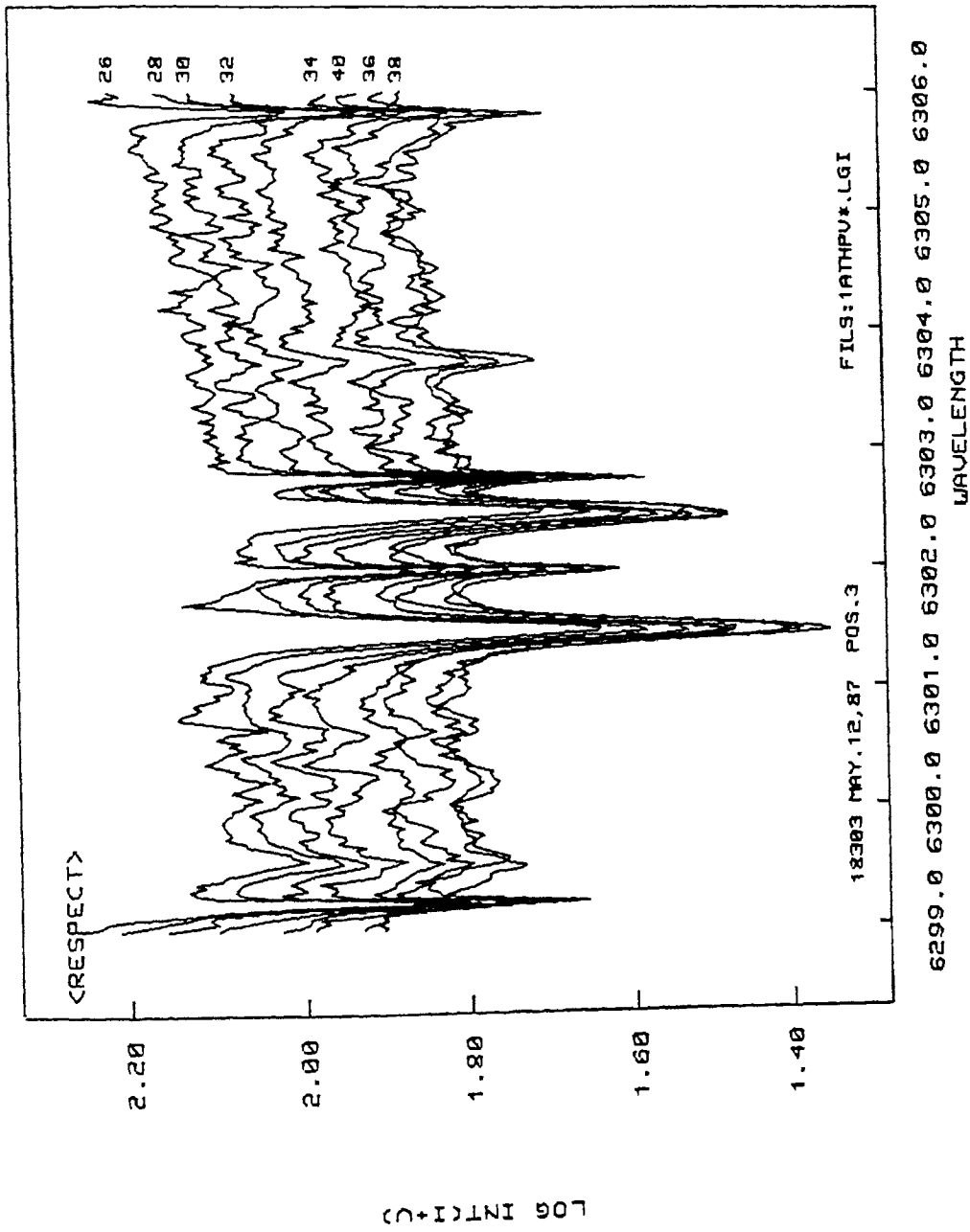


Fig.III-3.2.7c I + V profiles for the same positions as in Fig.III-3.2.7a.

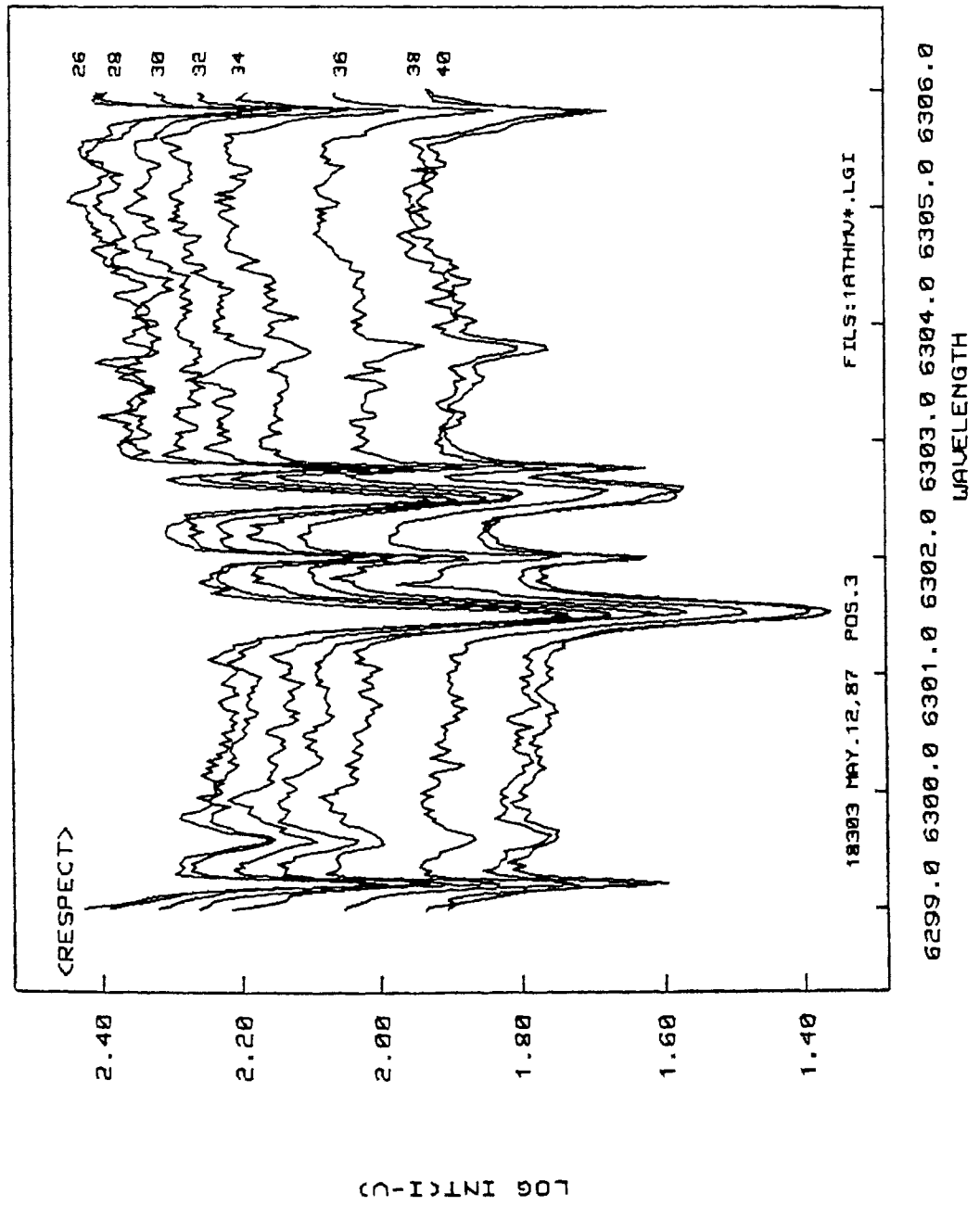


Fig. III-3.2.7d I - V profiles for the same positions as in Fig. III-3.2.7a.

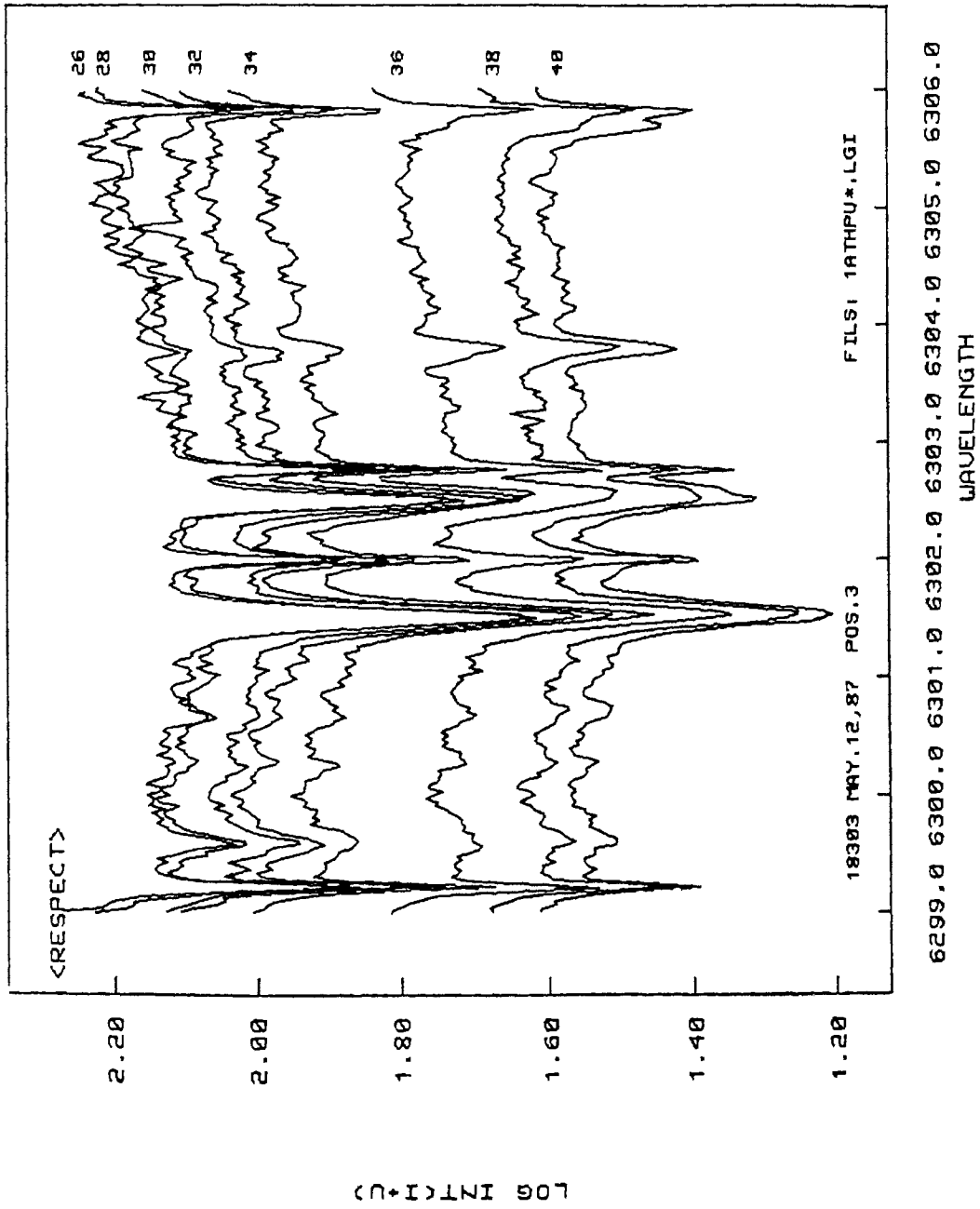


Fig. III-3.2.7e I + U profiles for the same positions as in Fig. III-3-2-7a.

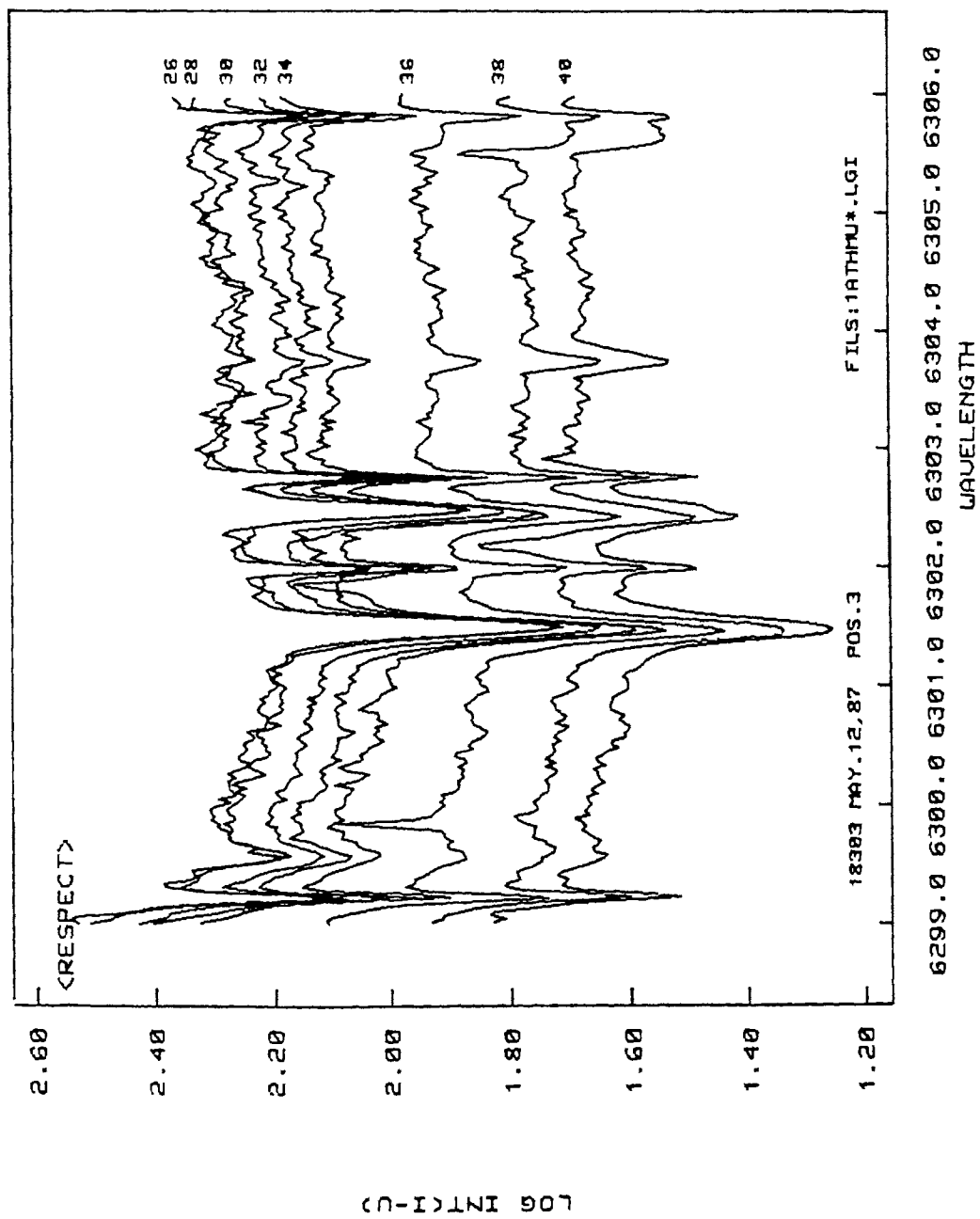


Fig.III-3.2.7f I - U profiles for the same positions as in Fig.III-3.2.7a.

3.2.8 Line-to-continuum ratios

An examination of the spectral continuum in *Figures* III-3.2.7a to III-3.2.7f shows that the response of the grating spectrograph is non-uniform as a function of wavelength. To overcome this problem it is necessary to determine the line-to-continuum ratio in the spectra shown in the above figures. Attempts were first made to fit a local continuum to the spectrum. The continuum bins were chosen from the *Liege Atlas*, (Delbouille *et al.* 1973). Two types of continuum fitting were tried, a polynomial fitting as well as a cubic spline fitting. Both the methods proved futile, as the ultimate test, of having a zero polarisation in the continuum of the Stokes Q, U and V when algebraic operations were performed on the I+Q, I-Q, I+V, I-V, I+U, I-U profiles, failed.

In order to overcome this problem, the solar spectrum between $\lambda\lambda$ 6299-6306 Å, obtained from the *Liege Atlas* was digitised and the continuum therein was taken as the true continuum. The digitised portion of the *Atlas* is reproduced in *Figure* III-3.2.8. Using continuum wavelength bins derived from this atlas, the ratio of the continuum intensity of the Atlas to the observed spectrum, in these bins was first derived. A cubic spline curve was fitted through these ratio points and the resulting curve was multiplied with the observed spectra to derive the line to continuum ratio's. Hence all the spectra reported here have their line-to-continuum ratios normalised to the Atlas spectrum.

3.2.9: Using the derived line-to-continuum the Stokes I+Q, I-Q, I+V, I-V, I+U, I-U spectra were added or subtracted to obtain the Stokes I, Q, U and V spectra. We are interested more in the polarised spectra, Q, U and V as the I spectrum is contaminated by both stray light as well as light from non-magnetic regions, sample profiles of the Stokes Q, U and V spectra for one position of the slit on the sunspot KKL 18303 observed on May 12, 1987, one

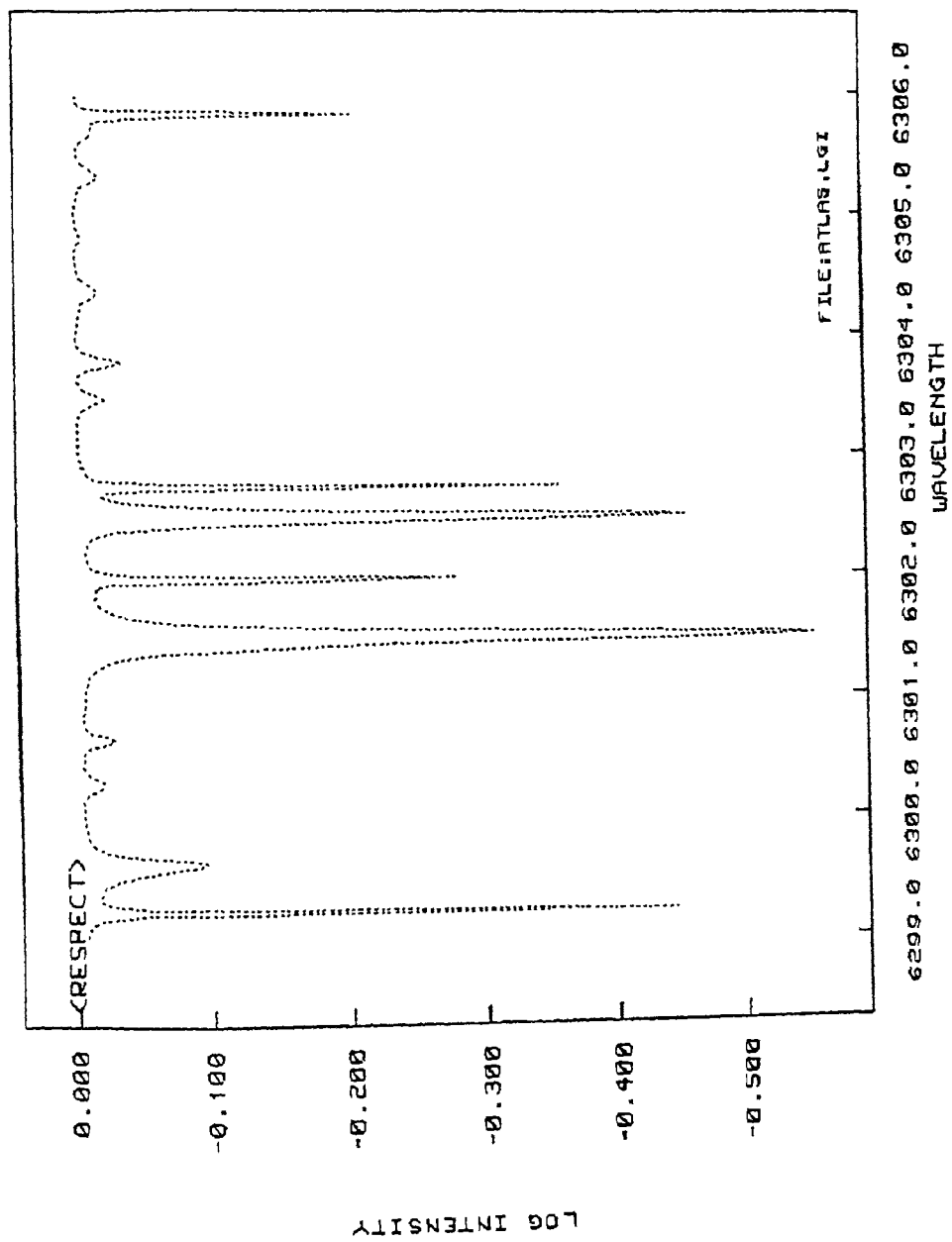


Fig. III-3.2.8 The Liege Atlas in the region of 6302 Å.

position of the slit are displayed in *Figures* III-3.2.9a, III-3.2.9b and III-3.2.9c, respectively.

4. CORRECTION FOR INSTRUMENTAL POLARISATION OF THE TELESCOPE

It is now necessary to correct the observed ~~the~~ polarisation profiles for the instrumental polarisation. The computer code based on the formalism derived in Chapter II was used to derive the inverted Mueller matrices for every set of observations, I+Q, I-Q, I+V, I-V, I+U, I-U. It may be recalled that the Mueller matrices depend on the geometry of the telescope and the coordinates of the Sun. Since every set of observations just took two minutes to complete, the time of observations used to derive the coordinates of the Sun was the average of the time between the beginning and the end of the observations. The coordinates of the Sun, for every set of observations, was derived from the *Almanac for Computers*, 1987 using a Chebychev polynomial fitting based on the coefficients given therein. The Mueller matrix is then inverted and the observed I, Q, U and V spectra are then subjected to this inverted Mueller matrix to obtain the true I, Q, U and V profiles. *Figures* III-3.2.9a, III-3.2.9b and III-3.2.9c (dot-dashed lines) shows the corrected Q, U and V profiles respectively. In comparing the two curves in *Figure* III-3.2.9b, for the Stokes U profile, one notices that there is a spurious Q like component in U before correction. Obtaining the true I, Q, U and V profiles also introduces an artificial bias in each of the I, Q, U and V profiles. This biasing is most markedly seen in the Q profile (*Figure* III-3.2.9a). Using the Tektronix 4115B color graphics monitor and the RESPECT command EXAMINE, each of these profiles have been individually corrected. Although we noticed that this biasing changes with the incident intensity, we have not yet attempted to quantify it. The biasing has been corrected for by shifting the position of the continuum

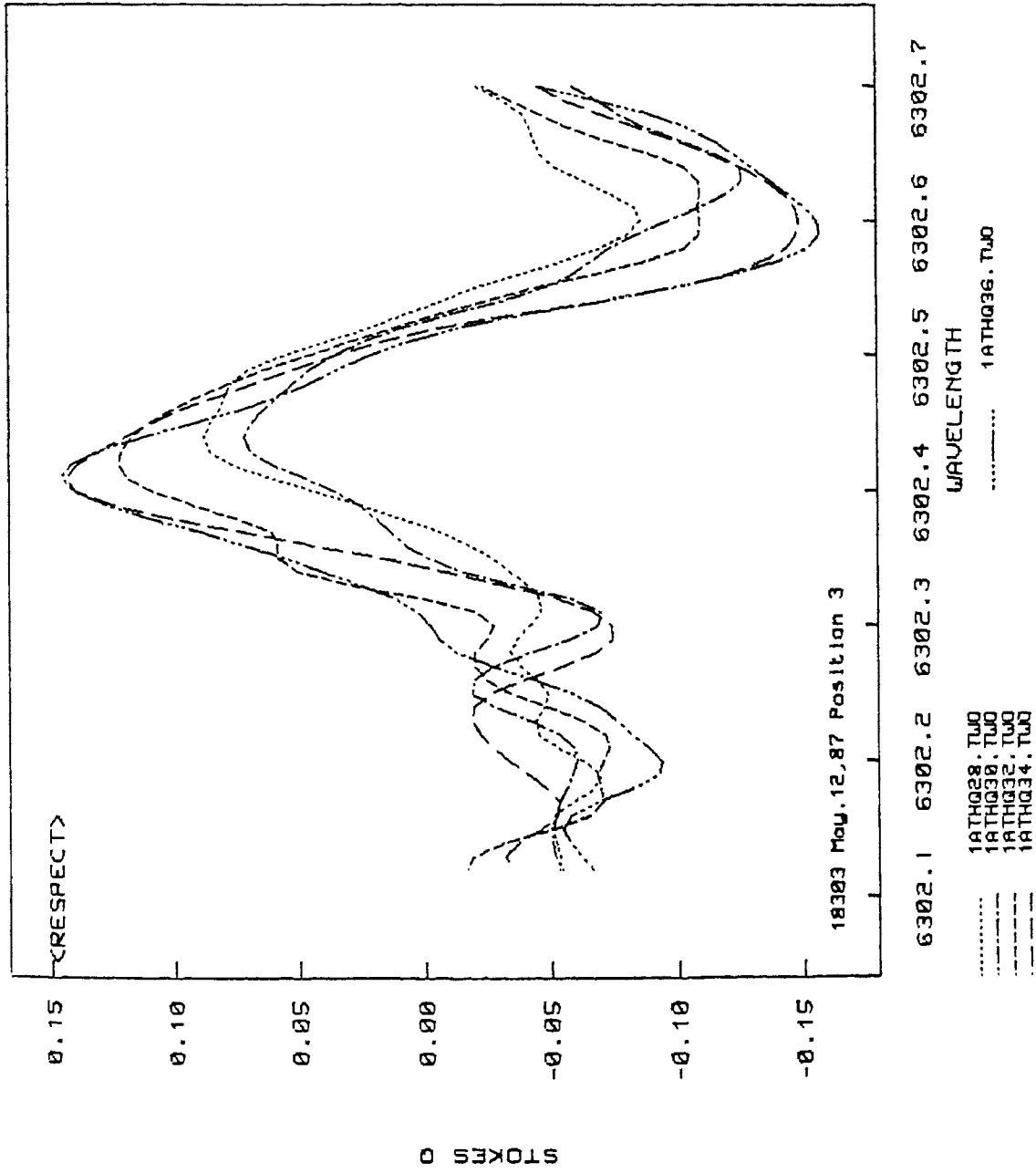


Fig.III-3.2.9a stokes Q profiles for four positions along the slit.

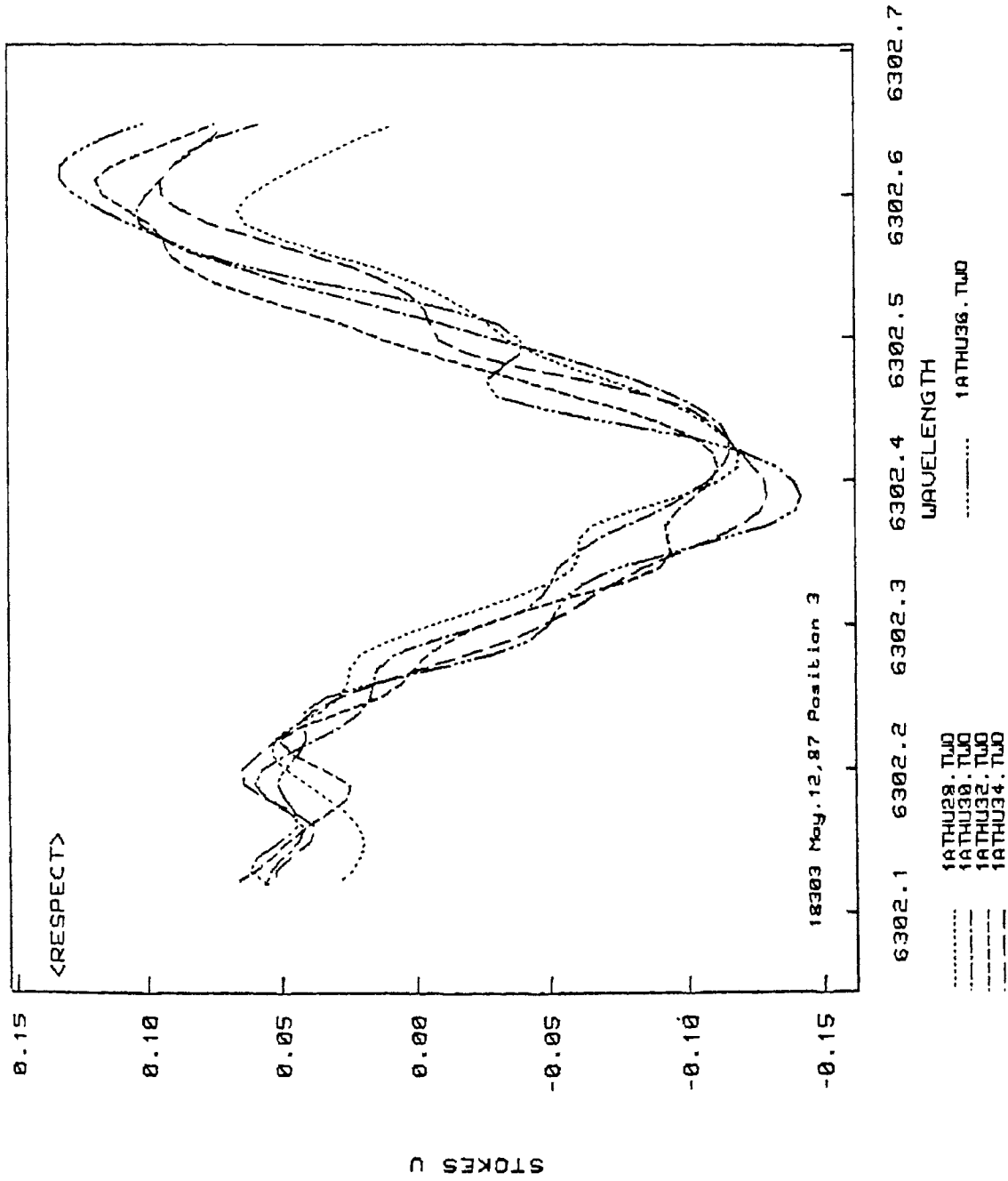


Fig.III-3.2.9b Stokes U profiles for the same positions as in Fig.III-3.2.9a.

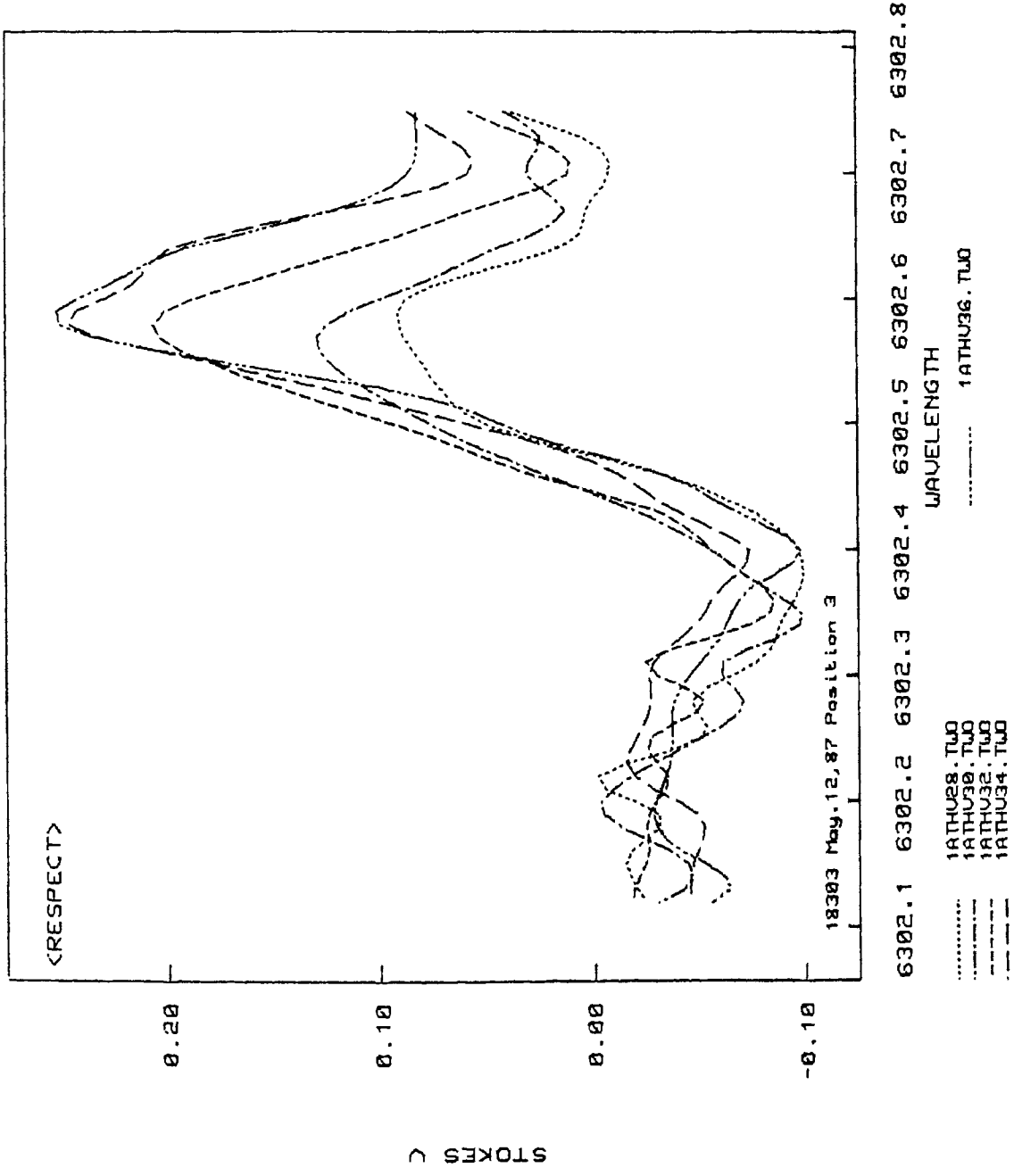


Fig. III-3.2.9c Stokes V profiles for the same positions as in Fig. III-3.2.9a.

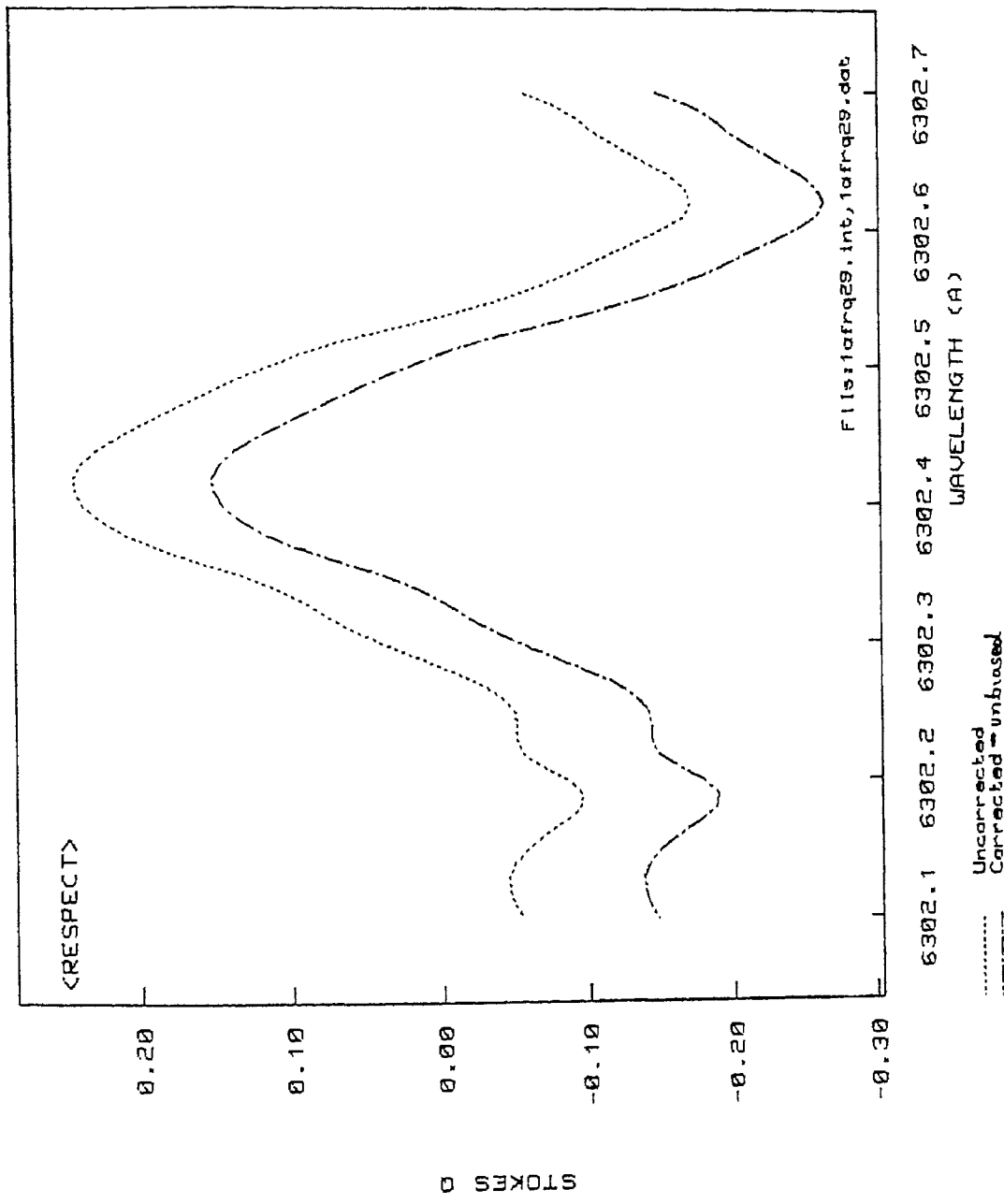


Fig. III-3.2.10a Comparison of Stokes Q profile at one location before and after correction for instrumental polarisation and continuum bias.

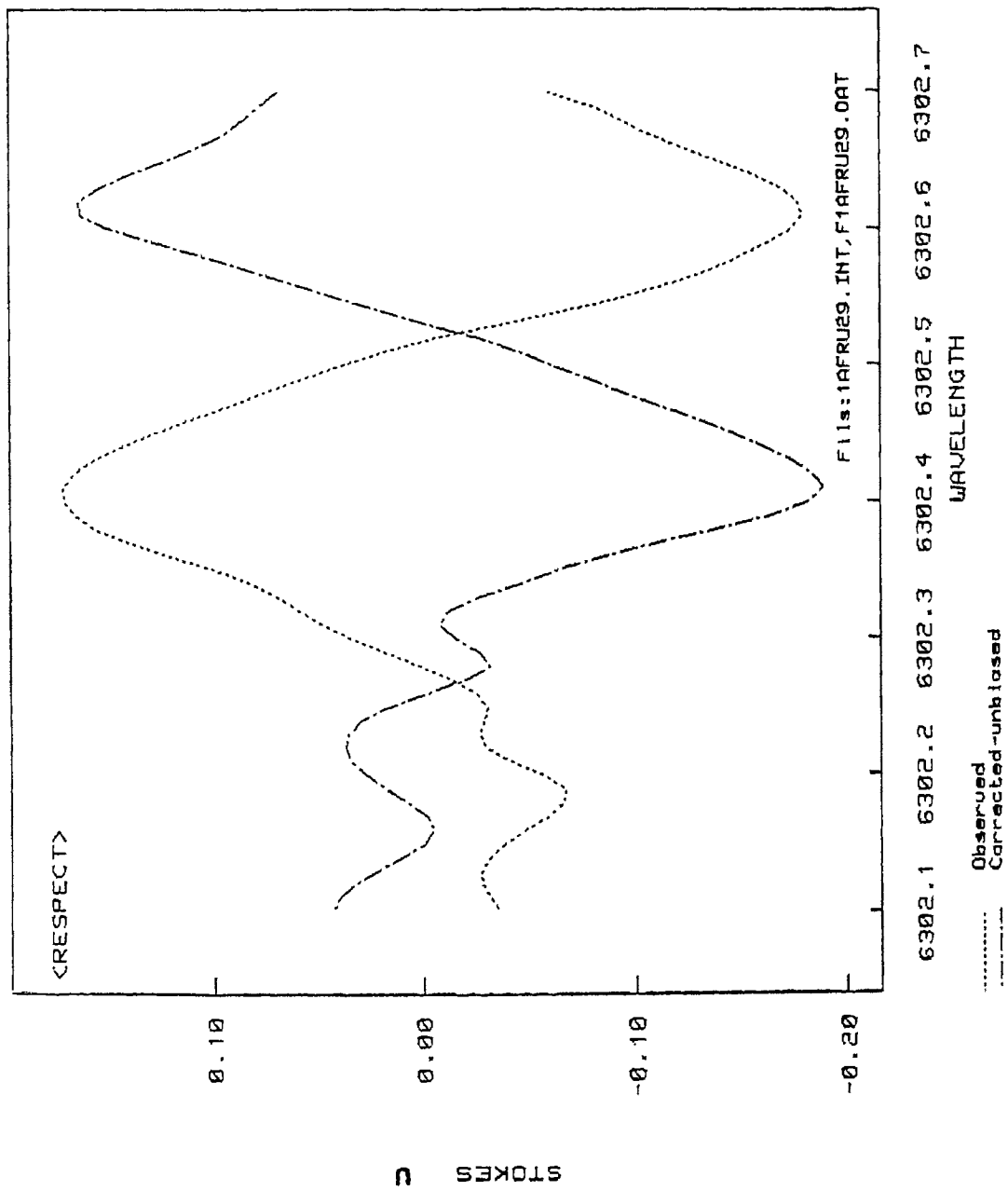


Fig.III-3.2.10b A similar comparison as in Fig.III-32.10a for Stokes U profile.

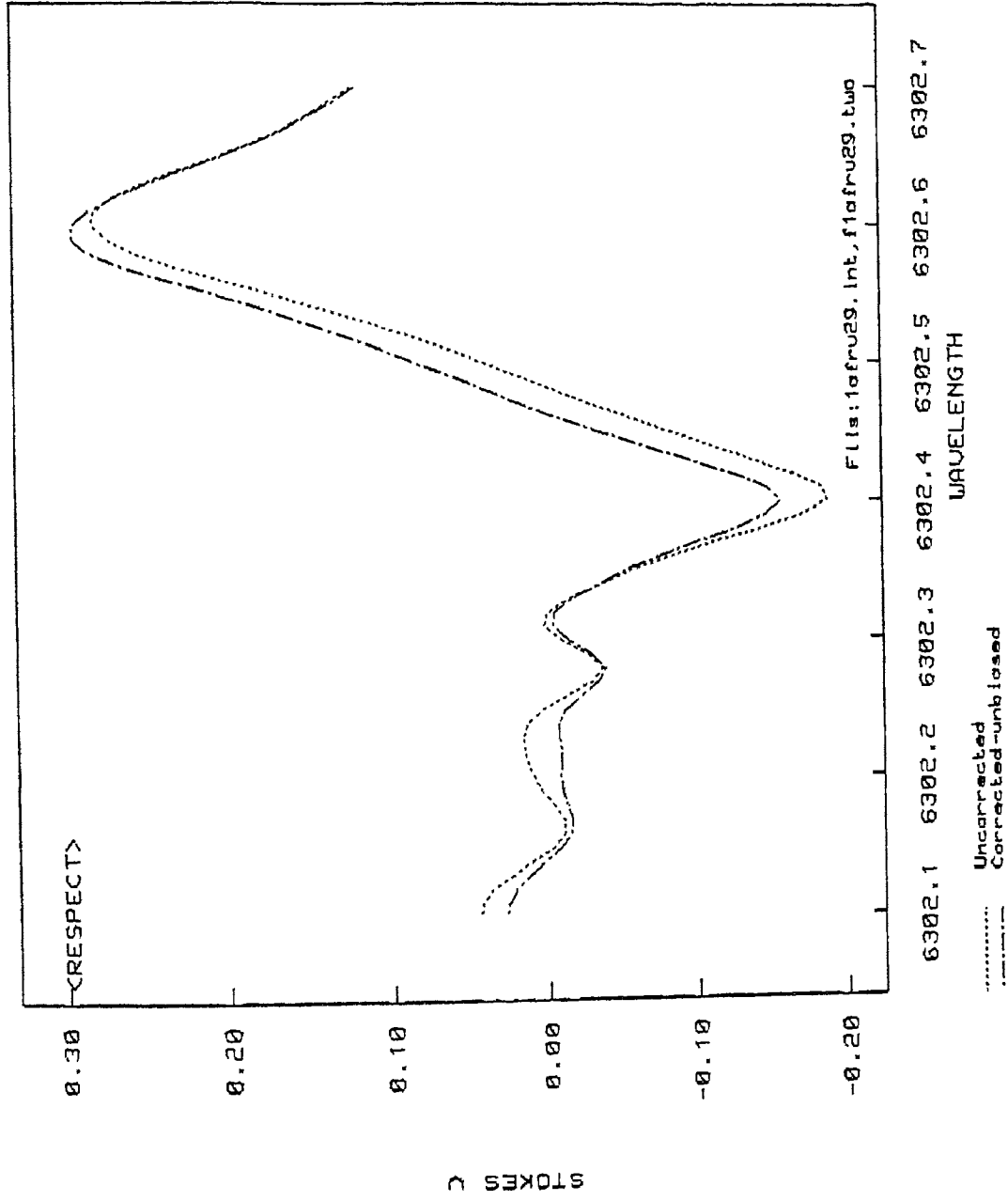


Fig. III-3.2.10c A similar comparison as in Fig. III-3.2.10a for Stokes V profile.

where the Q, U and V polarisations are expected to be zero. Sample spectra of the true Q, U and V profiles individually corrected for the biasing are shown in *Figures* III-3.2.10a, III-3.2.10b, III-3.2.10c. These profiles are from the recordings of the same sunspot KKL 18303, on May 12, 1987, at position 3. The legend at the bottom of the figure should be read as: sunspot number (1 = 18303), day of observation (A = May 12, 1987), position number (TH), Stokes profile (Q) and reference point from fiducial mark (28 etc.) and the spectral line (TWO = $\lambda 6302.5 \text{ \AA}$ line).

One may also notice in these figures, that the Q, U and V amplitudes in the red wing of the line drastically increases with the increase in magnetic field strength. The reason may be partially attributed to the blending of the telluric line $\lambda 6302.76 \text{ \AA}$ with the red wing of the $\lambda 6302.5 \text{ \AA}$ line, but we feel that blending itself may be only a minor cause, the major cause being at the source itself.

CHAPTER IV
INVERSION OF STOKES PROFILES

1. THE EQUATIONS OF RADIATIVE TRANSFER

Under the assumptions of (a) the solar atmosphere, where the spectral line is formed, is in a stationary state and its physical properties depend only on the geometric depth, (b) the continuum is formed under local thermodynamic equilibrium (LTE) and is unpolarised, (c) the atomic levels involved in the transition do not show atomic polarisation, the equations of polarised radiative transfer in the presence of magnetic fields, where the spectral lines are broadened due to the Zeeman effect, read as

$$\mu \frac{d I}{d \tau} = \eta_o (I - B_T) + \eta_I (I - S) + \eta_Q Q + \eta_U U + \eta_V V$$

$$\mu \frac{d Q}{d \tau} = \eta_Q (I - S) + (\eta_o + \eta_I) Q + \rho_V U - \rho_U V$$

$$\mu \frac{d U}{d \tau} = \eta_U (I - S) - \rho_V Q + (\eta_o + \eta_I) U + \rho_Q V$$

$$\mu \frac{d V}{d \tau} = \eta_V (I - S) + \rho_U Q - \rho_Q U + (\eta_o + \eta_I) V$$

-----IV-1.1

where μ is the cosine of the viewing angle between the line of sight and the normal to the solar surface at the point of observation. B_T is the local Planck function at a temperature T , S is the source function calculated in terms of LTE departure coefficients and I, Q, U, V are the local Stokes parameters (*Landi Degl'Innocenti and Landi Degl'Innocenti, 1972; Landi Degl'Innocenti 1976*). The elements of the Mueller matrix, following their papers, are given by

$$\eta_I = 0.5(\eta_p \sin^2 \gamma + 0.5(\eta_b + \eta_r)(1 + \cos^2 \gamma))$$

$$\eta_Q = 0.5(\eta_p - 0.5(\eta_b + \eta_r)) \sin^2 \gamma \cos(2\zeta)$$

$$\eta_U = 0.5(\eta_p - 0.5(\eta_b + \eta_r)) \sin^2 \gamma \sin(2\zeta)$$

$$\eta_V = 0.5(\eta_r - \eta_b) \cos \gamma$$

----- IV-1.2

and

$$\rho_Q = 0.5(\rho_p - 0.5(\rho_b + \rho_r)) \sin^2 \gamma \cos(2\zeta)$$

$$\rho_U = 0.5(\rho_p - 0.5(\rho_b + \rho_r)) \sin^2 \gamma \sin(2\zeta)$$

$$\rho_V = 0.5(\rho_r - \rho_b) \cos \gamma$$

----- IV-1.3

where,

$$\eta_p = \eta_o \sum_M S_M^{(2)} H(\alpha, \nu - \nu_M^{(2)})$$

$$\eta_b = \eta_o \sum_M S_M^{(1)} H(\alpha, \nu - \nu_M^{(1)})$$

----- IV-1.4

$$\eta_r = \eta_o \sum_M S_M^{(3)} H(\alpha, \nu - \nu_M^{(3)})$$

and

$$\rho_p = \eta_o \sum_M S_M^{(2)} Z F(\alpha, \nu - \nu_M^{(2)})$$

$$\rho_b = \eta_o \sum_M S_M^{(1)} Z F(\alpha, \nu - \nu_M^{(1)})$$

$$\rho_r = \eta_o \sum_M S_M^{(3)} Z F(\alpha, \nu - \nu_M^{(3)})$$

----- IV-1.5

Here, η_o is the ratio of the optical depth at the line centre wavelength (λ_o), and the same quantity at the reference wavelength (λ). ν is the inclination of the magnetic field vector to the line of sight and ζ is the azimuth of the magnetic field vector.

$$H(\alpha, \nu) = \frac{a}{\pi} \int_{-\pi}^{+\pi} \exp(-y^2) / ((\nu-y)^2 + a^2) dy \quad \text{-----IV-1.6}$$

and

$$F(\alpha, \nu) = \frac{1}{2\pi} \int_{-\pi}^{+\pi} (\nu-y) \exp(-y^2) / ((\nu-y)^2 + a^2) dy \quad \text{----IV-1.7}$$

are the Voigt and Faraday-Voigt function respectively, and α is the damping constant of the spectral line.

The quantities $S_M^{(i)}$ and $\nu_M^{(i)}$ are respectively the strengths of the Zeeman split components, and are functions of the L, S, J quantum numbers of the atomic levels involved in the transition (see *Table I* of *Landi Degl'Innocenti, 1975*). The splitting of the Zeeman components given by,

$$\nu_M = 1.6686 \times 10^{-13} \lambda_0^2 H ((G - G')M - G'(2-i)) / \Delta\lambda_D \quad \text{----- IV-1.8}$$

where λ_0 is expressed in Angstroms, H in Gauss. G and G' are the Lande' g factors of the lower and upper levels of the atomic transition in question given by the expression (*White, 1934*)

$$G = 1 + [J(J+1) - L(L+1) + S(S+1)] / [2 J(J+1)] \quad \text{-----IV-1.9}$$

The superscripts (i=1,2,3) in any of the above expressions refers to any of the Zeeman split components and M refers to the magnetic quantum number.

$\nu = (\lambda - \lambda_0) / \Delta\lambda_D$ is the distance from the line centre in Doppler broadening ($\Delta\lambda_D$) units and is given by

$$\Delta\lambda_D = \frac{\lambda_0 \sqrt{(\xi^2 + (2kT/M_a))}}{c} \quad \text{-----IV-1.10}$$

here ξ, k, T, c, M_a refer to the microturbulent velocity, Boltzmann constant, temperature, velocity of light and mass of atom under consideration, respectively.

2. ANALYTICAL SOLUTIONS OF THE POLARISED RADIATIVE TRANSFER EQUATIONS

The analytical solutions of the polarised radiative transfer equations in terms of the Stokes parameters have been derived by *Landolfi and Landi Degl'Innocenti* (1982). Consider the spectral line being formed in a plane parallel atmosphere. Let the line of sight axis (s), be at an angle $\cos^{-1} \mu$ to the outward normal. Let τ be the continuum optical depth defined by:

$$d\tau/\mu = -\kappa_c ds \quad \text{-----IV-2.1}$$

where κ_c is the continuous extinction coefficient at the reference wavelength. Under the assumption of the Milne-Eddington atmosphere, the source function varies linearly with optical depth τ ,

$$B(T_e) = B_0 + B_1 \tau, \quad \text{-----IV-2.2}$$

and the opacity ratio η_0 , the line damping α and Doppler width $\Delta\lambda_D$ are constants. Assuming that the magnetic vector and the line of sight velocity are constants then the η 's and ρ 's in Equation IV-1.2 are also constant.

The analytical solutions read as,

$$\begin{aligned} I &= B_0 + \mu B_1 \Delta^{-1} [(1+\eta_I) \{ (1+\eta_I)^2 + \rho_Q^2 + \rho_U^2 + \rho_V^2 \}] \\ Q &= -\mu B_1 \Delta^{-1} [(1+\eta_I)^2 \eta_Q + (1+\eta_I) (\eta_V \rho_U - \eta_U \rho_V) + \rho_Q R] \\ U &= -\mu B_1 \Delta^{-1} [(1+\eta_I)^2 \eta_U + (1+\eta_I) (\eta_Q \rho_V - \eta_V \rho_Q) + \rho_U R] \\ V &= -\mu B_1 \Delta^{-1} [(1+\eta_I)^2 \eta_V + \rho_Q R] \end{aligned} \quad \text{-----IV-2.3}$$

where,

$$\Delta = (1+\eta_I)^2 [(1+\eta_I)^2 - \eta_Q^2 - \eta_U^2 - \eta_V^2 + \rho_Q^2 + \rho_U^2 + \rho_V^2] - R^2 \quad \text{-----IV-2.4}$$

and,

$$R = (\eta_Q \rho_Q + \eta_U \rho_U + \eta_V \rho_V) \quad \text{-----IV-2.5}$$

It may be noted that for a normal Zeeman triplet (e.g., the Fe I λ 6302.5 Å line) the absorption profiles (η 's) and the anomalous dispersion profiles (ρ 's) are given by

$$\begin{aligned} \eta_p &= \eta_o H(\alpha, \nu) \\ \rho_p &= 2 \eta_o F(\alpha, \nu) \\ \eta_{b;r} &= \eta_o H(\alpha, \nu \pm \nu_H) \\ \rho_{b;r} &= 2 \eta_o F(\alpha, \nu \pm \nu_H) \end{aligned} \quad \text{-----IV-2.5}$$

here

$$\nu_H = (4.6686 \times 10^{-13} \lambda_o^2 H) / \Delta \lambda_D \quad \text{-----IV-2.6}$$

is the Zeeman splitting due to magnetic field H (normal Zeeman effect).

3. THE INVERSION SCHEME

The non-linear least square fitting technique - The Marquardt Algorithm.

From the observed data one needs to derive the vector magnetic field and other physical parameters. This can be done by (a) synthesising the spectrum (e.g., Wittmann, 1974) and then comparing the observed and synthesised profiles. (b) use of Q-U diagrams to obtain the magneto-optical effects in comparison with theory and neglecting the magneto-optical effects. To determine the magnetic field strength and inclination and other physical parameters using the Unno theory. (Kawakami, 1983). (c) Skumanich and Lites (1987) have used the non-linear least square fitting technique to recover the vector magnetic field parameters and other physical quantities, using the analytical solution of the Stokes Q, U and V

profiles.

The non-linear least square method of Marquardt attempts to optimally fit the Q, U and V profiles based on the assumptions used to derive the analytical solutions of these profiles.

A set of eight parameters, a_j ($j=1, n$), are used to compare all the three Stokes profiles Q, U and V, simultaneously. The parameters are

- i. the magnetic field strength - H
- ii. inclination of the magnetic field vector - γ
- iii. azimuth of the magnetic field vector
- iv. opacity ratio - η_0
- v. damping constant - α
- vi. line centre wavelength - λ_0
- vii. Doppler width - $\Delta\lambda_D$
- viii. cosine of the heliocentric angle times the slope of the source function - μB_1 .

We use the spectral line Fe I λ 6302.5 Å for the non-linear least square method. This line has a Lande' g factor of 2.5 (*Beckers* 1969).

The problem under consideration is that of minimising a sum of the squares of several non-linear functions $r_i(\vec{a})$ of many variables (\vec{a})

$$y(\vec{a}) = \sum_{i=1}^m [r_i(\vec{a})]^2 \quad \text{-----IV-3.1}$$

where $\vec{a} = (a_1, a_2, \dots, a_n)^T$, where $m \geq n$. where $r_i(\vec{a})$ is the residual difference between the observed and the predicted quantities. The Levenberg-Marquardt Scheme (*Levenberg* 1944; *Marquardt* 1963; *Fletcher* 1971) is as follows:

If the $m \times n$ Jacobian matrix J is defined as

$$J_{ij} = \partial r_i / \partial a_j \quad \text{-----IV-3.2}$$

then for every step of iteration, one can write

$$\vec{a}^{(k+1)} = \vec{a}^{(k)} + \vec{\delta}^{(k)} \quad \text{-----IV-3.3}$$

where $\vec{\delta}$ is the solution of a set of linear equations

$$(A + \lambda_c I) \vec{\delta} = -\vec{v} \quad \text{-----IV-3.4}$$

where $A = J^T J$ and $\vec{v} = J^T \vec{r}$ are evaluated at $\vec{a}^{(k)}$, λ_c is an adjustable parameter used to control the iteration.

On any one iteration, A and \vec{v} are fixed so that $\vec{\delta}$ may be considered a step function, $\vec{\delta}(\lambda_c)$ of λ_c . Then as $\lambda_c \rightarrow \infty$, $\vec{\delta}(\lambda_c) \rightarrow \vec{v}/\lambda_c$ which is an incremental step along the direction of the steepest descent of $y(\vec{a})$. as $\lambda_c \rightarrow 0$ then $\vec{\delta}(\lambda_c) \rightarrow -A^{-1} \vec{v}$ which is the correction predicted by the Gauss-Newton or the generalised least squares method. Steepest descent methods converge surely, but slowly, whereas the Gauss-Newton methods rapidly converge but the convergence is not reliable.

In the Marquardt scheme, as described in *Bevington* (1969), the parameter λ_c is arbitrarily fixed at a value of 10^{-3} at the beginning of the first iteration and then multiplied or divided by constant value of 10 depending upon the minimisation of the sum of residuals (or the chi-square test). If the residual is less than zero then increase λ_c by a factor of 10 and if greater than zero decrease λ_c by a factor of 10. In *Bevington's* scheme, χ^2 is evaluated twice per iteration, once before the incremental of a_j and once after it.

The disadvantage is that one cannot choose the step length of the increments, as defined by its fairness or nearness to the solution. Moreover it takes a longer computer time to evaluate the Jacobian twice per

iteration.

In the Fletcher's scheme of the Modified Marquardt algorithm, λ_c is evaluated by comparing $y = y(\vec{a}_j^{(k)})$ and $y' = y(\vec{a}_j^{(k)} + \vec{z}^{(k)})$. Then λ_c is predicted from the following:

If $\phi(\vec{a})$ represents the predicted sum of squares, then the predicted reduction is given by

$$\phi(\vec{a}_j^{(k)}) - \phi(\vec{a}_j^{(k)} + \vec{z}) = -2\vec{z}^T \vec{v}^{(k)} - \vec{z}^T A^{(k)} \vec{z} \quad \text{----IV-3.5}$$

The strategy adopted for choosing λ_c is: if the ratio of the actual reduction to the predicted reduction is close to 1 then decrease λ_c , and if the ratio is near or less than 0 then increase λ_c . For intermediate values, keep λ_c fixed.

3.1.SIMULTANEOUS FITTING OF THE STOKES Q, U AND V PROFILES

For the simultaneous fitting of the three Stokes profiles Q, U and V, we have used the function

$$r_i^2(\vec{a}) = (Q_{\text{fit}} - Q_{\text{obs}})^2 + (U_{\text{fit}} - U_{\text{obs}})^2 + (V_{\text{fit}} - V_{\text{obs}})^2 \quad \text{----IV-3.6}$$

where the suffix 'obs' corresponds to the observed data points and 'fit' corresponds to the fitted data point using the analytical solution of Q,U and V.

3.2.CALCULATION OF STOKES Q, U AND V PROFILES AND THEIR DERIVATIVES.

a) The Profiles

The calculation of the Stokes profiles from the analytical solutions requires test values of the 8 parameters. Using them the profiles are evaluated from the Voigt and Faraday-Voigt functions, $H(a,v)$ and $F(a,v)$, using fast algorithms given by *Matta and Reichel* (1971). The

codes for evaluating these functions has been well tested by *Nagendra and Periah* (1985) and have been adopted from them.

b) The Derivatives

The derivatives of the Stokes Q, U and V profiles enter the calculations via the Jacobian and need to be evaluated.

(i) Derivatives of Q, U and V with respect to azimuth, ζ and inclination, γ . The derivatives of Q, U and V profiles with respect to both these quantities will mean obtaining the derivatives of η_I , η_Q , η_U and η_V . Since these functions are mere sine or cosine functions of ζ and γ , they are easily evaluated.

(ii) Derivatives of Q, U and V with respect to damping, a , Doppler width, $\Delta\lambda_D$, magnetic field strength, H , and velocity function $(\lambda - \lambda_0)$.

The derivatives of Q, U and V with respect to these functions depend on the derivatives of the Voigt and Faraday-Voigt functions with respect to damping and velocity. Following *Nagendra and Periah* (1985),

$$K(a,v) = 2 H(a,v)$$

and hence from *Heinsel* (1978),

$$H^v = 2(K.a - H v)$$

$$H^a = 2[H.a + K v - (1/\sqrt{\pi})]$$

$$K^v = - 2[H.a + K v - (1/\sqrt{\pi})]$$

$$K^a = H^v$$

where obvious symbols within brackets are left out (e.g. $H(a,v) \cong H$ etc.). The superscript 'v' and 'a' refer to the derivatives of functions H and K with respect to each one of them.

(iii) Derivatives with respect to μB_1

Since the source function enters the Stokes Q,U and V profiles, it represents a simple scaling factor, and hence

the derivatives of Q , U and V with respect to μB_1 are the same as Q , U and V , but the scaling is now unity.

3.3 TEST ON THE NON-LINEAR LEAST SQUARE FITTING ALGORITHMS

We generated the synthetic Stokes profiles from the analytical solutions defined by equation IV-2.3, for various test cases.

3.3.1 Bevington's scheme

We attempted to check the algorithm by using Bevington's scheme. Frequent encountering of numerical overflow ($>10^{34}$) or underflow ($<10^{-34}$) with the VAX 11/780 computer problems hampered the task. Since the increase or the decrease in step-lengths were fixed, it took a longer time to converge.

3.3.2 Fletcher's scheme.

Since Bevington's scheme imposed a large number of numerical problems, the next attempt was at using Fletcher's Scheme. In this case, it did improve the speed of computations, with little or no improvements on the convergence.

3.3.3 Modifications of Bevington's scheme to include the tunability of λ_c as the solution approaches the minimum. The experience gained in these tests helped to modify the Bevington scheme as follows:

For the synthetically generated profiles the values of χ^2 minimised with 20 iterations (takes about 15 minutes of CPU time on the VAX 11/780 computer). In order to help in the convergence we started with λ_c equal to 15. At every stage of improved χ^2 , as χ^2 became smaller, the value of λ_c was chosen to be smaller, so that when χ^2 attained a value of about 10^{-10} , λ_c was as small as 1.2. This was because we preferred to have a sure convergence, albeit a rather slow one.

3.3.4. Test runs on the modified scheme are shown in *Table IV-1*. After 20 iterations all the parameters have been recovered perfectly well when compared with the inputs to the synthetic profiles, showing that the algorithm works well.

3.3.5. However one must be very cautious in the use of Marquardt algorithm to simultaneously fit the Stokes Q, U and V profiles. In no case of real data, did the value of χ^2 go less than 10^{-4} , indicating that in real data the situation is more complicated. Moreover, a complete model atmosphere for the profiles were generally not used, resulting in χ^2 values as large as 10^{-4} compared to test cases on synthetic profiles which were as small as 10^{-14} . The average value of χ^2 at the beginning of the first iteration was between 2-1 and decreased to values between 10^{-3} to 10^{-7} . In line of this, the values of λ_c at the initial iteration was kept at 20 and decreased successively as χ^2 kept decreasing in units of 3.

4. TEST RUNS ON REAL DATA

The Stokes Q, U and V profiles, after correction correction for all instrumental errors were subjected to the Marquardt algorithm. The data base for this purpose was four positions out of six shown in *Figure III-1.1* for the sunspot 18303 on May 12, 1987.

5. RESULTS OF NON-LINEAR LEAST SQUARE FITTING ALGORITHM

We applied the above mentioned modified scheme of the Marquardt algorithm to the sunspot KKL 18303 for positions 2, 3, 4 and 5 (see *Figure III-1.1*). Of the eight parameters recovered from the fit, the least values recovered were that of line centre wavelength, the magnetic field strength, inclination and azimuth.

Sample plots of the observed and fitted Q, U and V profiles for position 3 are shown in *Figures IV-5.1a,*

TABLE IV-1

T [†] No	Ite No	Line λ_0 in Å	Doppler $\Delta\lambda$ in Å	Damp. const.	η_0	$\mu.B_1$	Magn. field*	Incli. ψ	Azim ζ	λ_c	χ^2
1	20	6302.56	0.035	1.30	4.00	3.0	2500	5.0	50	15E-8	.92
		6302.50	0.070	0.03	2.00	7.0	1500	25.0	20		
		6302.56	0.035	1.30	4.00	3.0	2500	5.0	50		
2	20	6302.56	0.035	1.30	4.00	3.0	2500	5.0	75	15E-8	.91
		6302.50	0.070	0.30	2.00	7.0	1500	25.0	20		
		6302.56	0.035	1.30	4.00	3.0	2500	5.0	75		
3	20	6302.56	0.035	1.30	4.00	3.0	2500	5.0	90	6.51	.75
		6302.50	0.070	0.30	2.00	7.0	1500	25.0	20		
		6302.56	0.035	1.30	4.00	3.0	2500	5.0	90		
4	16	6302.56	0.035	1.30	4.00	3.0	2500	5.0	120	12.20	.85
		6302.56	0.060	0.30	3.13	3.3	1951	12.2	133		
		6302.56	0.035	1.30	4.00	3.0	2500	5.0	120		
5	89	6302.56	0.035	1.30	4.00	3.0	2500	5.0	120	8.30	.75
		6302.50	0.070	0.30	2.00	7.0	1500	25.0	140		
		6302.56	0.035	1.30	4.00	3.0	2500	5.0	120		

Table IV-1 continued...

6	76	6302.56	0.035	1.30	4.00	3.0	2500	5.0	160	2.20	.69
		6302.50	0.070	0.30	2.00	7.0	1500	25.0	140		
		6302.56	0.035	1.30	4.00	3.0	2500	5.0	160		
7	28	6302.56	0.035	1.30	4.00	3.0	2500	20.0	70	0.39	.82
		6302.50	0.070	0.30	2.00	7.0	1500	25.0	10		
		6302.56	0.035	1.30	4.00	3.0	2500	20.0	430		
8	19	6302.56	0.035	1.30	4.00	3.0	2500	60.0	70	0.43	7.9
		6302.50	0.070	0.30	2.00	7.0	1500	25.0	10		
		6302.56	0.035	1.30	4.00	3.0	2500	60.0	1150		

NOTE: † The three entries against each test (T.No) corresponds to

TRUE, TRIAL and RECOVERED values respectively in that order;

* Magnetic field measured in Gauss.

‡ In units of 10^{-14}

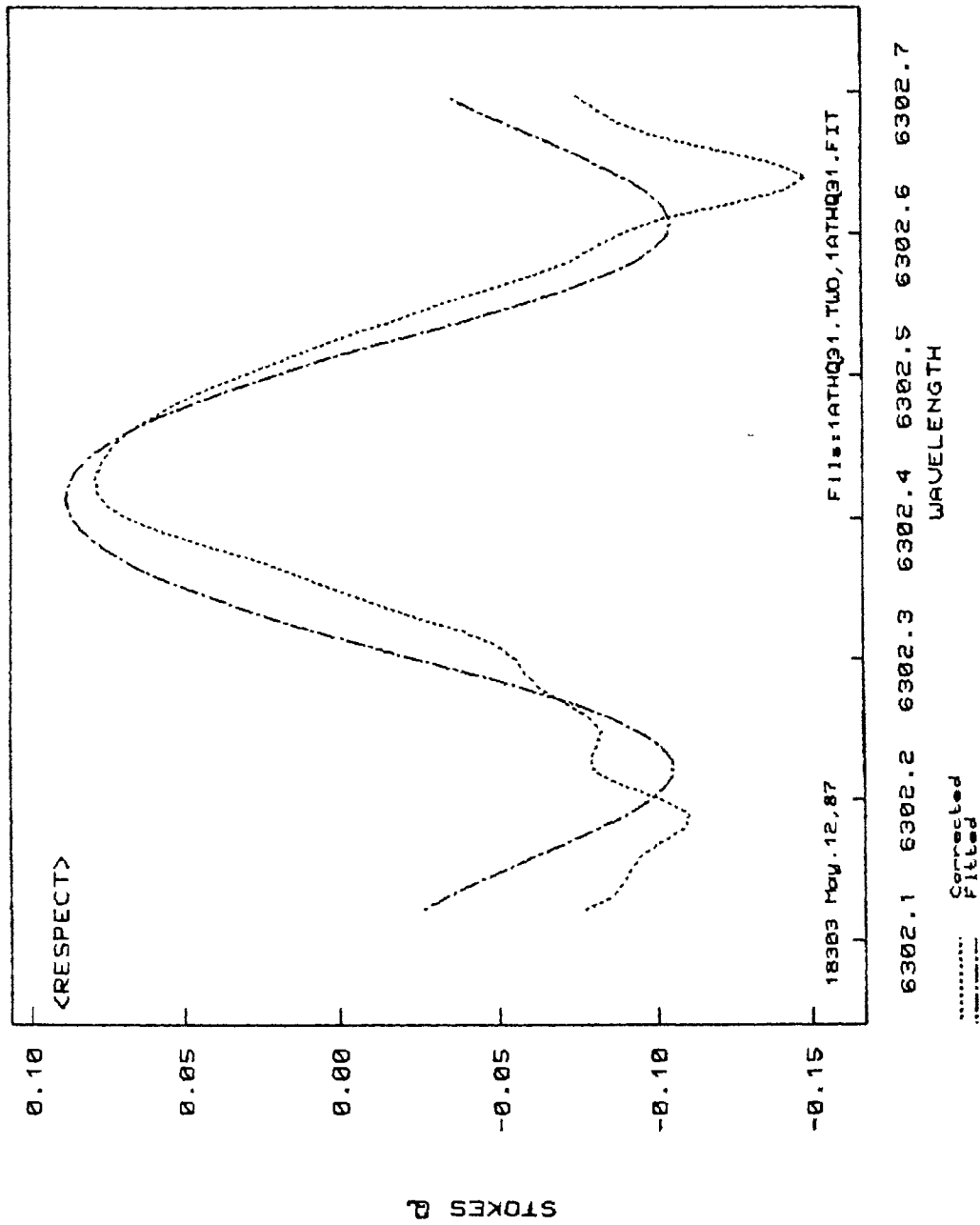


Fig. IV-5.1a Observed Stokes Q profile (dashed line) for the sunspot KKL 18303, position 3, pixel 31, compared with the one computed (dotted line) using the non-linear least-square technique following the Marquardt algorithm.

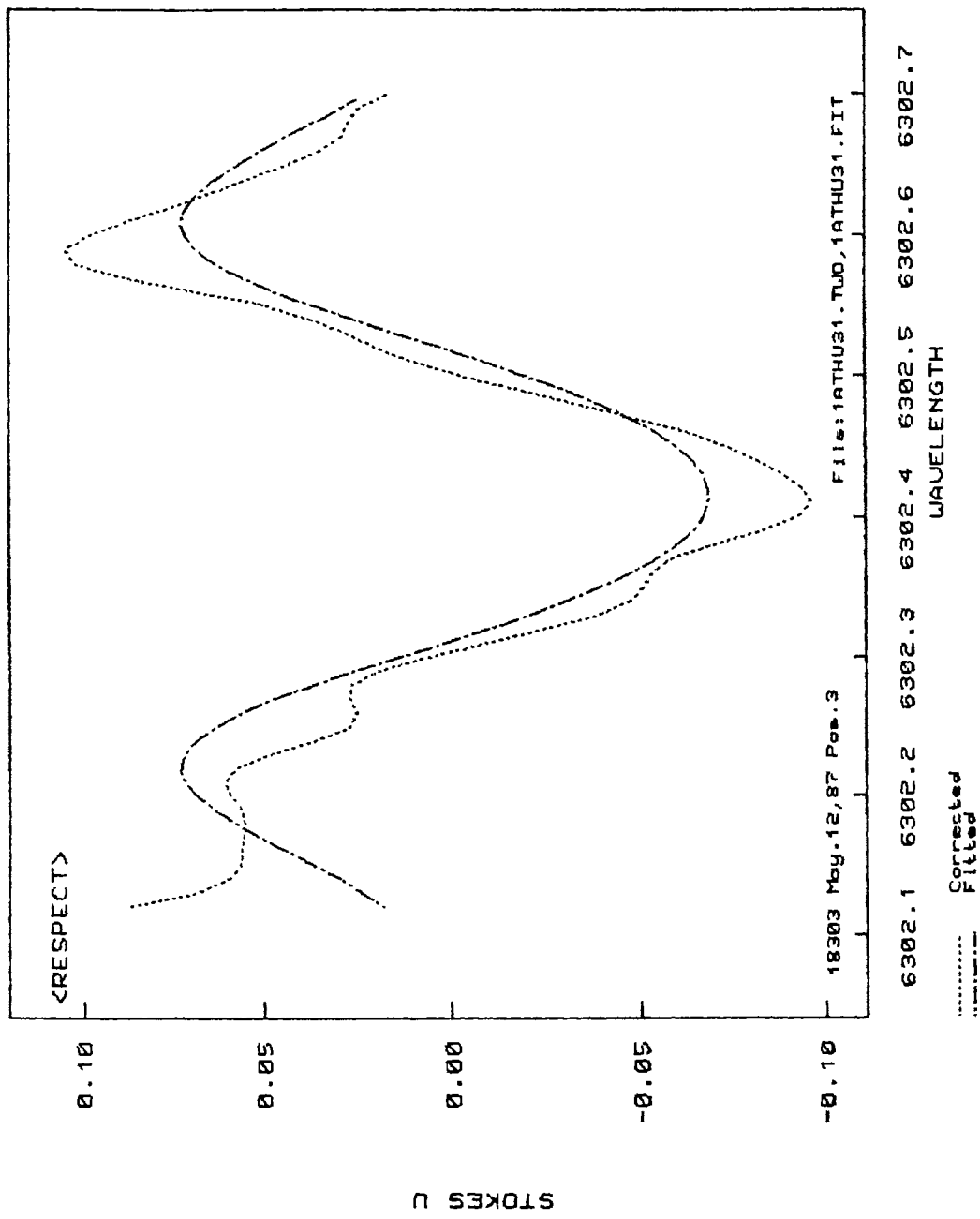


Fig. IV-5.1b Observed (dashed) and computed (dotted) Stokes U profiles for the same position as in Fig. IV-5.1a.

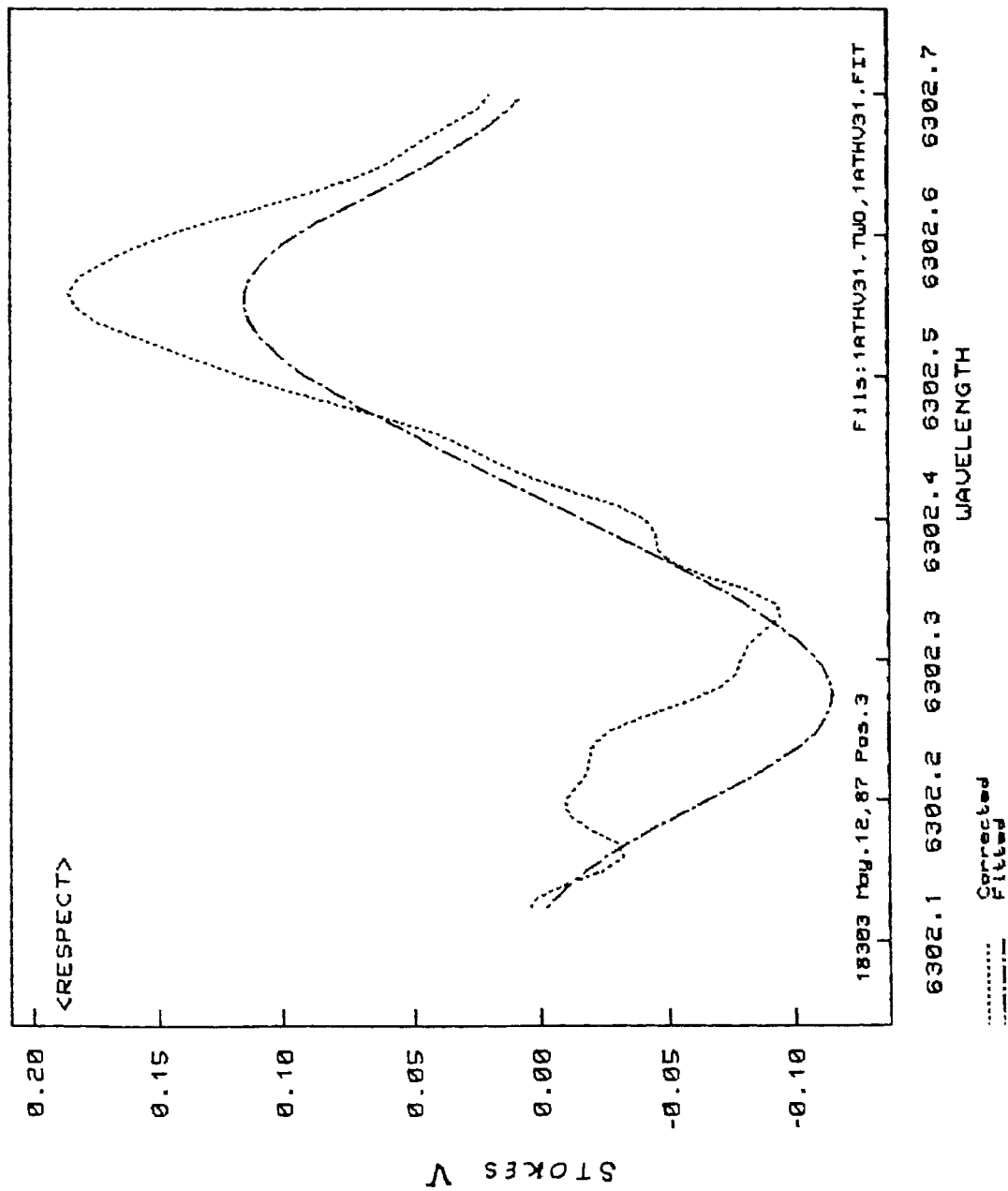


Fig. IV-5.1c Observed (dashed) and computed (dotted) Stokes V profiles for the same position as in Fig. IV-5.1a.

IV-5.1b and IV-5.1c for pixel number 31 . Similar plots are shown in *Figures* IV-5.2a, IV-5.2b and IV-5.2c for the same position with pixel 30.

In all these figures , the fitting of the observed profiles with those of the computed ones, to recover the parameters is good.

Notice that the V profile does not change sign. Thus we are looking at one side of the observed polarity inversion line (neutral line). Since the sunspot is not at the disc centre , ($\mu=0.88$), the line of sight is approximately 30° to the normal to the photosphere. Thus the inclination should monotonically increase or decrease as one moves from the penumbra towards the umbra, depending on the side of the inversion line being looked at. *Figure* IV-5.3 shows the plot of the inclination of the magnetic field as a function of the position across the sunspot (pixel number reckoned from the fiducial mark; each pixel number corresponds to 200 microns i.e. 1.1 arcseconds). The inclination increases as one moves towards the umbra. Thus we seem to be looking at the inner portion of the umbra. The above conclusion is consistent with the strong total magnetic field strengths seen in *Figure* IV-5.4 as well as from the position of the slit on the sunspot as seen in *Figure* III-1.1.

The field strengths show values between 500-4300 Gauss. Without more data, it would be premature to comment on the structures seen in these figures.

Figure IV-5.5 shows a decrease in the slope of the source function (μB_1), as one goes towards the umbra. If one could interpret this as a decrease in the temperature gradient, as one moves towards the umbra, then this indicates a smaller heat flux in the umbra.

Figure IV-5.6 depicts the line centre wavelength

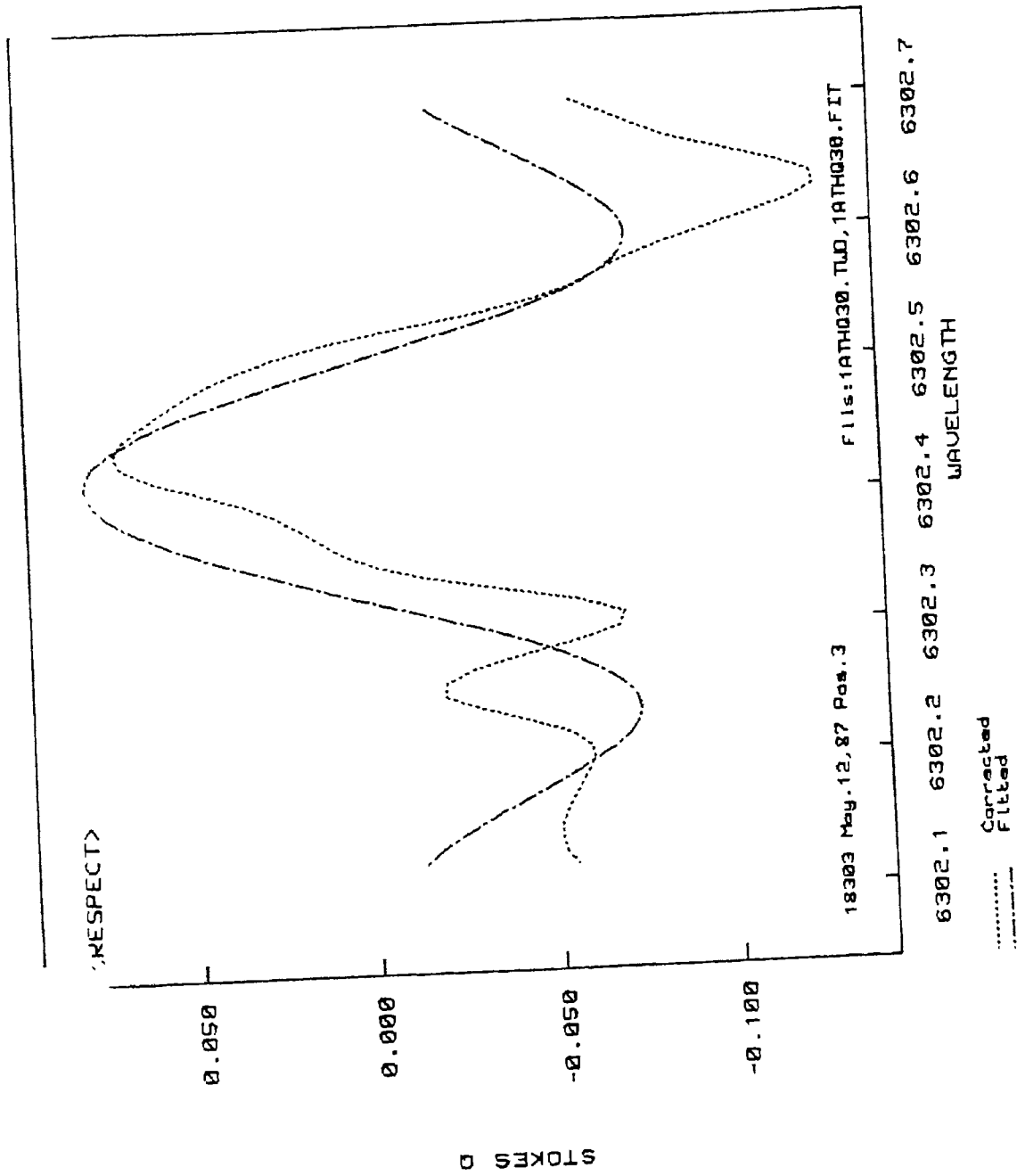


Fig. IV-5.2a
 Observed Stokes Q profile (dashed line) for the sunspot KKL 18303, position 3, pixel 30, compared with the one computed (dotted line) using Marquardt algorithm.

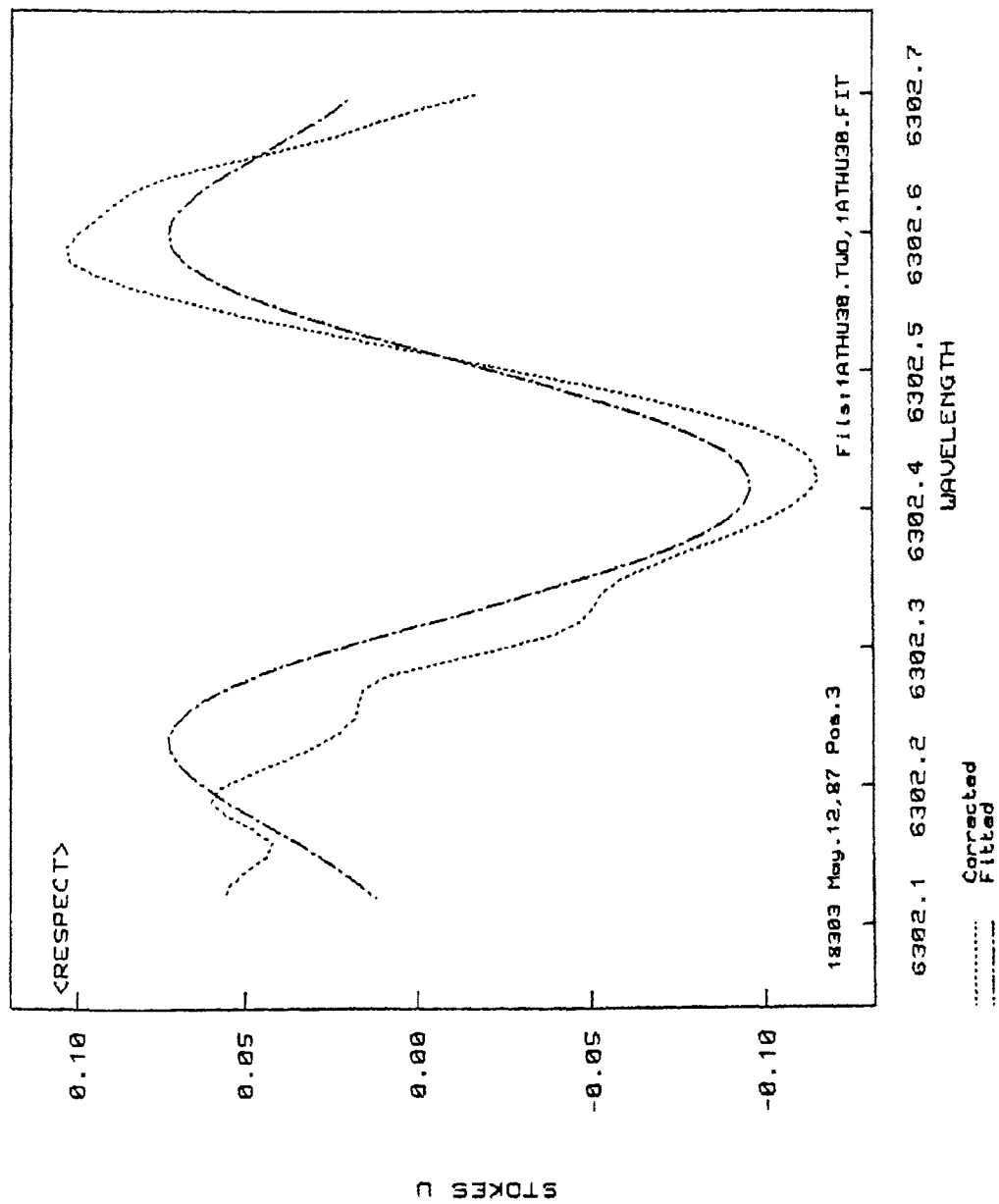


Fig. IV-5.2b Observed (dashed) and computed (dotted) Stokes U profiles for the same position as in Fig. IV-5.2a.

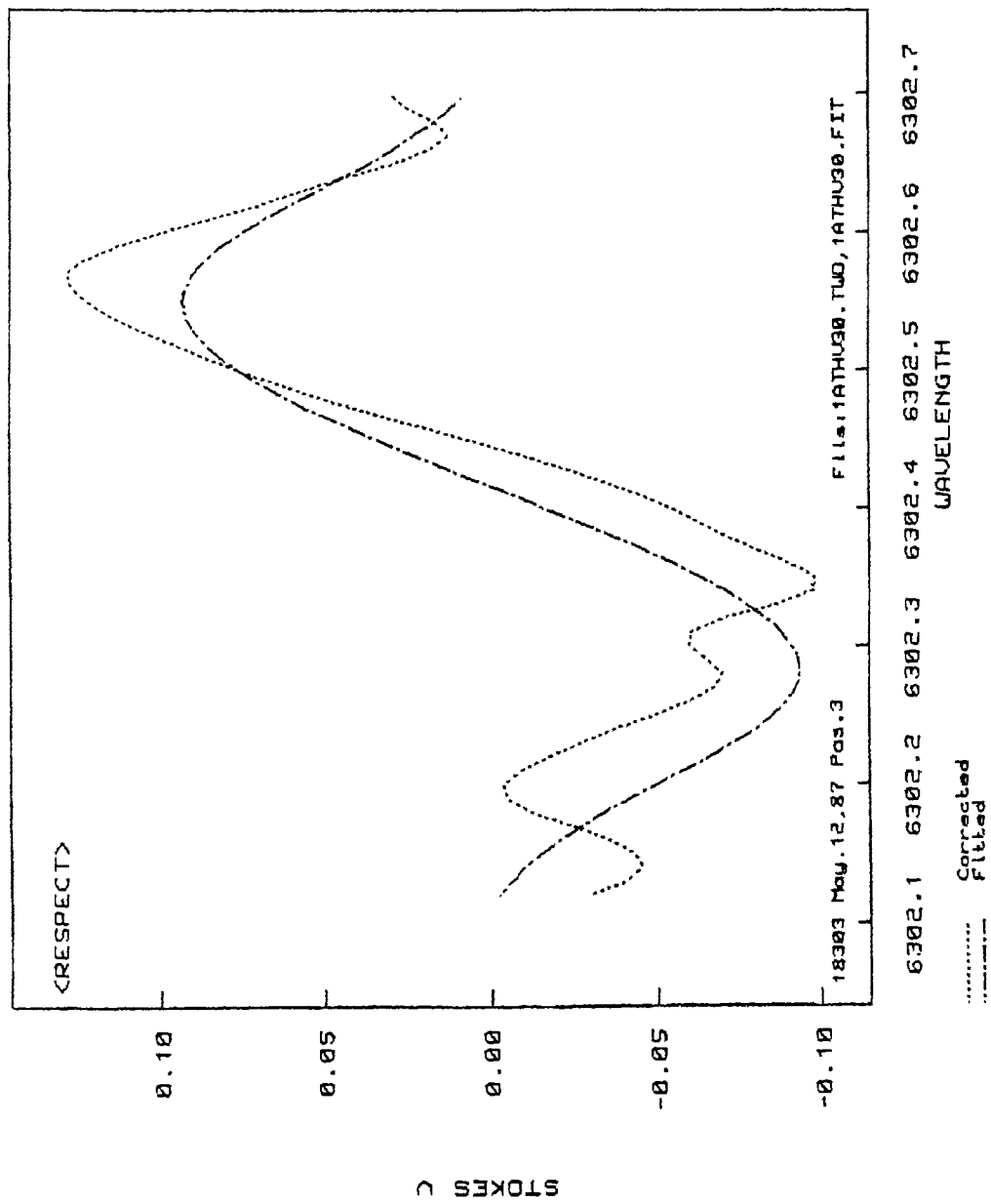


Fig. IV-5.2c Observed (dashed) and computed (dotted) Stokes V profiles for the same position as in Fig. IV-5.2 c.

18303 May. 12, 1987 Position 3

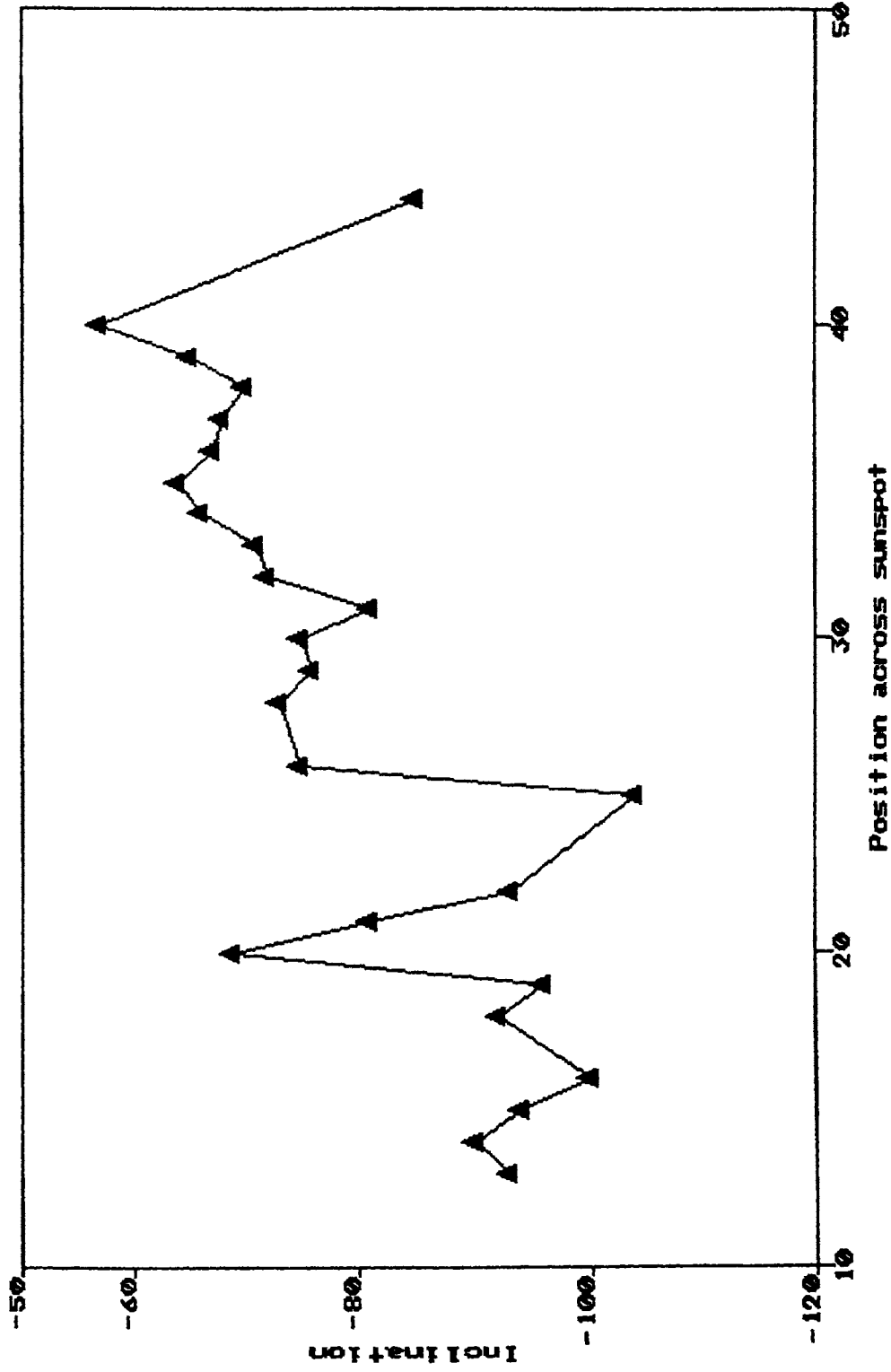


Fig. IV-5.3 A plot of the inclination of magnetic field lines across the sunspot KKL 18303, position 3, observed on May 12, 1987. The position is in units of 1.1 arcsec. Note the trend in the inclination to increase from the penumbra (left) to the umbra (right).

18303 May. 12, 1987 position 3

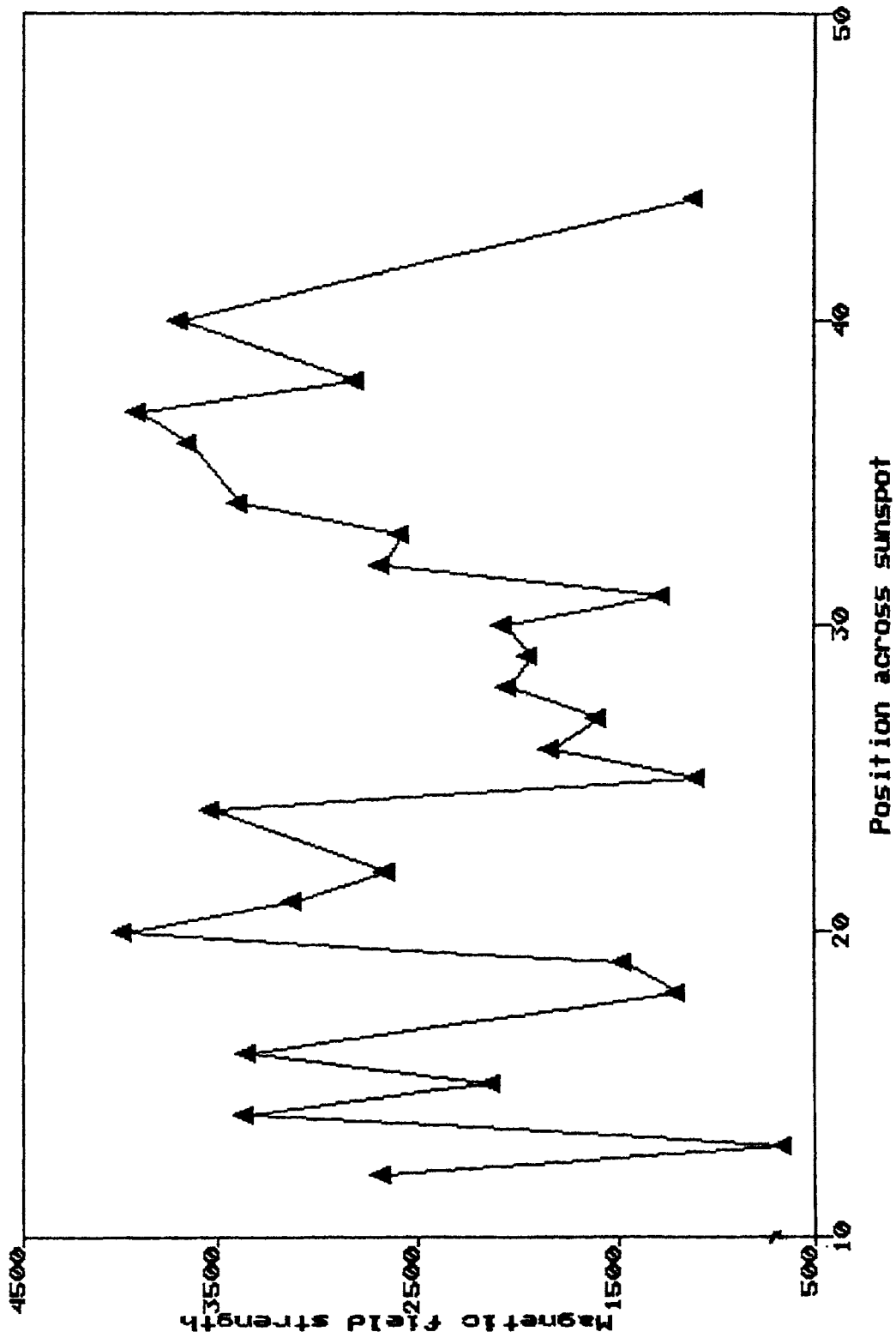


Fig. IV-5.4 The total magnetic field strength across the sunspot KKL 18303 along slit position 3.

18303 May. 12, 1987 Position 3

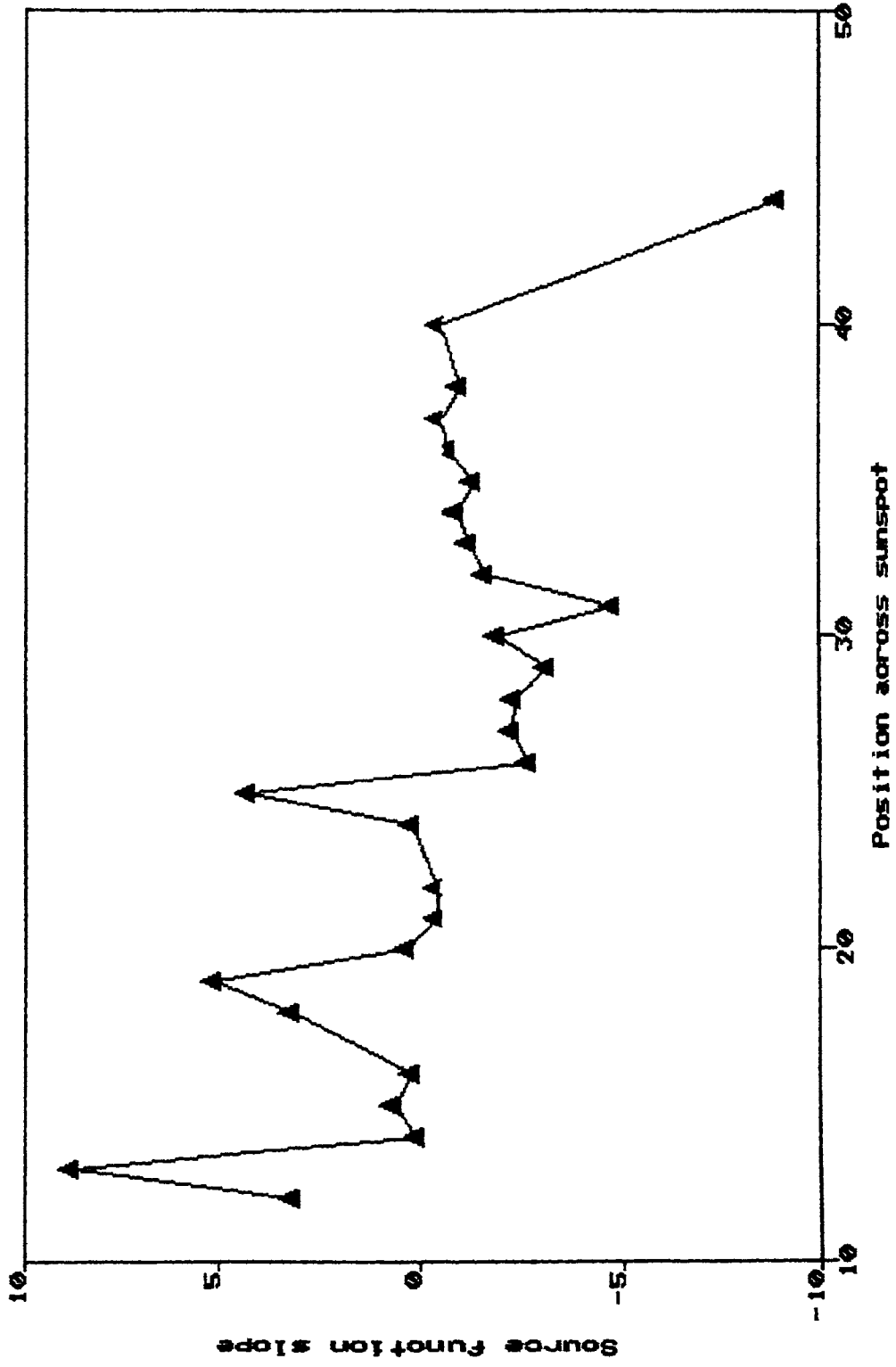


Fig. IV-5.5 Variation of the slope of the source function as one moves from the penumbra to the umbra (see text).

18303 May. 12, 1987 Position 3

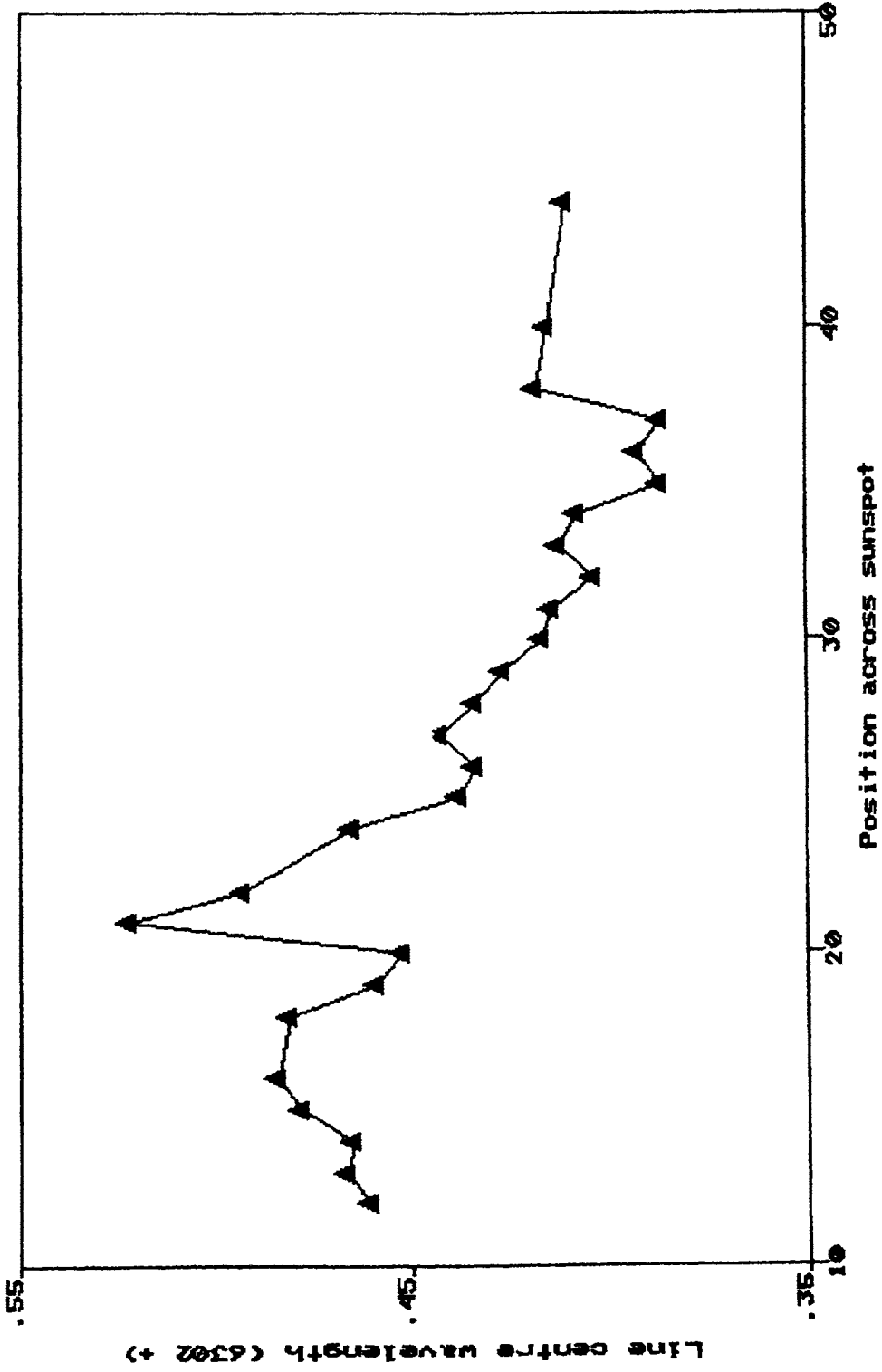


Fig. IV-5.6 The variation of the line-centre wavelength recovered using the Marquardt algorithm for the sunspot KKL18303.

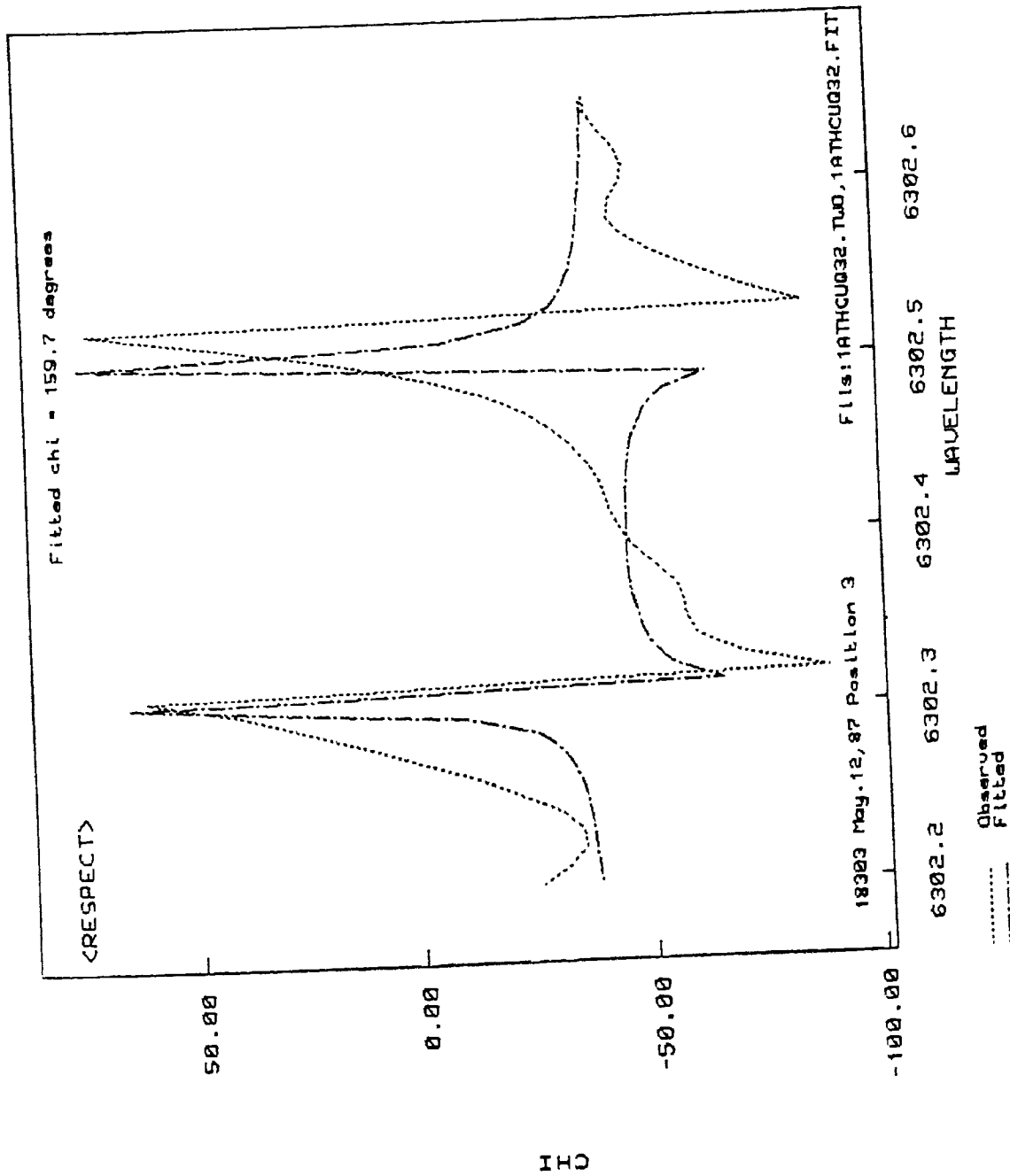


Fig. IV-5.7 The azimuth plots derived from $\tan^{-1}(U/Q)$ for the observed and fitted curves. Notice the sharp changes in linear polarisation as one moves from the spectral line wings towards the line centre.

decreasing towards the umbra which indicates that the umbral region shows a line of sight blue shift relative to the penumbral region.

The azimuth is not shown for these positions because this is a single scan across the sunspot, and the 180° ambiguity in the azimuth would be difficult to resolve in the absence of H- α pictures corresponding to these observations. In *Figure IV-5.7* a wavelength plot of the azimuth as recovered from $\tan^{-1}(U/Q)$, for position 3, at pixel number 32 is shown. The fitted curves from the same, as determined from the non-linear least square fitting is also shown. Notice that the shape of the curves is consistent with the sudden change in the values at the spectral line wings, which is consistent with the change in the linear polarisation from one orthogonal form to another, as decided by the Zeeman effect.

CHAPTER V

SUMMARY AND CONCLUSIONS

1. OVERVIEW.

The aim of this thesis has been measurement of Stokes profiles and vector magnetic fields in sunspots using the Kodaikanal Tower/Tunnel Telescope and spectrograph. Although this coelostat telescope had been constructed with no polarisation measurements in mind, it has been possible to make such measurements given its limitation of oblique reflections and its advantages of very high spectral and spatial resolution. It is this advantage of high spectral and spatial resolution that made it possible to measure the Stokes profiles and derive both vector magnetic fields as well as physical parameters of the solar photosphere in the region of magnetic concentration.

Starting with an extensive study of the polarisation introduced by the instrument and its effect on the recorded Stokes polarisation profiles, we have attempted the design and construction of a simple polarimeter. This has only a few optical components in the path of a light beam, which minimises the instrumental polarisation. Using this polarimeter, we have photographically recorded the Stokes polarisation profiles, in the $\lambda 6300 \text{ \AA}$ region, across a few sunspots in an effort to derive both vector magnetic fields as well as the physical parameters across sunspots.

Our next effort has been to establish a regular working procedure for the reductions of the spectral lines into a useable form. One of the major reasons why full line Stokes polarimetry is not used to produce two dimensional maps of sunspots and other active regions, is the enormous quantity of data to be handled as well as computer time needed. To our knowledge only Kawakami's work has made any attempt in that direction. The present

study has also been motivated to understand the data handling problems.

From the observed Stokes profiles that have been corrected for the instrumental polarisation, we proceed to recover the vector magnetic fields and other physical parameters through an inversion technique. The inversion technique is still in its infancy, and we are yet to appreciate many of its advantages and understand its limitations. Once again, we have come across only the attempt of *Skumanich and Lites* (1987) to use this technique and test it on real data. We have attempted to tune the algorithm for better fitting.

On the instrumental front, using the photographic emulsion has been a disadvantage. Our the signal to noise ratios indicate that the measurement of polarisation is accurate to the order of 2%. One needs to undertake detailed modelling in various situations to translate these quantities into uncertainties of the vector magnetic field and other physical parameters.

The work done here complements the broad-band polarisation work done at several observatories, particularly those of the NASA MSFC system as well as the Tokyo Astronomical Observatory.

In principle cross talk from V into Q could be made very small in this method and thus make the measurements of umbral fields more reliable compared to the ones obtained using instruments that employ electro-optic modulators. One might expect non-potentiality of sunspot umbrae to have a dominant influence on manifestations of solar activity such as solar flares, eruptive filaments, disarations brusgues. Thus reliable measurement of vector fields in the umbral is crucial for the understanding of these processes. It is for this reason

we wish to pursue Stokes polarimetry as a mode of measuring vector fields despite difficulties encountered in both acquisition and interpretation of data.

2. FUTURE IMPROVEMENTS.

The background and practical experience gained from this exercise has shown the need for several improvements.

2.1 The polarimetric system:

In order to record polarisation spectral line profiles of Zeeman sensitive lines in the solar spectrum anywhere between 3000 to 7000 Angstroms it is necessary to redesign the polarimeter. The major changes envisaged include: a) replacing the existing $\lambda/4$ plate (6302 Å) with an achromatic rotating quarter wave plate also known as the Pancharathnam plate. The rotation of the achromatic $\lambda/4$ plate is intended to chop the polarisation beam and thus to improve the signal-to-noise ratio, b) Replacing the existing polaroid with a Glan-Thompson polariser, as polaroids are not 100% efficient. We also intend to keep the polariser fixed so as to always have linear polarisation of the output beam with the electric vector vibrating along the direction of the grating rule to exploit the full efficiency of the grating.

2.2 The detector system:

In conjunction with what has been mentioned in the previous section, the next obvious goal is to have a better two-dimensional detector system preferably a charged-coupled-device to improve the quantum efficiency, reduce noise and to increase time resolution. This would help in achieving better polarimetric accuracies.

2.3 Reduction of scattered light and improvements to telescope seeing:

A system of baffles needs to be designed both at the

the telescope as well as the spectrograph, to prevent spatially scattered light reaching the telescope image plane and to prevent spectrally scattered light within the spectrograph contaminating the recorded spectrum.

2.4 An on-line seeing monitor cum image guiding system hooked to the telescope to enable a raster scanning facility at image plane.

2.5 Auxiliary information in the form of H α spectroheliograms at the same spatial resolution with near simultaneity is imperative to resolve the 180° ambiguity of the vector field.

2.6 The existing algorithms for the non-linear least-square fitting need to be modified because of its slow convergence. It may be necessary to search for better inversion techniques compared to the Marquardt algorithm.

APPENDIX

A PROTOTYPE ELLIPSOMETER TO MEASURE THE REFRACTIVE INDICES OF ALUMINIUM COATED ON THE SURFACE OF COELOSTAT MIRRORS.

Since the reflectivity of aluminium changes with time, the real part, n of the complex refractive index \hat{n} and the extinction coefficient k (imaginary part of \hat{n}) vary with time. Our purpose in designing and constructing a prototype ellipsometer is to monitor these changes. So far, in all measurements of magnetic fields on the Sun, only the laboratory values of the of the indices $n=1.13$ and $k=6.39$ have been used (*Makita and Nishi. 1970; Schulz and Tangerlini 1954*).

A.1. THE METHOD.

Our purpose here is to measure n and k . Let

$$\chi = \frac{R_{\perp}}{R_{\parallel}}$$

where R_{\perp} and R_{\parallel} represent the intensity reflection coefficients perpendicular and parallel to the plane of incidence, respectively. As the angle of incidence slowly changes from 0° to 90° , R_{\parallel} passes through a minimum; the angle of incidence at which this occurs is called the principal angle ψ_p (*Clarke and Grainger 1971*). At the principal angle the phase difference τ between the R_{\parallel} and R_{\perp} components is $\pi/2$.

If linearly polarised light is incident on the mirror surface, with the vibration direction making an angle of 45° with the plane of incidence, then the reflected light is elliptically polarised. If we further introduce a phase difference of $\pi/2$ between the orthogonal components of this elliptically polarised light, then it will be converted to

linearly polarised light. A polaroid in the path of the reflected beam, when rotated about the propagation direction, will then, at some orientation of the polaroid transmission axis, completely extinguish the beam (i.e., when the polaroid transmission axis is orthogonal to the vibration direction of the linearly polarised beam).

The azimuth γ , the angle subtended between the polaroid transmission axis and the perpendicular to the plane of incidence, measured in an anticlockwise sense, is called the principal azimuth. The principal angle i_p is found to obey the law (Clarke and Grainger 1971)

$$[\sin i_p \tan i_p]^4 = (n^2 + k^2)^2 - 2(n^2 - k^2) \sin^2 i_p - n^4 i_p^4$$

The principal azimuth follows the approximate relationship

$$\frac{k}{n} = \tan \gamma$$

A.2. THE DESIGN.

With the above relationships in mind, we have designed an ellipsometer to measure n and k . The spectral lines that are used for the measurement of the vector magnetic fields are Fe I $\lambda 6301.5 \text{ \AA}$ and Fe I $\lambda 6302.5 \text{ \AA}$. Since we require n and k about this wavelength, the light source used is a Spectra-Lase Helium-Neon laser at $\lambda 6328 \text{ \AA}$.

The design drawing of the ellipsometer is shown in *Figure A-1*. The two arms of the ellipsometer, one containing the light source and the other containing the detector are moveable, about the normal of the mirror, from angles 0° through 86° , symmetrically. A semi-circular graduated steel plate holds the arms of the ellipsometer and can be clamped onto the mirror cell of any one of the coelostat mirrors. The scale can be read off to an accuracy of 0.25° . The angle range of 10° to 80° is restricted because of mechanical constraints of positioning

the coelostat. The motion of each arm of the ellipsometer is achieved by mechanical rollers that rest in two positions about the steel plate. Each arm is held in position by a wing-nut. When the arms of the ellipsometer are at very large angles to the normal of the mirror surface, the wing-nuts can fasten the arms with the help of a detachable lever-spanner.

The arms of the ellipsometer are made of brass tubes. One arm containing the light source consists of the following parts:

I. The helium-neon laser source which is held in position by a clamped arrangement so that the laser beam passes through the geometric centre of the tube.

II. A sheet polaroid mounted in a cell. This enables the polaroid to be rotated about an axis normal to the laser beam. A graduated scale (with an accuracy of 0.5°) at the periphery of the cell helps to measure the orientation of the polaroid transmission axis. In this case, the transmission axis of the polaroid is kept fixed, at an angle of 45° to the plane of incidence.

The beam emerging from the tube gets reflected by the mirror surface to enter the other tube containing the detector arm. The detector arm contains the following components:

I. The quarter wave plate assembly for the conversion of elliptically polarised light to linearly polarised light.

II. This is followed by another polaroid assembly that acts as an analyser for the emergent linearly polarised light. Both the quarter-wave plate as well as the polaroid are mounted in rotatable cells similar to the polaroid cell in the light source arm.

III. Following the polaroid is an assembly to mount an optional depolariser.

IV. A movable dekker, with various size apertures for preventing scattered light, allows the laser beam to fall on the detector which is a Light Sensitive Resistor.

The detector is connected in a simple Wheatstone bridge circuit that has a 15-volt input supply. The output is connected to a voltmeter from which the signal can be read-off. Since we seek a minimum signal when the polaroid completely extinguishes the linearly polarised light emerging from the quarter-wave plate at the principal angle, this simple arrangement is adequate.

Initial tests of this prototype ellipsometer on the third mirror located at the bottom of the tower have proved to be encouraging. Certain modifications, however, need to be incorporated before the ellipsometer is made operational. These include strengthening the steel plate as there is flexure on the steel plate, polishing of the grooves in the steel plate holding the guide rollers so that a smooth movement of the arms can be achieved and configuring an arrangement such that each of the arms of the ellipsometer acts as a counter-weight to the other.

REFERENCES

1. Adams, M.J.: 1963, Mon. Not. Roy. Astron. Soc, **126**, 135.
2. Anupama, G.C.: 1987, Paper presented at 'Workshop on Astronomical Instrumentation in India - Past, Present and Future'. Kodaikanal.
3. Auer, L.H., Heasley, J.N., House, L.L.: 1977, Solar Physics, **55**, 47.
4. Babcock, H.W.: 1953, Astrophys. J, **118**, 387.
5. Babcock, H.W.: 1961, Astrophys. J. **133**, 572.
6. Babcock, H.W. and Babcock, H.D.: 1955, Publ. Astron Soc Pac. **64**, 282.
7. Bachman, G. and Pflug, K.: 1983, Publ. Debrecen Heliophysical Obs. **5**, 589.
8. Balasubramaniam, K.S.: 1986, Proc. Workshop. 'Role of fine scale magnetic fields on the structure of the solar atmosphere' (In press).
9. Balasubramaniam, K.S., Venkatakrishnan, P., Bhattacharyya, J.C.: 1985. Solar Phys. **99**, 333.
10. Bappu, M.K.V.: 1967, Solar Phys. **1**, 151.
11. Beckers, J.M.: 1969, Solar Phys. **9**, 372.
12. Beckers, J.M.: 1969, Solar Phys. **10**, 262.
13. Beckers, J.M., Bridges C.A., Gilliam, L.B.: 1976, AFGL-TR-0126. Vols. I, II. A high resolution spectral atlas of the solar irradiance from 380-700 nanometers.
15. Bevington, P.R.: 1969, Data Analysis and Error Analysis for the Physical Sciences, Mc Graw-Hill, New York.
17. Bhattacharyya, J.C.: 1969, D.Phil Thesis, Univ. Calcutta.
18. Bigelow: 1889, 'The Solar Corona, Smithsonian Institution.
19. Bray R.J., Loughhead, R.E.: 1964, Sunspots, Dover Publ. Inc, New York.
20. Breckinridge, J.B.: 1970, M.S. Thesis, Univ. Arizona.
21. Breckinridge, J.B.: 1972, Appl. Optics **10**, 286.
22. Bumba, V.: 1962, Bull. Astr. Inst. Cze. **30**, 95.
23. Caccin, B., Cavallini, F., Capatelli, G., Righini, A., and Sambuco, A.M.: 1985, Astron. Astrophys. **140**, 357.

24. Clarke, D. and Grainger, J.F.:1971, Polarised Light and Optical Measurements, Pergamon, New York.
25. Condon, E.U., Shortley, G.H.: 1935, Theory of Atomic spectra, Cambridge Univ. Press.
26. de Vaucouleurs,G: 1968, Appl. Optics, **7**, 1513.
27. Delbouille, L., Rowland, G., Naven L.: 1973, Photometric atlas of the Solar Spectrum from λ 3000- 10000 Å. Inst. de Astrphys. de L'Universit. de Liege and Observatoire de Belgique.
28. Deslandres,:1912 , Comptes Rendus, Dec 30.
29. Fletcher, R.: 1971 , U.K.Atomic Energy Estbl. Tech Rep. AREE 6799.
30. Hale, G.E. :, 1913, Astrophys. J.**38**, 27; Contr. Princeton Obs 71.
31. Harvey J, Brault, J, Stenflo, J.O., Zwan, C.: 1980, Bull. Amer. Astron Soc. **12**, 476.
32. Hagyard, M.J., Cumings,N.P.:West, E.A., 1983, Proceeding of a Workshop on solar physics and interplanetary travelling phenomena. Sp. Sc. Lab Preprint-84-116.
33. Hagyard, M.J., Cumings. N.P. West, E.A., 1983 , Smith, J.E.: 1982 solar Phys. **80**, 33.
34. Heinzel,P: 1978, Bull astron. Inst. Czec. **20**, 159.
35. Hutley, M.C.: 1982, Diffraction Grating, Academic Press, London.
36. Illing, R.M.E., Landman, D.A. Mickey, D.L. 1974, Astr. Astrophys.**35**,327.
37. Kawakami, H.:1983, Publ. Astron. Soc. Japan. **35**,459.
38. Kemp, J.C., Henson, G.D., Steiner, C.T., Bowell, E.R.: 1987, Nature, **326**, 270.
39. Landi Degl'Innocenti, E., Landi Degl'Innocenti, M. 1972, Solar Phys.**27**, 319.
40. Landi Degl'Innocenti,E.,Landi Degl'Innocenti,M: 1976,Astr. Astrophys. Supl. Ser., **25**, 379.
41. Landi Degl'Innocenti, E., Landi Degl'Innocenti, M: 1977, Solar Phys.**31**, 299.
42. Landolfi. M.,Landi Degl'Innocenti, E.: 1982.Solar Phys.**78**, 355.

43. Landi Degl'Innocenti, E., Landi Degl'Innocenti, M.:
1985, Il. Nuovo Cimento, **27B**, 134.
44. Landolfi, M, Landi Degl'Innocenti, E., Areana, P.:1984,
Solar Phys.**93**, 269.
45. Leighton, R.B.: 1956, Astrophys. J, **130**, 366.
46. Levenberg, K.: 1944, Quart. Appl. Maths. **2**, 164.
47. Lindgren, H.: 1975, Rep. Obs. Lund. **6**, 15.
48. Livingston, W. and Harvey, J.:1971, Kitt Peak Natl.
Obs. Contribution No. 558.
49. Livingston, W. and Harvey, J., Slaughter, C.,
Trumbo, D.:1976, Appl. Optics. **15**, 40.
50. Makita, M., Hamana, S., Nishi, K.: 1985, in NASA
CP-2374, p173. Measurements of Solar Vector Magnetic
Fields. Ed. M.J. Hagyard.
51. Makita, M. and Nishi, K.:1970, Ann. Tokyo Astron. Obs.
253, 2857.
52. Marquardt, D.W.: 1963, J. SIAM, **11**, 431.
53. Mickey, D.L.: 1985, in NASA CP-2374, p183. Measurements
of Solar Vector Magnetic Fields. Ed. M.J. Hagyard.
54. Moe, O.K.:1968, Solar Physics, **4**, 267.
55. Moe, O.K.:1986, Inst. Theor. Astrophys. Rep. No.27,
Univ. Oslo.
56. Moore, C.E., Minnaert, M.G.J., Houtgast, J: 1966, The
Solar Spectrum 2395 Å - 8770Å. Nat. Bur. Stan.
Monograph. 61.
57. Nagendra, K.N., Periah, A.: 1985, Astrophys. Space
Sci.**117**, 121.
58. Nikulin, N.S.: 1960, Publ. Crim. Astrophys. Obs. **22**, 3.
59. Pierce, A.K., Breckinridge, J.B.: 1973, The Kitt Peak
Table of Photographic Solar Spectrum Wavelengths.
KPNQ Contribution No. 559.
60. Prabhu, T.P., Anupama, G.C., Giridhar, S.: 1987, Bull.
Astron. Soc. India, **15**, 98.
61. Rachkovsky, D.N.: 1962, Izv. Crim. Astrophys. Obs. **27**,
148.
62. Rees, D.E.: 1969, Solar Physics, **10**, 268.
63. Schuster :1892, Rep. B.A.A.S., 634.
64. Schuster :1912, Proc. Phys. Soc. London, **24**, 121.

65. Sears, F.H.:1913, *Astrophys. J.*, **38**,27.
66. Severny, A.B.:1964, *Publ. Crim. Astrophys. Obs.*,**31**,126.
67. Severny, A.B.:1964, *Publ. Crim. Astrophys. Obs.*,**31**,209.
68. Severny, A.B.:1965, *IAU Symposium 22*, Ed . R.Lust.
D. Reidel.
69. Skumanich, A., Lites, B.W.: 1987, *Astrophys. J.* **322**,
473.
70. Smart, W.M.:1979, *Textbook on Spherical Astronomy*,
Vikas Publishing House, New Delhi.
71. Solanki, S.K.: 1986, *Astron. Astrophys.***168**, 329.
72. Solanki, S.K., Stenflo, J.O.: 1984. *Astron.*
*Astrophys.***140**,185.
73. Solanki, S.K., Stenflo, J.O.: 1985. *Astron.*
*Astrophys.***148**,123.
74. Stenflo, J.O.: 1973. *Solar Physics.***32**,41.
75. Stenflo, J.O., Harvey, J.W., Brault, J.W., and
Solanki,S *Astron. ,Astrophys.*, **131**, 333.
76. Stepanov, V.E.:1958, *Publ. Crim. Astrophys. Obs.*,**18**,
156.
77. Stepanov, V.E.:1958, *Publ. Crim. Astrophys. Obs.*,**10**, 20.
78. Stepanov, V.E.:1960, *Publ. Crim. Astrophys. Obs.*,**22**, 42.
79. Stepanov, V.E.:1960, *Publ. Crim. Astrophys. Obs.*,**23**,
291.
80. Stepanov, V.E.:1960, *Publ. Crim. Astrophys. Obs.*,**24**,
293.
81. Stepanov, V.E., Severny, A.B.:1962, *Publ. Crim.*
Astrophys. Obs. **28**, 166.
82. Stone, J.M.: 1963, *Radiation in Optics*, Mc Graw-Hill
New York.
83. Stromer: 1892, *Comptes Rendus*, Feb.20, p 1911.
84. Treanor, P.J.: 1960, *Mon. Not. Roy. Astron. Soc.* **120**,
412.
85. Unno, W.: 1956, *Publ. Astron. Soc. Japan.* **8**, 108.
86. West, E.A., Hagyard, M.J.: 1983, *Solar Physics*, **88**, 51.
87. White, H.E.: 1934, *Introduction to Atomic Spectra*.
McGraw-Hill, New York.
88. Wittmann, A.D.:1974. *Solar Phys.*, **33**, 107.
89. Wittmann, A.D.:1974. *Solar Phys.*, **36**, 11.

90. Wittmann, A.D.: 1977. *Astron. Astrophys.* **54**, 175.
91. Zeeman, P.: 1896 *Proc. R. Acad. Amsterdam*, **5**, 181.